



Article

Discovery of Bispecific Antagonists of Retinol Binding Protein 4 That Stabilize Transthyretin Tetramers: Scaffolding Hopping, Optimization, and Preclinical Pharmacological Evaluation as a Potential Therapy for Two Common Age-Related Comorbidities

Christopher L. Cioffi, Parthasarathy Muthuraman, Arun Raja,
Andras Varadi, Boglarka Racz, and Konstantin Petrukhin

J. Med. Chem., **Just Accepted Manuscript** • DOI: 10.1021/acs.jmedchem.0c00996 • Publication Date (Web): 03 Sep 2020

Downloaded from pubs.acs.org on September 3, 2020

Just Accepted

“Just Accepted” manuscripts have been peer-reviewed and accepted for publication. They are posted online prior to technical editing, formatting for publication and author proofing. The American Chemical Society provides “Just Accepted” as a service to the research community to expedite the dissemination of scientific material as soon as possible after acceptance. “Just Accepted” manuscripts appear in full in PDF format accompanied by an HTML abstract. “Just Accepted” manuscripts have been fully peer reviewed, but should not be considered the official version of record. They are citable by the Digital Object Identifier (DOI®). “Just Accepted” is an optional service offered to authors. Therefore, the “Just Accepted” Web site may not include all articles that will be published in the journal. After a manuscript is technically edited and formatted, it will be removed from the “Just Accepted” Web site and published as an ASAP article. Note that technical editing may introduce minor changes to the manuscript text and/or graphics which could affect content, and all legal disclaimers and ethical guidelines that apply to the journal pertain. ACS cannot be held responsible for errors or consequences arising from the use of information contained in these “Just Accepted” manuscripts.

1
2
3
4
5
6
7
8
9
10
11
12
13
14
15
16
17
18
19
20
21
22
23
24
25

Discovery of Bispecific Antagonists of Retinol Binding Protein 4 That Stabilize Transthyretin Tetramers: Scaffolding Hopping, Optimization, and Preclinical Pharmacological Evaluation as a Potential Therapy for Two Common Age-Related Comorbidities

26
27
28
29
30
31
32
33
34
35
36
37

Christopher L. Cioffi,^{*†} Parthasarathy Muthuraman,[†] Arun Raja,[†] Andras Varadi,[§] Boglarka Racz,[§] and Konstantin Petrukhin^{*§}

†Albany College of Pharmacy and Health Sciences, Departments of Basic and Clinical Sciences and Pharmaceutical Sciences, 106 New Scotland Ave, Albany, NY 12208

§Department of Ophthalmology, Columbia University Medical Center, New York, NY 10032

38
39
40
41
42
43
44
45
46
47
48
49
50
51
52
53
54
55
56
57

Abstract: Accumulation of cytotoxic lipofuscin bisretinoids may contribute to atrophic age-related macular degeneration (AMD) pathogenesis. Retinal bisretinoid synthesis depends on influx of serum all-*trans*-retinol (**1**) delivered via a tertiary retinol-binding protein 4 (RBP4)–transthyretin (TTR)–retinol complex. We previously identified selective RBP4 antagonists that dissociate circulating RBP4-TTR-retinol complexes, reduce serum RBP4 levels, and inhibit bisretinoid synthesis in models of enhanced retinal lipofuscinogenesis. However, release of TTR by selective RBP4 antagonists may be associated with TTR tetramer destabilization and, potentially, TTR amyloid formation. We

1
2
3 describe herein identification of bispecific RBP4 antagonists – TTR tetramer kinetic
4 stabilizers. Standout analogue (\pm)-**44** possesses suitable potency for both targets,
5
6 significantly lowers mouse plasma RBP4 levels, and prevents TTR aggregation in a gel-
7
8 based assay. This new class of bispecific compounds may be especially important as a
9
10 therapy for dry AMD patients who have another common age-related comorbidity, senile
11
12 systemic amyloidosis, a non-genetic disease associated with wild-type TTR misfolding.
13
14
15
16
17
18
19

20 INTRODUCTION

21
22
23 All-*trans*-retinol (vitamin A, **1**) (Figure 1) is an essential vitamin that serves as a precursor
24
25 for the biosynthesis of retinoic acid (**2**),¹ 11-*cis*-retinal (**3**),² and many other key retinoids
26
27 involved in multiple cellular processes and numerous critical biological functions
28
29 throughout the body. Extracellular delivery of fat-soluble **1** from the liver to vitamin A-
30
31 dependent tissues is accomplished via a protein transport complex involving the lipocalin
32
33 protein retinol binding protein 4 (RBP4) and transthyretin (TTR, thyroxine binding
34
35 prealbumin).³ The majority of circulating RBP4 is synthesized in the liver (~60%), where it
36
37 requires the binding of **1** (holo-RBP4) prior to secretion. The tertiary complex between
38
39 holo-RBP4 and TTR is required as the small size of RBP4 (21 kDa) makes it susceptible to
40
41 rapid glomerular filtration.⁴ Formation of the complex depends on binding of **1** to RBP4
42
43 as apo-RBP4 associates with TTR poorly.
44
45
46
47
48
49
50
51
52
53
54
55
56
57
58
59
60

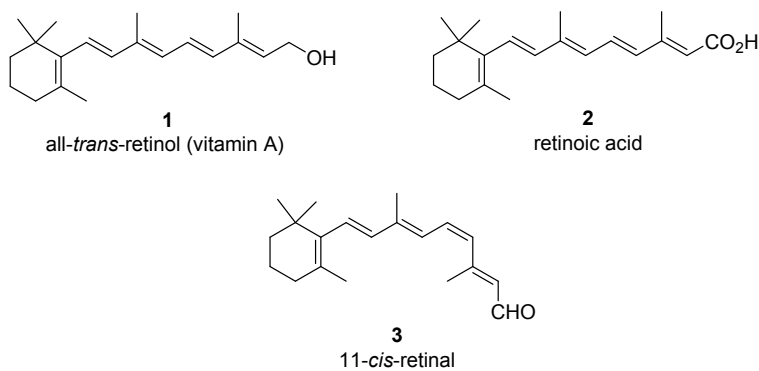


Figure 1. All-*trans*-retinol (**1**), retinoic acid (**2**) (a vital retinoid involved in morphogenesis), and 11-*cis*-retinal (**3**) (a key retinoid required for phototransduction).

TTR is a 55-kDa homotetrameric protein largely synthesized in the liver for systemic circulation and by the choroid plexus for secretion into the cerebral spinal fluid (CSF).⁵ In plasma, TTR mainly functions as a transporter of holo-RBP4 while also serving as a secondary transporter for the thyroid hormone thyroxine (T4, **4**) (Figure 2). Thyroxine-binding globulin (TBG) is the major T4 transport carrier in plasma with approximately 10-15% bound to TTR.

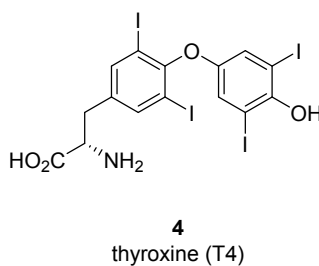


Figure 2. The thyroid hormone thyroxine (T4) (**4**).

1
2
3 The quaternary structure of TTR is composed of a dimer of dimer arrangement that
4 features two identical C2 symmetric binding sites for T4 at the central channel of the
5 tetramer formed where the dimers interface (Figure 3, A).⁵ Each dimer subunit is
6 constructed from two 127-residue β -sheet-rich polypeptide monomers that associate via
7 their edge β -strands. The dimer-dimer interface at the T4 binding sites is weak, and the
8 breakage of it constitutes the first step in the TTR tetramer dissociation process.⁶
9

10
11
12
13
14
15
16
17
18 Complexation between RBP4 and TTR requires that **1** be initially bound to RBP4. The
19 structure of RBP4 contains a cylindrical binding cavity for **1** and analysis of Protein Data
20 Bank (PDB) X-ray crystallographic data for holo-RBP4 (PDB 1RBP)⁷ shows the isoprene tail
21 of **1** occupying the tunnel with its pendant trimethyl cyclohexene ring projecting within
22 the inner hydrophobic β -ionone cavity. The hydroxyl group of **1** resides near the binding
23 cavity opening and is exposed to solvent. Binding of **1** to RBP4 induces conformational
24 changes to exterior loops⁸ that provide favorable protein-protein interaction surfaces for
25 facile TTR engagement. These conformational changes permit two-fold axis of symmetry
26 docking to TTR (Figure 3, B). TTR features two equivalent binding sites for holo-RBP4,
27 providing a complex stoichiometry of one TTR tetramer to two holo-RBP4 molecules
28 (Figure 3, C).⁵ However, a 1:1 molar complex is typically observed due limiting
29 concentrations of plasma RBP4. Lastly, an H-bond between the hydroxyl group of **1** and
30 TTR further stabilizes the protein transport complex⁹ and allows it to fully-conceal the
31 hydrophobic vitamin as it is transported in serum.
32
33
34
35
36
37
38
39
40
41
42
43
44
45
46
47
48
49
50
51
52
53
54
55
56
57
58
59
60

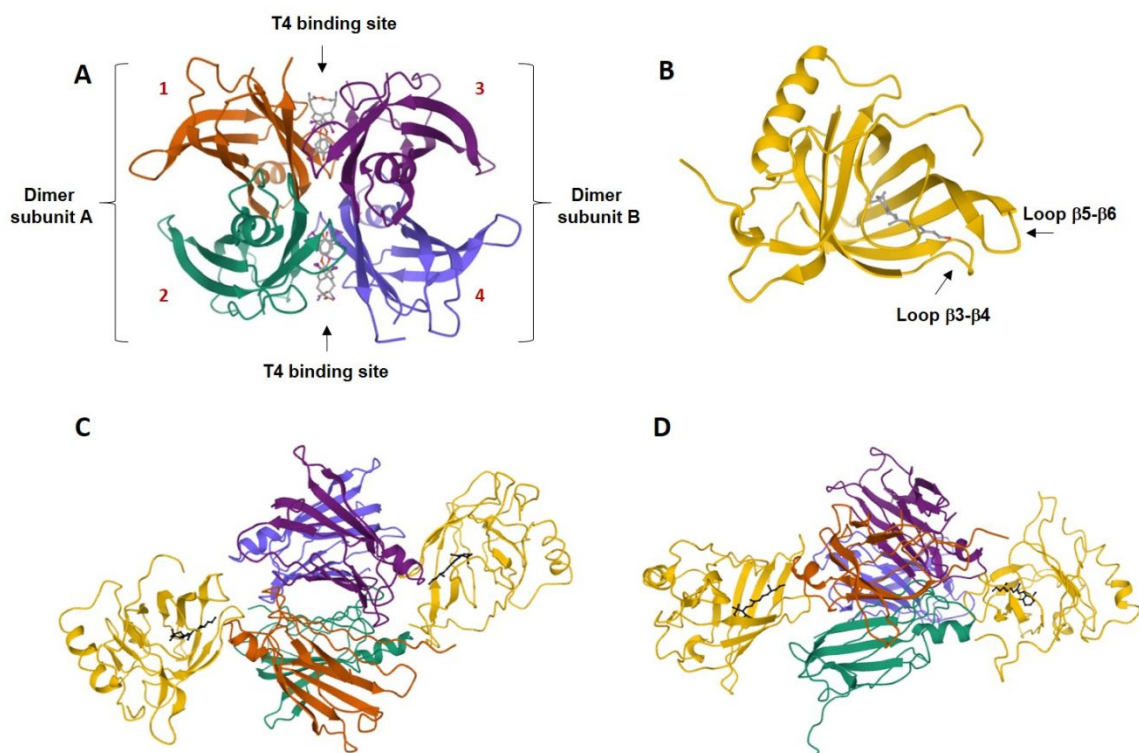


Figure 3. Three-dimensional structures of TTR, holo-RBP4, and the holo-RBP4-TTR tertiary complex. (A) Ribbon diagram of the quaternary homotetrameric structure of TTR with **4** bound (PDB 2ROX).^{5c} The dimers are shown as dimer subunit A and dimer subunit B and each monomer subunit of the tetramer (labeled 1, 2, 3 and 4) is shown with its secondary structural elements and colored differently. The monomer components of dimer A are shown in orange (monomer 1) and cyan (monomer 2). The monomer components of dimer B are shown in violet (monomer 3) and blue (monomer 4). The dimers are associated back-to-back creating a large channel through the center of the tetramer that presents two C_2 symmetrical T4-binding sites. The binding of **4** in both T4 binding pockets of TTR is shown in ball and stick format (grey). (B) Ribbon diagram of holo-RBP4 (PDB 1RBP).⁷ RBP4 is shown as yellow and **1** is depicted in ball and stick format (grey) bound within the RBP4 hydrophobic β -barrel binding cavity. (C) The holo-RBP4-TTR tertiary complex (PDB 1QAB)¹⁰ colored by chain and viewed from the front. The TTR tetramer is located at the

1
2
3 center of the complex with two holo-RBP4 molecules docked at a twofold axis of symmetry that
4 is orthogonal to the T4 binding sites. Compound **1** is depicted in ball and stick format (black). (D)
5
6 The holo-RBP4-TTR tertiary complex (PDB 1QAB)¹⁰ colored by chain and viewed from the side.
7
8 Compound **1** is depicted in ball and stick format (black).
9
10
11
12
13

14 It was hypothesized that reducing systemic levels of circulating RBP4 and **1** via
15 selective antagonists could impede the biosynthesis of retinal bisretinoids and prevent
16 geographic lesion formation and growth associated with late-stage dry (atrophic) age-
17 related macular degeneration (AMD) and Stargardt disease.^{11, 12} All-*trans*-retinol-
18 competitive antagonists of RBP4 prohibit holo-RBP4-TTR complexation, thereby inducing
19 reductions with circulating RBP4 and **1** levels via rapid renal clearance. A diminished influx
20 of **1** to the RPE results in a reduction of cytotoxic bisretinoid accumulation in the retina,
21 which is believed to underlie parts of the pathophysiology of dry AMD and Stargardt
22 disease.^{11a, 13-16} The approach is supported by proof-of-concept data obtained for
23 fenretinide (**5**) (Figure 4), which was studied preclinically with *Abca4*^{-/-} transgenic mice
24 and in a Phase II proof-of-concept study with dry AMD patients.¹⁷ Thorough analysis of
25 the human data with **5** indicated that a reduction in serum RBP4 levels below the 1 μ M
26 threshold was required to significantly hinder expansion of demarcated atrophic lesions.
27
28 The non-retinoid RBP4 antagonist A1120⁸ (**6**) was reported disrupt holo-RBP4-TTR
29 complexation *in vitro* and reduce rodent RBP4 plasma levels by >70% and reduce retinal
30 bisretinoid accumulation in *Abca4*^{-/-} mice.¹³ Our selective and orally bioavailable non-
31 retinoid RBP4 antagonists **7**¹⁸ and BPN-14136¹⁹ (**8**) displayed favorable pharmacokinetic
32 (PK) profiles and induced dose-dependent circulating RBP4 reductions in rodents.
33
34
35
36
37
38
39
40
41
42
43
44
45
46
47
48
49
50
51
52
53
54
55
56
57
58
59
60

1
2
3 Compound **8** also robustly lowered serum RBP4 levels and exhibited excellent
4 pharmacokinetic-pharmacodynamic (PK-PD) correlations in non-human primates upon
5 oral administration.²⁰ Lastly, **8** inhibited production of fluorophore bisretinoid N-
6 retinylidene-N-retinylethanolamine (A2E) while restoring homeostatic complement
7 system protein expression in the *Abca4*^{-/-} mouse retina without altering visual cycle
8 kinetics.¹⁴
9
10
11
12
13
14
15
16
17

18 In addition to transporting **1** to targeted tissues, RBP4 has also been identified as an
19 adipokine potentially involved in metabolic disorders including type 2 diabetes,²¹
20 obesity,²² insulin resistance,²³ cardiovascular disease,²⁴ and hepatic steatosis.²⁵ Thus, the
21 pharmacological reduction of circulating RBP4 serum levels may also hold promise for the
22 treatment of a myriad of metabolic diseases. Indeed, we have recently reported that our
23 antagonist **10** significantly lowered serum RBP4 levels in rodents (>80%), reduced the
24 concentration of circulating RBP4 produced in the adipose tissue, and ameliorated
25 hepatic steatosis in transgenic adi-hRBP4 mice. These data provide evidence that RBP4
26 antagonists may hold therapeutic promise for treating non-alcoholic fatty liver disease
27 (NAFLD).²⁶
28
29
30
31
32
33
34
35
36
37
38
39
40
41
42
43
44
45
46
47
48
49
50
51
52
53
54
55
56
57
58
59
60

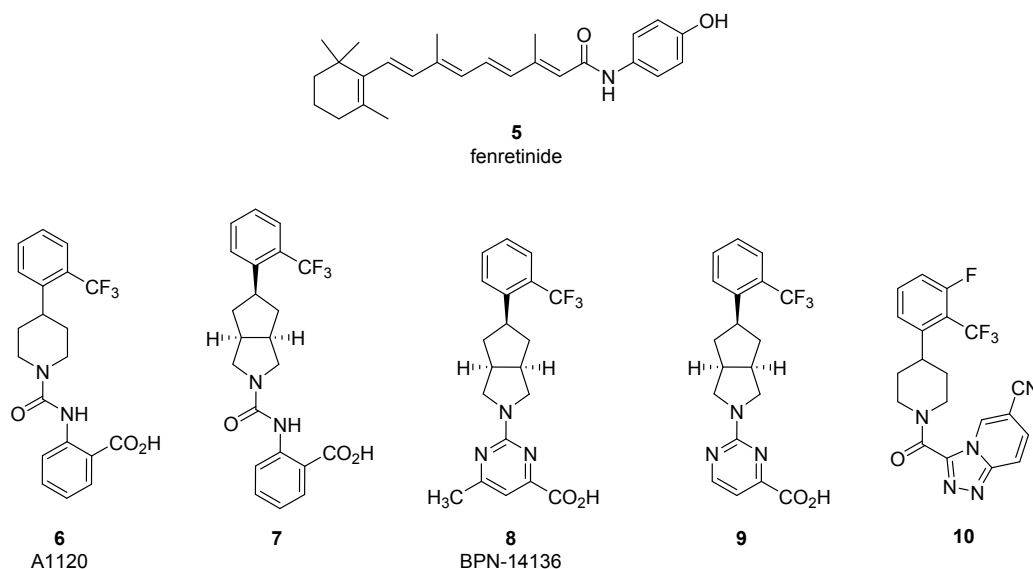


Figure 4. Examples of previously reported RBP4 antagonists that include fenretinide (**5**), A1120 (**6**), and previously identified RBP4 antagonists **7**, BPN-14136 (**8**), **9**, and **10**.

The formation of amyloid aggregates derived from either mutant or wild-type underlies TTR amyloidosis (ATTR) diseases such as senile systemic amyloidosis (SSA), peripheral polyneuropathy (ATTR-PN), and cardiomyopathy (ATTR-CM).^{6, 27} As was noted above, the breakage of the dimer-dimer interface in TTR tetramers constitutes the first step in the TTR tetramer dissociation process that leads to TTR misfolding. Approximately 50% of serum TTR is associated with RBP4 and it is suggested that tertiary holo-RBP4-TTR complexation serves to stabilize this fraction of serum TTR tetramers and prevent them from dissociation and misfolding.^{28, 29} Based on the *in vitro* observation that RBP4-TTR interaction is capable of conferring an additional stabilization to tetrameric TTR,^{28, 29} it seems plausible that the release of TTR tetramers from RBP4-TTR-retinol complexes

1
2
3 induced by selective RBP4 antagonists may lead to tetramer destabilization and its
4
5 enhanced dissociation to dimer subunits. The resulting dimers may then further
6
7 dissociate into monomers that can misfold, aggregate, oligomerize, and eventually form
8
9 insoluble TTR amyloid fibrils.^{28, 29} While selective RBP4 antagonists can be a safe and
10
11 effective therapy for the majority of dry AMD patients, this class of compounds may
12
13 potentially be counter-indicated for a fraction of AMD patients who may be prone to
14
15 developing ATTR. In addition to individuals with rare genetic forms of ATTR caused by pro-
16
17 amyloidogenic TTR mutations, the use of selective RBP4 antagonists may not be optimal
18
19 in patients with SSA, a late-onset non-genetic disease associated with misfolding and
20
21 aggregation of wild-type TTR. SSA affects approximately 25% of patients over the age of
22
23 80³⁰ and based on the high population frequency of this disease and dry AMD, significant
24
25 comorbidity between the two conditions is expected. In addition, the use of selective
26
27 RBP4 antagonists may not be optimal in older African-American patients with dry AMD
28
29 who have the increased chance of carrying a relatively high frequency pro-amyloidogenic
30
31 V122I mutation in the TTR gene.³¹ It is undesirable for an effective chronic treatment for
32
33 one of the two conditions to be counter-indicated for the use in patients with another
34
35 one, and developing an optimal therapy for dry AMD that can be safely used in patients
36
37 with ATTR comorbidities is an important objective.
38
39
40
41
42
43
44
45
46

47 ATTR pathophysiology begins with the sequential dissociation of TTR tetramers into
48
49 pro-amyloidogenic monomers with tetramer dissociation into dimer subunits as the rate-
50
51 limiting step in the process.⁶ While thyroxine binding was reported to stabilize TTR
52
53 tetramers,³² the majority of TTR in circulation (up to 90%), including TTR in a complex with
54
55
56
57
58
59
60

1
2
3 holo-RBP4, is not bound to its natural ligand.²⁸ Current therapeutic approaches to treat
4
5 ATTR-CM include small molecule kinetic stabilizers of TTR tetramers that bind at the T4
6
7 binding sites and increase the energy barrier of tetramer dissociation.³³ Two orally
8
9 bioavailable kinetic stabilizers clinically investigated to date include FDA-approved
10
11 tafamidis (**11**) (Figure 5),³⁴ and AG10 (**12**).³⁵ TTR stabilizer **11** is currently approved to treat
12
13 familial amyloid polyneuropathy and ATTR-CM patients, and **12** has demonstrated near-
14
15 complete stabilization of TTR in ATTR-CM patients with symptomatic, chronic heart failure
16
17 in Phase II clinical trials (a Phase III trial is ongoing).³⁶ In addition, the repurposed FDA-
18
19 approved non-steroidal anti-inflammatory drug diflunisal (**13**)³⁷ and catechol-O-methyl
20
21 transferase inhibitor tolcapone (**14**)³⁸ are examples of additional small molecules that also
22
23 exhibit TTR tetramer kinetic stabilization activity and have been investigated for clinical
24
25 efficacy against ATTR-PN. Lastly, recently reported saturation transfer difference (STD)-
26
27 NMR data by Gemino and coworkers show that β -amyloid (A β) peptides bind at the RBP4
28
29 binding pockets of TTR and that stabilization of the TTR tetramer by iododiflunisal
30
31 (structure not shown) may be facilitating the TTR-A β interaction.³⁹ These STD-NMR
32
33 binding experiments may shed some light on the mechanism by which iododiflunisal
34
35 produces its ameliorating effects in animal models for Alzheimer's disease.⁴⁰
36
37
38
39
40
41
42
43
44
45
46
47
48
49
50
51
52
53
54
55
56
57
58
59
60

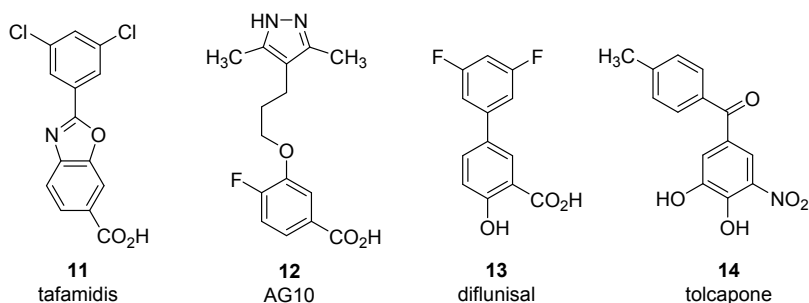


Figure 5. Examples of reported small molecule TTR tetramer kinetic stabilizers that include tafamidis (**11**), AG10 (**12**), diflunisal (**13**), and tolcapone (**14**).

Our goal was to develop a treatment for dry AMD and ATTR comorbidities based on bispecific ligands that can serve as both an RBP4 antagonist and TTR tetramer kinetic stabilizer. Such drugs are predicted to provide therapeutic benefits associated with reducing circulating RBP4 levels while simultaneously stabilizing unliganded TTR tetramers released from the holo-RBP4-TTR complex, thus circumventing potential risks of amyloid fibril formation as schematized in Figure 6. Furthermore, a polypharmacological approach consisting of single bispecific molecule capable of exhibiting dual activity for both targets may present advantages over the co-administration of single agent for each target. Such advantages include improving patient compliance, minimizing complex PK, and avoiding potential drug-drug interactions that could arise from multiple drug intake.⁴¹

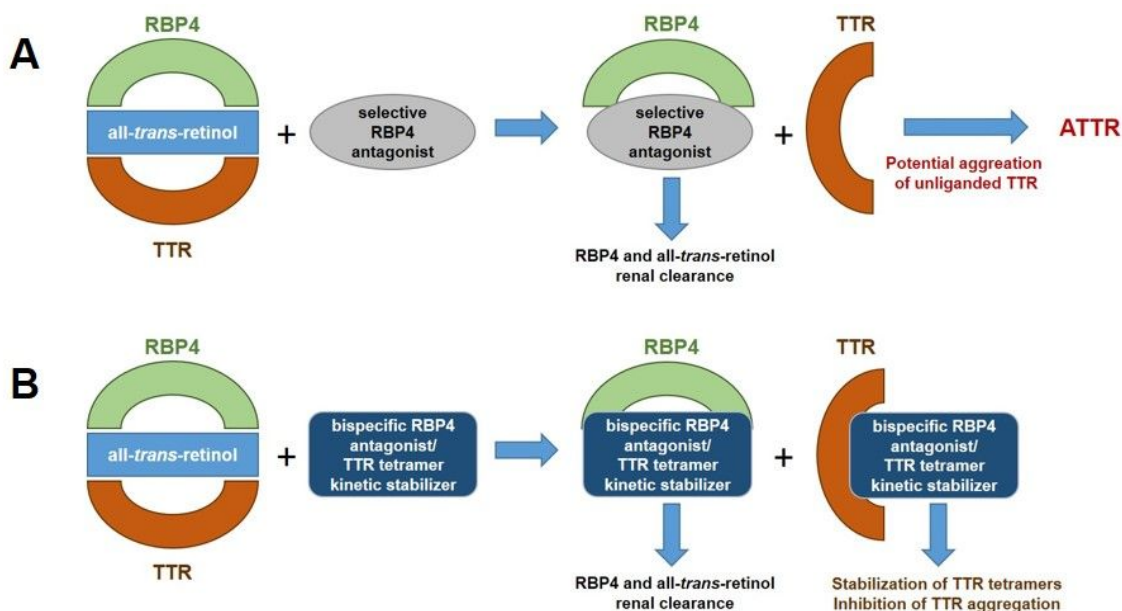


Figure 6. Bispecific RBP4 antagonists and TTR tetramer kinetic stabilizers for treating RBP4 indications with potential ATTR comorbidities. (A) Schematic illustrating the use of selective RBP4 antagonists for disrupting the holo-RBP4-TTR protein-protein interaction and inducing serum reduction of **1** and RBP4. The concomitant release of unliganded TTR may induce its aggregation, potentially contributing to ATTR in predisposed patients. (B) Bispecific ligands with dual RBP4 antagonist and TTR tetramer kinetic stabilization activity may induce reductions in circulating levels of RBP4 and **1** while also preventing potential TTR aggregation and insoluble amyloid fibril formation.

In our work reported herein, we initiated a structure-based drug design effort to identify a novel class of non-retinoid bispecific compounds capable of exhibiting dual RBP4 antagonist and TTR tetramer kinetic stabilization activity. The primary desirable attributes for the newly designed analogues were: 1) to contain a non-retinoid framework so as to avoid potential off-target activity at retinoic acid receptors, 2) to effectively compete with **1** and antagonize the all-*trans*-retinol-dependent RBP4-TTR interaction, 3)

1
2
3 to induce robust *in vivo* serum RBP4 reduction by >70%, and 4) to bind to unliganded TTR
4
5 tetramers and effectively prevent TTR dissociation and aggregation as judged in a gel-
6
7 based wild-type TTR aggregation assay. It is for these reasons in our program that
8
9 compounds were measured for binding potency to non-TTR associated RBP4 via
10
11 competition with **1** (scintillation proximity assay (SPA) to generate dose-response IC₅₀
12
13 values in the presence of fixed concentrations of [³H]-all-*trans*-retinol), compound
14
15 binding potency to unliganded TTR tetramers (fluorescence polarization assay (FP) to
16
17 generate dose-response IC₅₀ values in the presences of a fixed concentration of a
18
19 fluorescence probe that binds at TTR tetramer T4 sites), and compound functional
20
21 antagonist potency for disruption of holo-RBP4-TTR complex formation (homogenous
22
23 time-resolved fluorescence assay (HTRF) to generate dose-response IC₅₀ values in the
24
25 presence of fixed concentrations of all-*trans*-retinol).
26
27
28
29
30
31
32
33
34

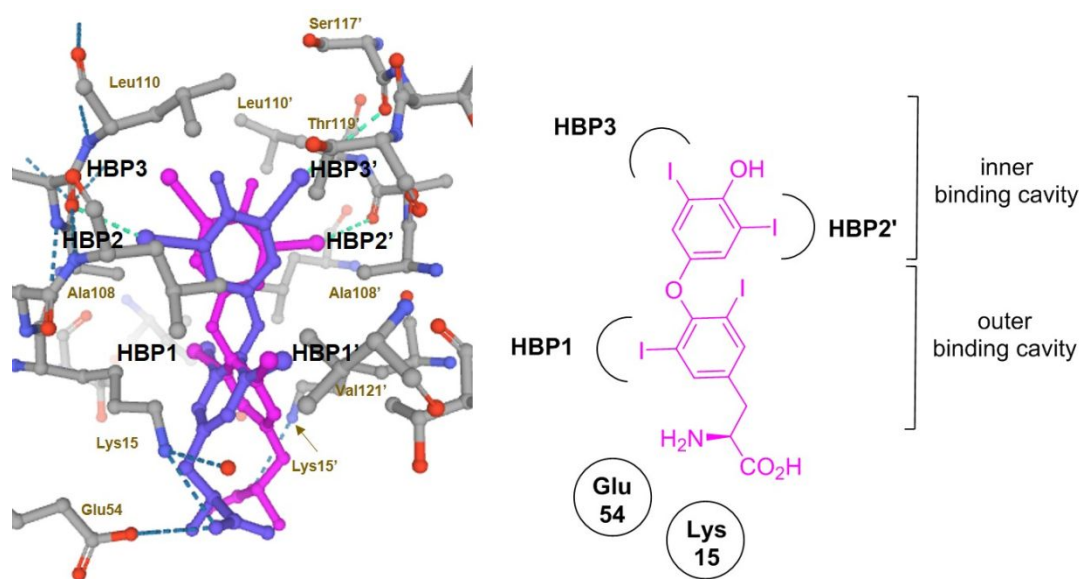
35 DESIGN OF BISPECIFIC ANALOGUES

36
37 We discovered that our previously disclosed series of RBP4 antagonists could serve as
38
39 suitable benchmark scaffolds for our novel bispecific analogue design efforts. RBP4
40
41 antagonists **7**¹⁸ (RBP4 SPA IC₅₀ = 72.7 nM, RBP4-TTR HTRF IC₅₀ = 0.294 μM) and **9**¹⁹ (RBP4
42
43 SPA IC₅₀ = 20.8 ± 0.5 nM, RBP4-TTR HTRF IC₅₀ = 79.7 nM) were found to exhibit significant
44
45 TTR tetramer binding potency (**7** TTR FP IC₅₀ = 2.4 μM; **9** TTR FP IC₅₀ = 2.5 μM). These data,
46
47 in addition to the exemplary PK-PD properties^{19, 20} and *in vivo* *Abca4*^{-/-} transgenic mouse
48
49 model efficacy¹⁴ exhibited by standout analogue **8** (RBP4 SPA IC₅₀ = 12.8 ± 0.4 nM, RBP4-
50
51 TTR HTRF IC₅₀ = 43.6 ± 10.5 nM), led us to focus our initial bispecific drug design efforts
52
53
54
55
56
57
58
59
60

1
2
3 starting from their common [3.3.0]-bicyclic core scaffold. Thus, our optimization strategy
4 was to identify novel compounds that presented the following attribute: 1) retaining or
5 improving *in vitro* activity observed for **7**, **8**, and **9**, 2) exhibiting TTR binding potency that
6 could provide adequate TTR tetramer stabilization and prevent aggregation at
7 therapeutic concentrations required for >70% serum RBP4 reduction, 3) maintaining the
8 largely favorable ADME profile observed for **7**, **8**, and **9**, and 4) maintaining the favorable
9 PK-PD properties of **7** and **8**. A potential drawback for **8** was its ancillary agonist activity
10 at the nuclear peroxisome proliferator-activated receptor-gamma (PPAR γ) (PPAR γ IC₅₀ =
11 3.6 μ M in the agonist-induced corepressor NCoR release assay). PPAR γ plays a critical role
12 in regulating energy homeostasis, metabolism, and inflammation and we sought to avoid
13 such off-target activity due to potential side effects often associated with PPAR γ agonists,
14 which include risk for fluid retention, weight gain, bone loss, and congestive heart
15 failure.⁴²

16
17
18
19
20
21
22
23
24
25
26
27
28
29
30
31
32
33
34
35 Our structure-based optimization approach sought to exploit potential similarities
36 presented within the binding pockets of both proteins. X-ray crystallographic data of **4**
37 bound to TTR (PDB 2ROX)^{5c} shows that the T4 binding sites are segregated by an inner
38 and outer binding cavity. The two-fold axis symmetry of the T4 binding cavity presents six
39 halogen binding pockets designated as HBP1, HBP1', HBP2, HBP2', HBP3 and HBP3'
40 (Figure 7).^{5c} The HBPs are defined according to the relative positions of the iodine atoms
41 of **4** that occupy them. The inner T4 binding pockets contain HBP3 and HBP3' and are
42 located between the Ser117, Leu110, Thr119, and Ala108 residues of both subunits. The
43 innermost Ser117 hydroxyl groups may either participate in bridging hydrogen bond
44
45
46
47
48
49
50
51
52
53
54
55
56
57
58
59
60

1
2
3 interactions with a resident structural water molecule or they may mediate hydrogen
4
5 bond interactions with bound TTR tetramer kinetic stabilizers, such as **12**.³⁵ The HBP2 and
6
7 HBP2' pockets are located between the inner and outer binding cavities and are highly
8
9 lipophilic as they contain Leu17, Ala108, Ala109 and Leu110 residues. Lastly, the HBP1
10
11 and HBP1' pockets reside near the outer binding cavity and feature residues Lys15, Glu54,
12
13 Leu17, Thr106, and Val121 of both subunits. The binding of **4** typically involves a forward
14
15 binding mode, which projects the bis-iodo phenol "head group" deep within the inner
16
17 cavity where the iodine atoms occupy HBP2 and HBP3 pockets. The linker phenyl ring
18
19 resides within the hydrophobic channel bridging the inner and outer cavities, with one of
20
21 its iodine atoms occupying a HBP1/HBP1' binding pocket. Lastly, the amino acid "bottom
22
23 group" motif of **4** resides near the periphery of the binding site opening and forms salt-
24
25 bridge interactions with ionizable residues Lys15/Lys15' and Glu54/Glu54'.^{5c}
26
27
28
29
30
31
32
33
34



1
2
3 **Figure 7.** The halogen binding pockets (HBPs) of the T4 binding site with **4** bound (PDB 2ROX).^{5c}
4
5 Compound **4** is shown in ball and stick format and both symmetry-related binding modes related
6
7 by a two-fold axis are presented (**4** is shown in violet and magenta). The iodine atoms of **4** occupy
8
9 the HBP1, HBP2, and HBP3 pockets while the amino acid appendage engages in ionic salt-bridge
10
11 interactions Lys15 and Glu54 near the opening of the binding site. Contacting amino acids are
12
13 designated and depicted in ball and stick form. Dashed blue lines represent H-bonds and dashed
14
15 cyan lines represent halogen bonds.
16
17
18
19
20

21
22 A common pharmacophore among small molecule RBP4 antagonists and TTR
23
24 tetramer kinetic stabilizers is a “bottom group” carboxylic acid appendage connected
25
26 through a core linker scaffold to an aromatic “head group” moiety. The X-ray
27
28 crystallographic data PDB 3FMZ⁸ provides insight as to how **6** and related analogues **7** and
29
30 **8** may bind to RBP4 (Figure 8, A). The binding pose of **6** involves the piperidine core linker
31
32 residing within the central cavity while the lipophilic phenyl ring bearing a trifluoromethyl
33
34 group extends into the inner lipophilic cavity in an orthogonal manner. The ionizable
35
36 anthranilic acid forms electrostatic binding interactions with Arg121 and a pair of H-bonds
37
38 with neighboring residues Tyr90 and Gln98. The structural data for **4** bound to the T4
39
40 binding site (PDB 2ROX)^{5c} reveals how both molecular targets present binding pockets of
41
42 comparable geometries and van der Waals surfaces areas of hydrophobicity and polarity.
43
44 Ligand **4** binds in the aforementioned forward binding mode with its lipophilic phenolic
45
46 head group projecting into the inner binding cavity and oriented orthogonally (Figure 8,
47
48 C). The linker phenyl ring of **4** resides within the hydrophobic channel bridging the inner
49
50 and outer cavities, and similar to RBP4 antagonist **6**, the ionizable amino acid appendage
51
52
53
54
55
56
57
58
59
60

resides near the opening of its respective binding site where it also engages in salt-bridge interactions.

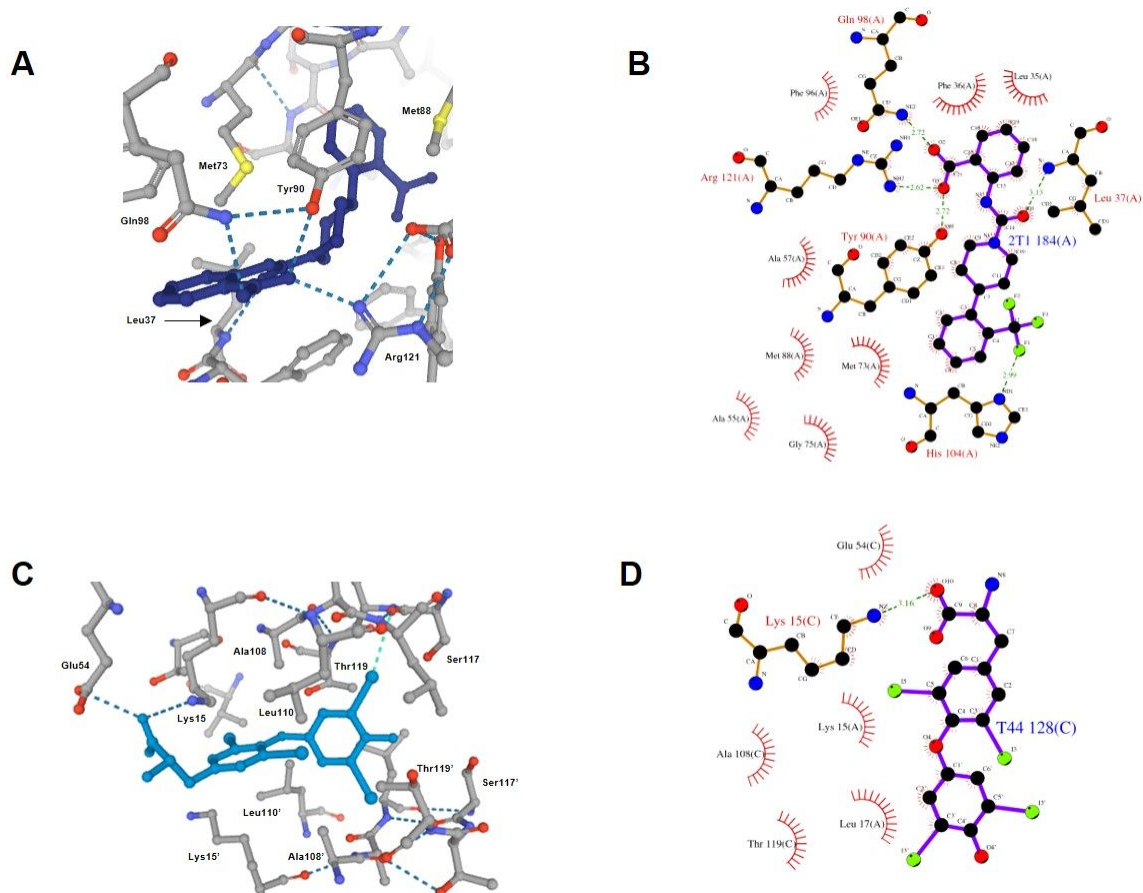


Figure 8. X-ray crystallographic data showing similar binding poses for **6** bound to RBP4 (PDB 3FMZ)⁸ and **4** bound to the T4 binding site (PDB 2ROX).^{5c} (A) RBP4 antagonist **6** is shown in ball and stick format (dark blue) with polar binding interactions (e.g., H-bonds and salt bridges) shown as blue dotted lines. (B) Ligand interaction diagram of **6** with RBP4 indicating key H-bonds and salt-bridge interactions. (C) TTR ligand **4** is shown in ball and stick format (light blue) with the phenolic aryl appendage projecting into the inner cavity in an orthogonal manner. The iodine atoms of the head group occupy the HBP2 and HBP3 pockets while the iodine atoms of the central

1
2
3 core phenyl ring occupy the HBP1 pockets. The amino acid appendage engages in ionic salt-bridge
4 interactions Lys15 and Glu54 near the opening of the binding site. Polar binding interactions (e.g.,
5 H-bonds and salt bridges) shown as dark blue dotted lines, halogen bonds shown as light-blue
6 dotted lines. (D) Ligand interaction diagram of **4** with TTR indicating the key salt-bridge
7 interaction.
8
9
10
11
12
13
14
15
16

17 We planned to develop novel bispecific ligands that retain the key pharmacophoric
18 elements described for ligands of both targets. Importantly, critical salt-bridge
19 interactions with the basic Arg121 and Lys15 residues of RBP4 and TTR, respectively, are
20 mediated by an aromatic carboxylic acid for many known RBP4 antagonists and TTR
21 ligands. Hence, this motif was not altered in our novel bispecific analogue design. From
22 an examination of PDB 3FMZ⁸ and PDB 2ROX^{5c}, we speculated that varying the length
23 and conformational flexibility in the [3.3.0]-bicyclic core linker of **8** might maintain RBP4
24 antagonist potency while potentially enhancing TTR activity. Figure 9 highlights how we
25 executed our sequential structure-activity relationship (SAR) plan by examining three
26 critical regions of our novel scaffolds.
27
28
29
30
31
32
33
34
35
36
37
38
39
40

41 We initially executed a scaffold hopping campaign that explored how altering the
42 shape and flexibility of the linker core of **8** (A-region) would affect potency at both targets.
43 We hypothesized that subtle changes to this region of the molecule may better position
44 an appropriately substituted aromatic head group to fully occupy both the RBP4 β -ionone
45 pocket and inner T4 binding cavity. We synthesized initial illustrative examples of **8**
46 containing alternative linker scaffolds that retained the *ortho*-trifluoromethylphenyl head
47 group and the 6-methylpyrimidine-4-carboxylic acid bottom group moieties. We chose to
48
49
50
51
52
53
54
55
56
57
58
59
60

1
2
3 maintain the *ortho*-trifluoromethylphenyl head group as it is an established head group
4
5 motif for optimal RBP4 binding affinity and it has served as a suitable head group for
6
7 previously disclosed oxime⁴³ and *N*-phenyl phenoxazine⁴⁴ TTR amyloid fibril inhibitors
8
9 (structures not shown). We postulated that the 6-methylpyrimidine-4-carboxylic acid
10
11 bottom group provides functionality for the aforementioned key ionic interactions while
12
13 also providing additional structural components that could also engage in favorable
14
15 binding interactions. For example, we hypothesized that the pyrimidine nitrogen *para* to
16
17 the carboxylic acid may be in a similar position as the urea carbonyl of **6** (PDB 3FMZ),
18
19 which hydrogen bonds with backbone Leu37.⁸ Furthermore, the nitrogen *ortho* to the
20
21 carboxylic acid group could also be within a suitable proximity to H-bond with
22
23 Glu98/Tyr80 of RBP4 (PDB 3FMZ)⁸ and/or Glu54 of TTR (PDB 2ROX).^{5c} Analysis of PDB
24
25 2ROX suggests that the pyrimidine ring 6-position, which previously provided informative
26
27 RBP4 SAR,¹⁹ could also potentially provide a handle to further probe the HBP1/HBP1'
28
29 pocket within the T4 binding site.^{5c}
30
31
32
33
34
35
36
37
38
39

40 The various scaffold hopping core linkers explored presented similar distances
41
42 between the aromatic head group and carboxylic acid bottom group of **4** and bicyclic
43
44 analogues **6**, **7**, and **8**. Once a novel A-region core linker with suitable activity at both
45
46 targets was identified, it was then used to explore the SAR of alternatively substituted
47
48 aromatic head groups (B-region). Lastly, we subsequently studied carboxylic acid bottom
49
50 group (C-region) SAR with an identified optimal A- and B-region scaffold. This C-region
51
52 SAR sample set included analogues featuring picolinic and nicotinic acids, positional
53
54
55
56
57
58
59
60

variation of the carboxylic acid, carboxylic acid isosteres, and carboxamides that were prepared and analyzed for potency effects at both targets.

Sequential SAR Approach Toward Novel Bispecific RBP4 Antagonists - TTR Tetramer Kinetic Stabilizers

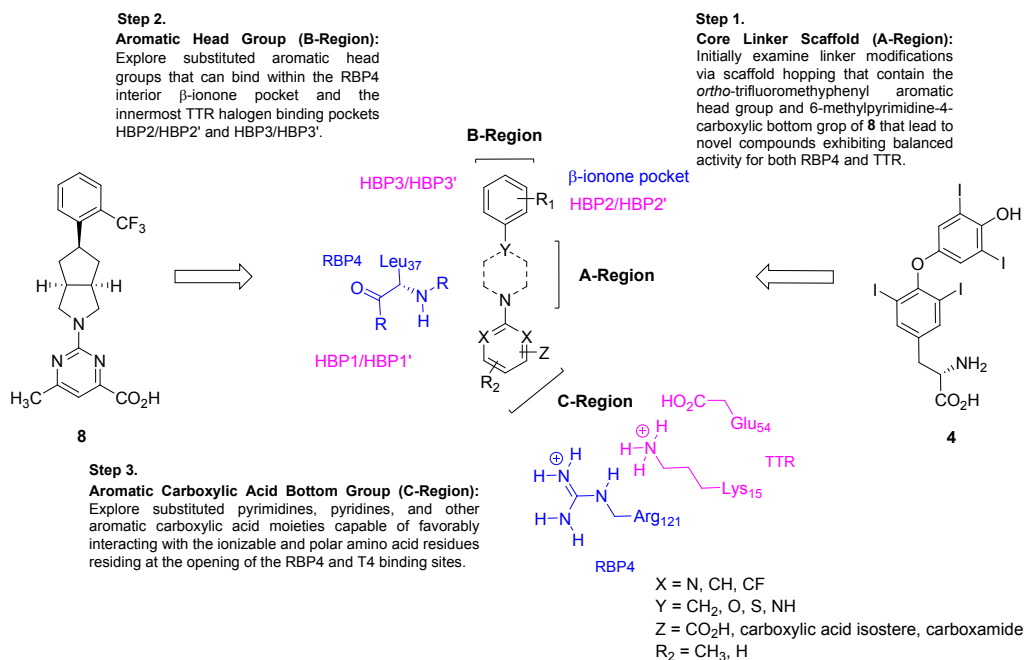
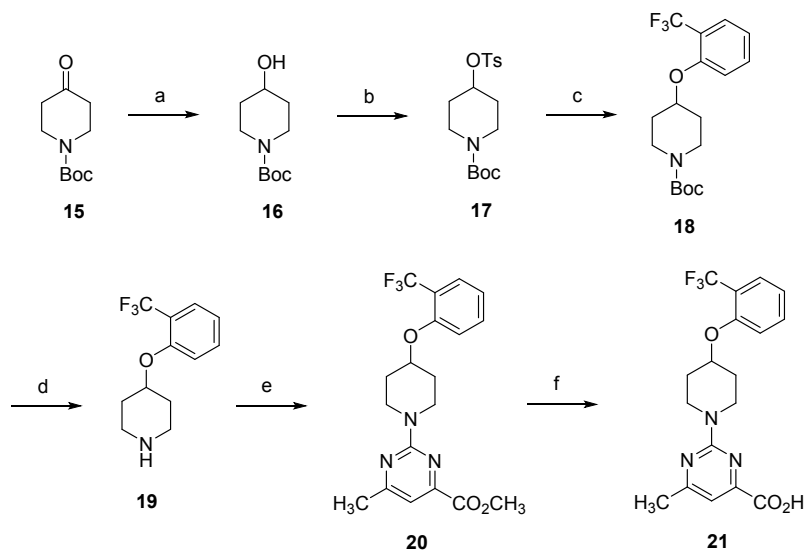


Figure 9. Medicinal chemistry strategy to identify bispecific RBP4 antagonists – TTR tetramer kinetic stabilizers. Novel analogues were rationally designed from benchmark RBP4 antagonist **8** and endogenous TTR ligand **4**. The initial SAR campaign involved scaffold hopping of the core linker (A-region) while maintaining the aromatic head group and aromatic carboxylic acid bottom group appendages of **8**. A subsequent SAR campaign of the RBP4 β -ionone and T4 inner cavities involved exploration of the aromatic head group (B-region) with a newly identified A-region core linker. Lastly, with an optimal A-region and B-region scaffold identified, aromatic carboxylic acid analogues (C-region) were then investigated. These analogues were designed to potentially engage in critical RBP4 H-bonding interactions with Arg121, Gln98 (not shown), and backbone

1
2
3 Leu37 (all RBP4 interactions shown in blue) while also engaging in key TTR binding interactions
4
5 with Lys15, Glu54 and within the HBP1/HBP1' (all TTR interactions shown in magenta).
6
7
8
9

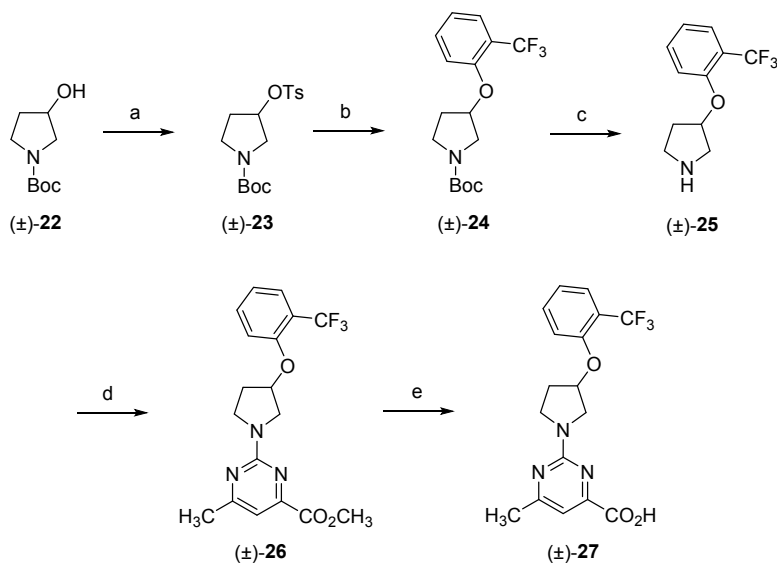
10 CHEMISTRY

11
12
13 The preparation of alkoxy piperidine analogue **21** shown in Scheme 1 begins with a
14
15 sodium borohydride (NaBH₄) reduction of *tert*-butyl 4-oxopiperidine-1-carboxylate (**15**)
16
17 to give alcohol **16**. Sulfonylation of **16** followed by bimolecular nucleophilic (S_N2)
18
19 displacement of the corresponding sulfonate ester **17** with 2-(trifluoromethyl)phenol led
20
21 to formation of phenoxyether **18**. Treatment of **18** with trifluoroacetic acid (TFA) provided
22
23 Boc-protected amine **19**, which when reacted with methyl 2-chloro-6-
24
25 methylpyrimidine-4-carboxylate, afforded pyrimidine methyl ester **20**. Hydrolysis of **20**
26
27 with lithium hydroxide (LiOH) followed by subsequent acidification of the lithium
28
29 carboxylate salt with 2 N aqueous hydrochloric acid (HCl) provided desired carboxylic acid
30
31
32
33
34
35 **21**.
36
37
38
39
40
41
42
43
44
45
46
47
48
49
50
51
52
53
54
55
56
57
58
59
60

Scheme 1^a

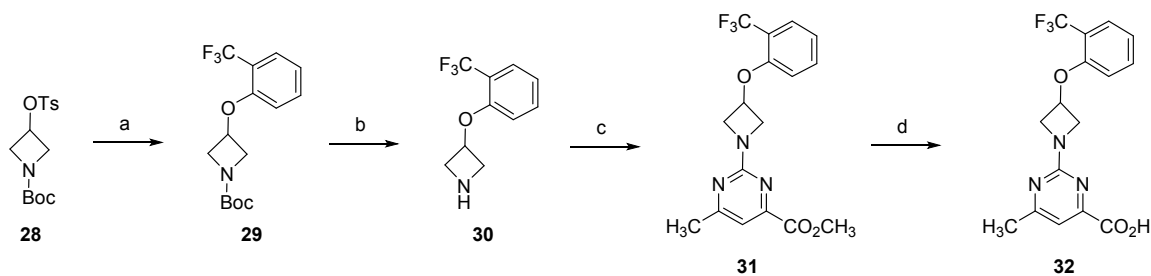
^aReagents and conditions: (a) NaBH₄, CH₃OH, 0 °C to rt, 8 h; (b) TsCl, DMAP, Et₃N, CH₂Cl₂, 0 °C to rt, 16 h; (c) 2-(trifluoromethyl)phenol, Cs₂CO₃, DMF, 80 °C, 16 h; (d) TFA, CH₂Cl₂, 0 °C to rt, 8 h; (e) methyl 2-chloro-6-methylpyrimidine-4-carboxylate, *i*-Pr₂NEt, THF, reflux, 16 h; (f) (i) LiOH, CH₃OH, THF, H₂O, rt, 16 h; (ii) 2 N aqueous HCl.

Scheme 2 highlights the preparation of racemic alkoxyproline analogue (\pm)-**27**. *Tert*-butyl 3-(tosyloxy)pyrrolidine-1-carboxylate ((\pm)-**23**) was generated via tosylation of commercially available racemic *tert*-butyl 3-hydroxypyrrrolidine-1-carboxylate ((\pm)-**22**). Treatment of sulfonate ester (\pm)-**23** with 2-(trifluoromethyl)phenol provided ether (\pm)-**24**, which was deprotected with TFA affording amine (\pm)-**25**. Conversion of (\pm)-**25** to the desired carboxylic acid (\pm)-**27** followed the same two-step process outlined in Scheme 1.

Scheme 2^a

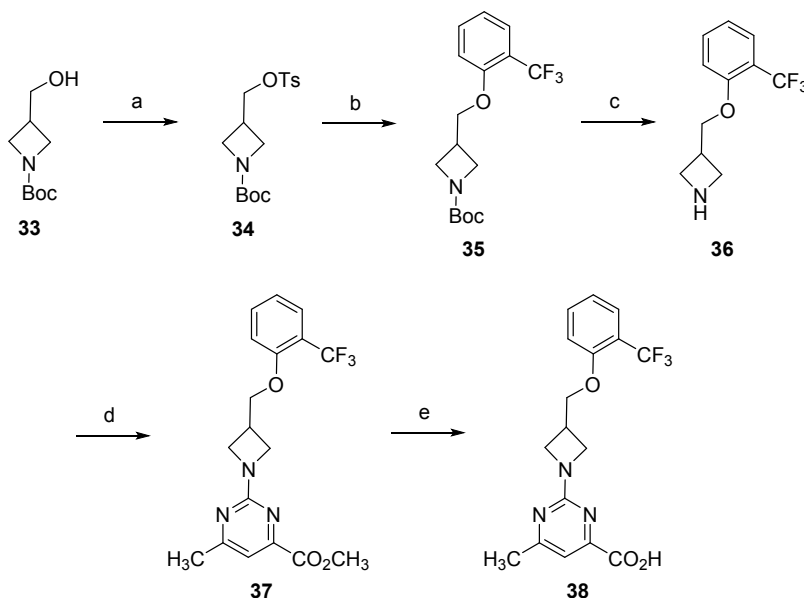
^aReagents and conditions: (a) TsCl, DMAP, Et₃N, CH₂Cl₂, 0 °C to rt, 16 h; (b) 2-(trifluoromethyl)phenol, Cs₂CO₃, DMF, 80 °C, 16 h; (c) TFA, CH₂Cl₂, 0 °C to rt, 8 h; (d) methyl 2-chloro-6-methylpyrimidine-4-carboxylate, *i*-Pr₂NEt, THF, reflux, 16 h; (e) (i) LiOH, CH₃OH, THF, H₂O, rt, 16 h; (ii) 2 N aqueous HCl.

O-alkylation of tosylated azetidine **28** with 2-(trifluoromethyl)phenol afforded phenyl ether **29** (Scheme 3). TFA-mediated Boc-deprotection of **29** followed by treatment with methyl 2-chloro-6-methylpyrimidine-4-carboxylate yielded pyrimidine **31**, which was hydrolyzed with LiOH to provide acid **32**.

Scheme 3^a

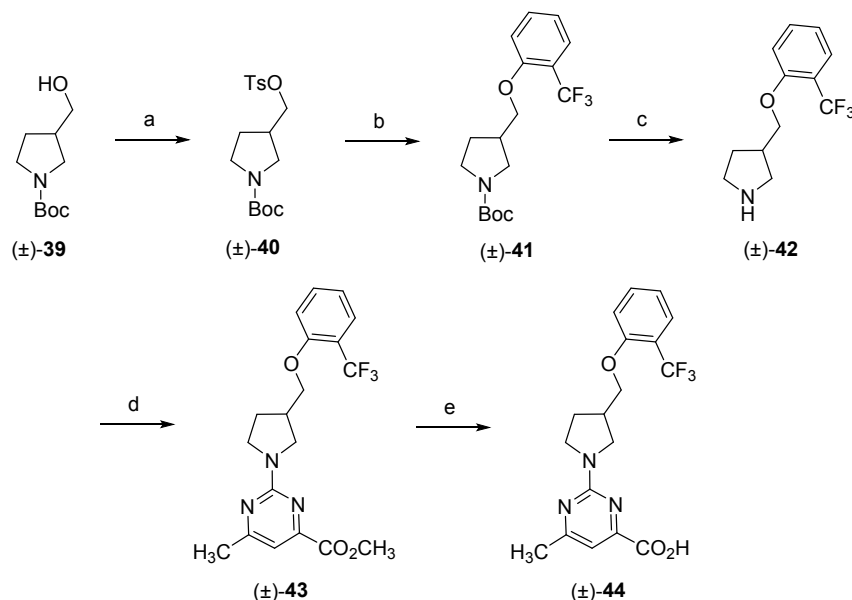
^aReagents and conditions: (a) 2-(trifluoromethyl)phenol, Cs₂CO₃, DMF, 80 °C, 16 h; (b) TFA, CH₂Cl₂, 0 °C to rt, 8 h; (c) methyl 2-chloro-6-methylpyrimidine-4-carboxylate, *i*-Pr₂NEt, THF, reflux, 16 h; (d) (i) LiOH, CH₃OH, THF, H₂O, rt, 16 h; (ii) 2 N aqueous HCl.

Construction of (hydroxymethyl)azetidine analogue **38** followed the route depicted in Scheme 4. Tosylation of alcohol **33** gave sulfonate ester **34**, which was subsequently treated with 2-(trifluoromethyl)phenol to provide phenyl ether **35**. TFA-mediated deprotection of **35** followed by reaction with methyl 2-chloro-6-methylpyrimidine-4-carboxylate provided analogue **37**. LiOH promoted hydrolysis of methyl ester **37** and subsequent acidification with 2 N aqueous HCl gave desired carboxylic acid **38**.

Scheme 4^a

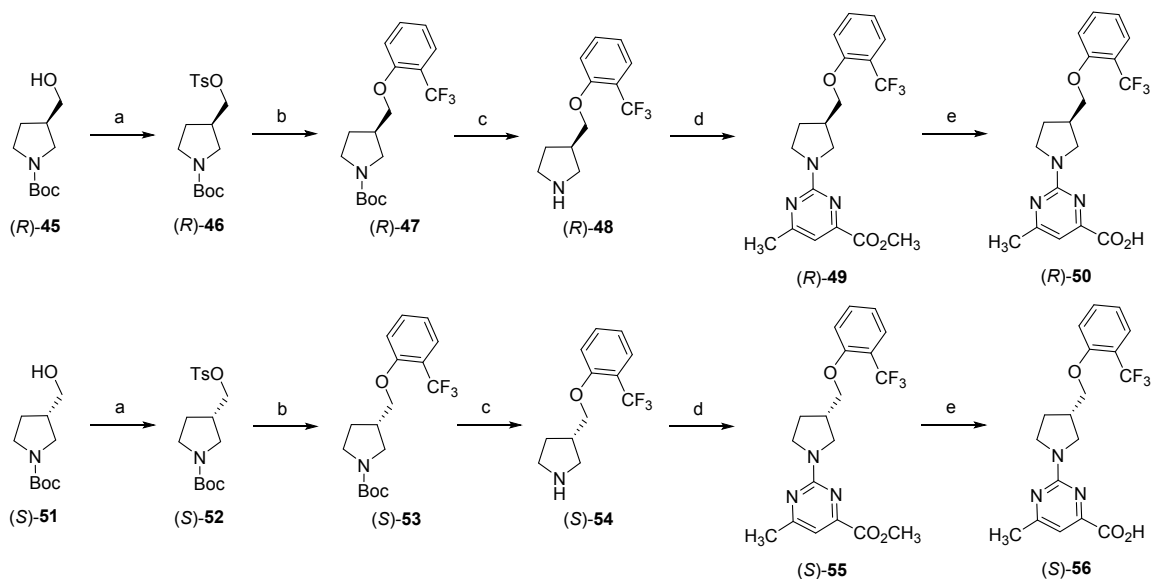
^aReagents and conditions: (a) TsCl, DMAP, Et₃N, CH₂Cl₂, 0 °C to rt, 16 h; (b) 2-(trifluoromethyl)phenol, Cs₂CO₃, DMF, 80 °C, 16 h; (c) TFA, CH₂Cl₂, 0 °C to rt, 8 h; (d) methyl 2-chloro-6-methylpyrimidine-4-carboxylate, *i*-Pr₂NEt, THF, reflux, 16 h; (e) (i) LiOH, CH₃OH, THF, H₂O, rt, 16 h; (ii) 2 N aqueous HCl.

Racemic 3-(hydroxymethyl)pyrrolidine (\pm)-**44** was achieved via the route shown in Scheme 5. Sulfonate ester formation of racemic alcohol (\pm)-**39** followed by S_N2 displacement with 2-(trifluoromethyl)phenol in the presence of cesium carbonate (Cs₂CO₃) gave O-alkylated product (\pm)-**41**. Treatment of (\pm)-**41** with TFA followed by reaction with methyl 2-chloro-5-methylpyrimidine-4-carboxylate yielded (\pm)-**43**, which was saponification with LiOH to provide desired racemic carboxylic acid (\pm)-**44**.

Scheme 5^a

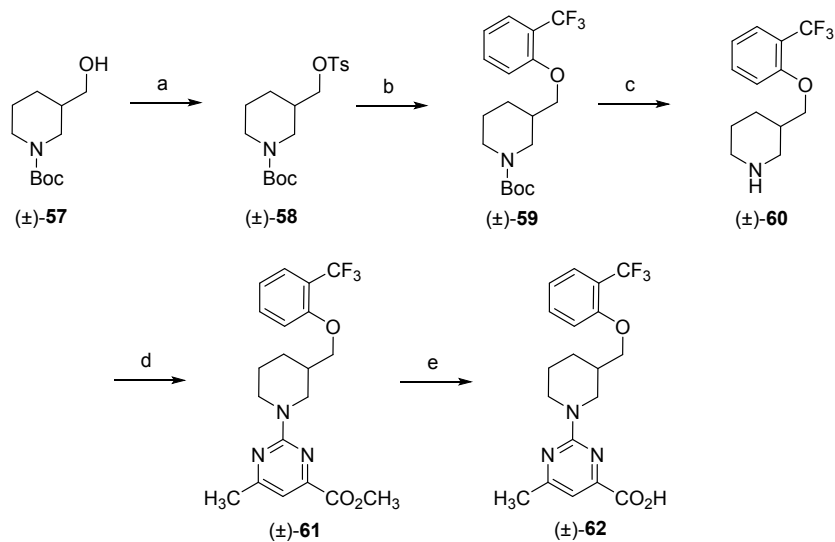
^aReagents and conditions: (a) TsCl, DMAP, Et₃N, CH₂Cl₂, 0 °C to rt, 16 h; (b) 2-(trifluoromethyl)phenol, Cs₂CO₃, DMF, 80 °C, 16 h; (c) TFA, CH₂Cl₂, 0 °C to rt, 8 h; (d) methyl 2-chloro-6-methylpyrimidine-4-carboxylate, *i*-Pr₂NEt, THF, reflux, 16 h; (e) (i) LiOH, CH₃OH, THF, H₂O, rt, 16 h; (ii) 2 N aqueous HCl.

Preparation of enantiomers (*R*)-50 and (*S*)-56 is highlighted in Scheme 6. The synthesis of the enantiopure analogues was achieved using the same route outlined in Scheme 5 but starting with either *tert*-butyl (*R*)-3-(hydroxymethyl)pyrrolidine-1-carboxylate ((*R*)-45) or *tert*-butyl (*S*)-3-(hydroxymethyl)pyrrolidine-1-carboxylate ((*S*)-51).

Scheme 6^a

^aReagents and conditions: (a) TsCl, DMAP, Et₃N, CH₂Cl₂, 0 °C to rt, 16 h; (b) 2-(trifluoromethyl)phenol, Cs₂CO₃, DMF, 80 °C, 16 h; (c) TFA, CH₂Cl₂, 0 °C to rt, 8 h; (d) methyl 2-chloro-6-methylpyrimidine-4-carboxylate, *i*-Pr₂NEt, THF, reflux, 16 h; (e) (i) LiOH, CH₃OH, THF, H₂O, rt, 16 h; (ii) 2 N aqueous HCl.

The preparation of the racemic piperidine carboxylic acid analogue (\pm)-**62** begins with S_N2 displacement of tosylate (\pm)-**58** with 2-(trifluoromethyl)phenol followed by treatment with TFA gave secondary amine (\pm)-**60** (Scheme 7). Reaction of amine (\pm)-**60** with methyl 2-chloro-5-methylpyrimidine-4-carboxylate yielded (\pm)-**61**, which upon saponification provided desired carboxylic acid (\pm)-**62**.

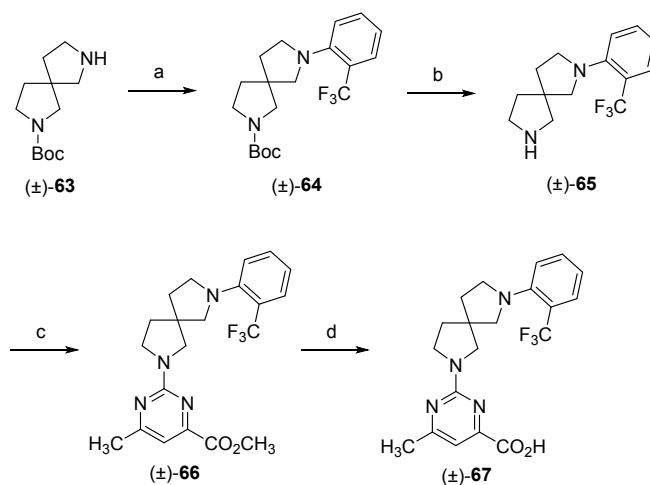
Scheme 7^a

^aReagents and conditions: (a) TsCl, DMAP, Et₃N, CH₂Cl₂, 0 °C to rt, 16 h; (b) 2-(trifluoromethyl)phenol, Cs₂CO₃, DMF, 80 °C, 16 h; (c) TFA, CH₂Cl₂, 0 °C to rt, 8 h; (d) methyl 2-chloro-6-methylpyrimidine-4-carboxylate, *i*-Pr₂NEt, THF, reflux, 16 h; (e) (i) LiOH, CH₃OH, THF, H₂O, rt, 16 h; (ii) 2 N aqueous HCl.

Racemic 2,7-diazaspiro[4.4]nonane analogue (±)-67 was designed to explore the SAR effects of introducing a ring-constrained core (Scheme 8). Aniline (±)-64 was generated via a palladium-catalyzed amination between (±)-63 and 1-bromo-2-(trifluoromethyl)benzene using tris(dibenzylideneacetone)dipalladium (0) (Pd₂(dba)₃) and 2-dicyclohexylphosphino-2',4',6'-triisopropylbiphenyl (XPhos). Boc-deprotection of (±)-64 with TFA gave amine (±)-65, which was subsequently reacted with methyl 2-chloro-5-methylpyrimidine-4-carboxylate to give pyrimidine (±)-66. Saponification of (±)-66 with

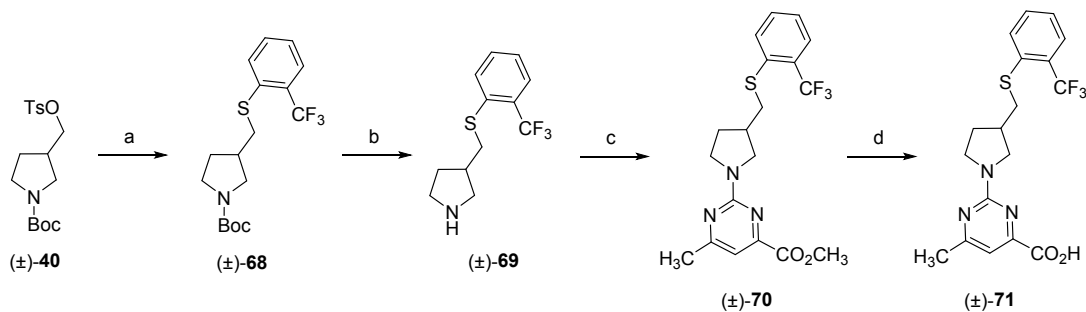
LiOH followed by acidification of the lithium carboxylate salt with 2 N HCl provided desired spirocycle (\pm)-**67**.

Scheme 8^a



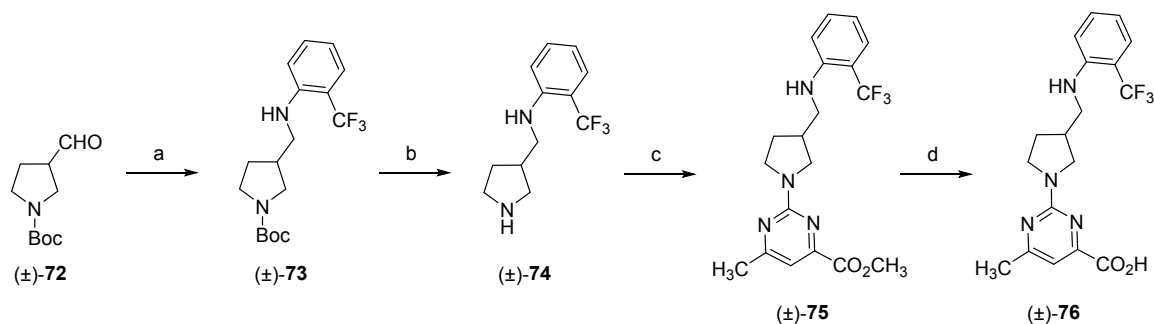
^aReagents and conditions: (a) 1-bromo-2-(trifluoromethyl)benzene, X-Phos, Pd₂(dba)₃, Cs₂CO₃, 1,4-dioxane, 110 °C, 16 h; (b) TFA, CH₂Cl₂, 0 °C to rt, 8 h; (c) methyl 2-chloro-6-methylpyrimidine-4-carboxylate, *i*-Pr₂NEt, THF, reflux, 16 h; (d) (i) LiOH, CH₃OH, H₂O, rt, 16 h; (ii) 2 N aqueous HCl.

Racemic thioether analogue (\pm)-**71** construction of is depicted in Scheme 9. The route use for the synthesis of (\pm)-**71** follows the aforementioned route described for (\pm)-**44** except that the S_N2 displacement of sulfonate ester (\pm)-**39** was conducted with 2-(trifluoromethyl)benzenethiol.

Scheme 9^a

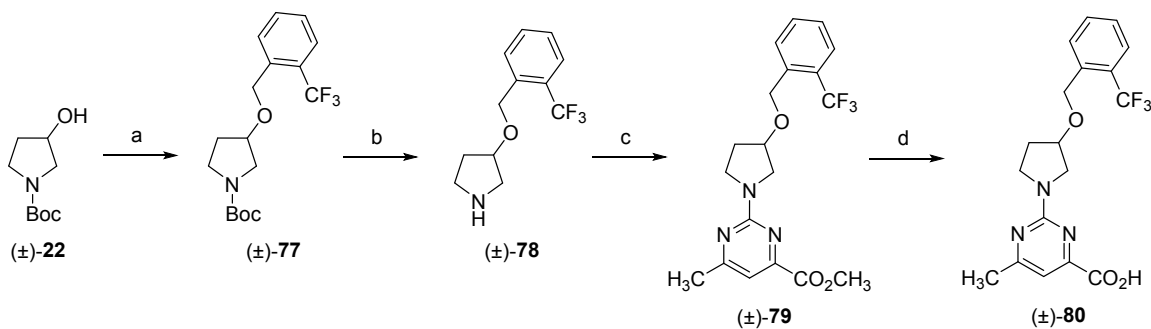
^aReagents and conditions: (a) 2-(trifluoromethyl)benzenethiol, Cs₂CO₃, DMF, 80 °C, 16 h; (b) TFA, CH₂Cl₂, 0 °C to rt, 8 h; (c) methyl 2-chloro-6-methylpyrimidine-4-carboxylate, *i*-Pr₂NEt, THF, reflux, 16 h; (d) (i) LiOH, CH₃OH, THF, H₂O, rt, 16 h; (ii) 2 N aqueous HCl.

Synthesis of amine linker (±)-76 was achieved via the synthetic route provided in Scheme 10. Reductive amination of *tert*-butyl 3-formylpyrrolidine-1-carboxylate ((±)-72) with 2-(trifluoromethyl)aniline with sodium triacetoxyborohydride (NaBH(OAc)₃) and acetic acid (HOAc) yielded compound (±)-73. Boc-deprotection of (±)-73 with TFA gave bis-amine (±)-74, which was converted to pyrimidine methyl ester (±)-75 via treatment with methyl 2-chloro-5-methylpyrimidine-4-carboxylate. Ester (±)-75 was hydrolyzed with LiOH, which yielded desired (±)-76 upon acidification.

Scheme 10^a

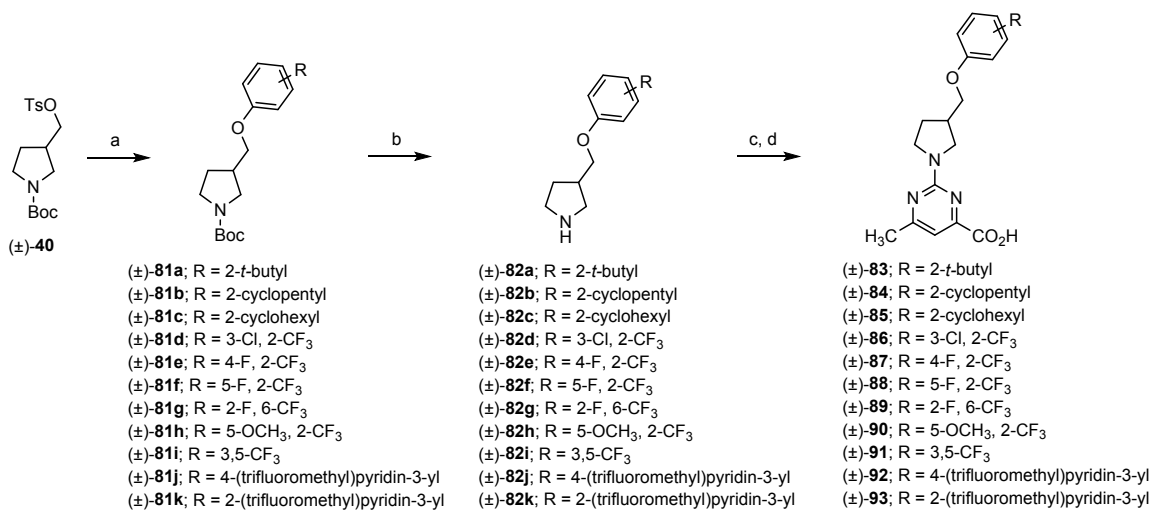
^aReagents and conditions: (a) 2-(trifluoromethyl)aniline, NaBH(OAc)₃, HOAc, CH₂Cl₂, rt, 16 h; (b) TFA, CH₂Cl₂, 0 °C to rt, 12 h; (c) methyl 2-chloro-6-methylpyrimidine-4-carboxylate, *i*-Pr₂NEt, DMF, 80 °C, 16 h; (d) (i) LiOH, CH₃OH, THF, H₂O, rt, 12 h; (ii) 2 N aqueous HCl.

The synthesis of racemic ether (±)-80 was accomplished via the route depicted in Scheme 11. Intermediate (±)-77 was produced via a Williamson ether synthesis between 1-(bromomethyl)-2-(trifluoromethyl)benzene and the sodium salt of racemic alcohol (±)-22. Treatment of ether (±)-77 with TFA provided Boc-deprotected (±)-78, which was subsequently reacted with methyl 2-chloro-5-methylpyrimidine-4-carboxylate to give (±)-79. Saponification of (±)-79 followed by acidification with 2 N aqueous HCl provided desired carboxylic acid (±)-80.

Scheme 11^a

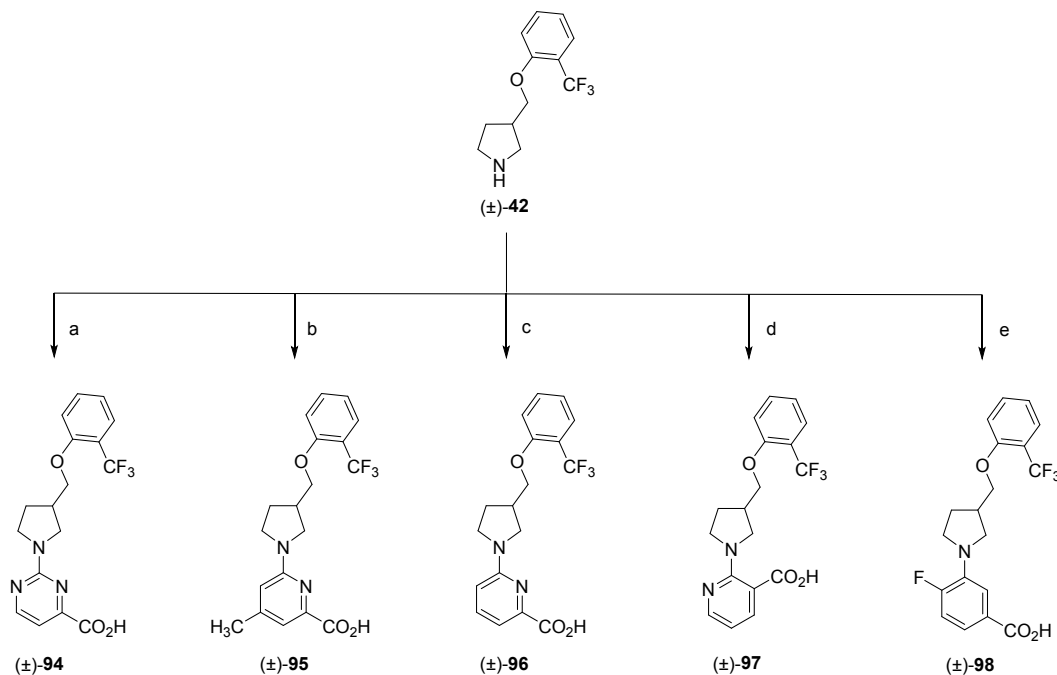
^aReagents and conditions: (a) 1-(bromomethyl)-2-(trifluoromethyl)benzene, NaH, DMF, 0 °C to rt, 16 h; (b) TFA, CH₂Cl₂, 0 °C to rt, 8 h; (c) methyl 2-chloro-6-methylpyrimidine-4-carboxylate, *i*-Pr₂NEt, THF, reflux, 16 h; (d) (i) LiOH, CH₃OH, THF, H₂O, rt, 16 h; (ii) 2 N aqueous HCl

A series of analogues derived from (±)-**44** that present varied aryl head groups ((±)-**83**-(±)-**93**) were prepared the manner depicted in Scheme 12. *O*-alkylation with tosylate (±)-**40** using an appropriately substituted phenol provided aryl ether intermediates (±)-**81a-k**. Boc-deprotection provided secondary amine intermediates (±)-**82a-k**, which when treatment with 2-methyl 2-chloro-6-methylpyrimidine-4-carboxylate followed by LiOH promoted saponification, gave the desired acids (±)-**83**-(±)-**93**.

Scheme 12^a

^aReagents and conditions: (a) substituted phenol, Cs₂CO₃, DMF, 80 °C, 16 h; (b) TFA, CH₂Cl₂, 0 °C to rt, 8 h; (c) methyl 2-chloro-6-methylpyrimidine-4-carboxylate, *i*-Pr₂NEt, THF, reflux, 16 h; (d) (i) LiOH, CH₃OH, THF, H₂O, rt, 16 h; (ii) 2 N aqueous HCl.

The production of the set of pyrimidine-substituted analogues (±)-**94**-(±)-**98** is shown in Scheme 13. Pyrimidine analogue (±)-**94** was prepared in the same manner as (±)-**44** starting from methyl 2-chloropyrimidine-4-carboxylate. For analogues (±)-**95**-(±)-**98**, the corresponding substituted chloro picolinic or nicotinic methyl esters and methyl 3-bromo-4-fluorobenzoate underwent palladium-catalyzed amination with amine (±)-**42**, Pd₂(dba)₃ and either 4,5-bis(diphenylphosphino)-9,9-dimethylxanthene (XantPhos) or XPhos in the presence of Cs₂CO₃. The resulting esters were hydrolyzed with LiOH and the lithium carboxylate salts were acidified with 2 N aqueous HCl.

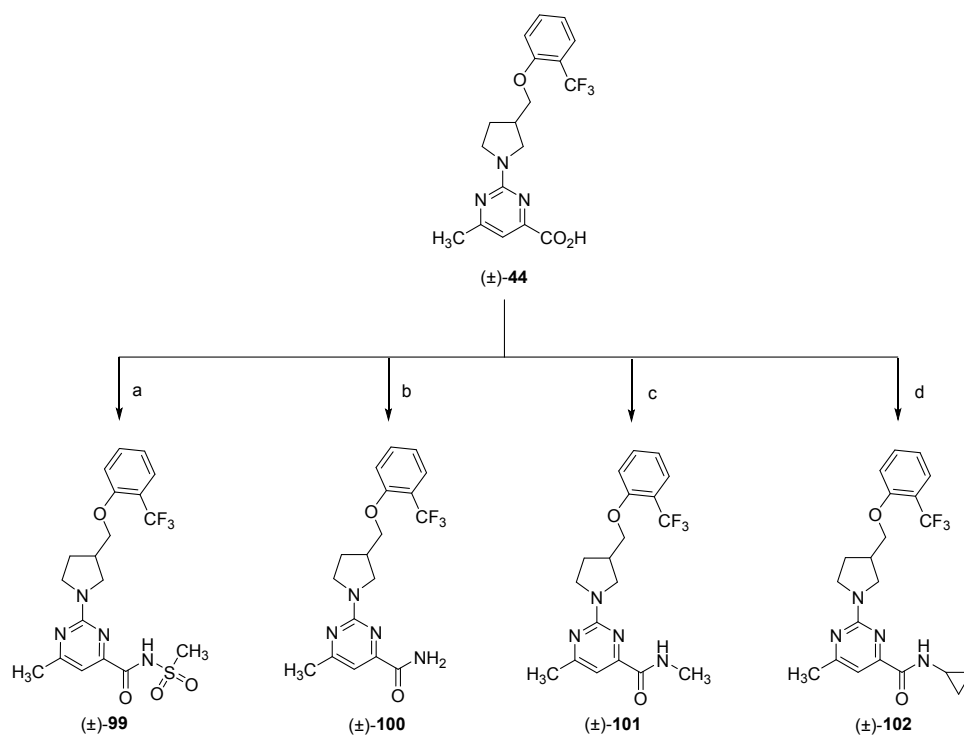
Scheme 13^a

^aReagents and conditions: (a) (i) methyl 2-chloropyrimidine-4-carboxylate, *i*-Pr₂NEt, THF, reflux, 16 h; (ii) LiOH, CH₃OH, H₂O, rt, 16 h; (iii) 2 N aqueous HCl; (b) (i) methyl 6-chloro-4-methylpicolinate, XantPhos, Pd₂(dba)₃, Cs₂CO₃, 1,4-dioxane, 80 °C, 16 h; (ii) LiOH, CH₃OH, H₂O, rt, 16 h; (iii) 2 N aqueous HCl; (c) (i) methyl 6-chloropicolinate, XantPhos, Pd₂(dba)₃, Cs₂CO₃, 1,4-dioxane, 80 °C, 16 h; (ii) LiOH, H₂O, CH₃OH, THF, rt, 16 h; (iii) 2 N aqueous HCl; (d) (i) methyl 2-chloronicotinate, XantPhos, Pd₂(dba)₃, Cs₂CO₃, 1,4-dioxane, 80 °C, 16 h; (ii) LiOH, H₂O, CH₃OH, THF, rt, 16 h; (iii) 2 N aqueous HCl; (e) (i) methyl 3-bromo-4-fluorobenzoate, XPhos, Pd₂(dba)₃, Cs₂CO₃, 1,4-dioxane, 110 °C, 16 h; (ii) LiOH, H₂O, CH₃OH, THF, rt, 16 h; (iii) 2 N aqueous HCl.

Preparation of analogues designed to explore the SAR of carboxylic acid isosteres and carboxamide analogues of (±)-44 is shown in Schemes 14 and 15. Generation of acylsulfonamide (±)-99 was achieved via a peptide coupling involving (±)-44, methane

1
2
3 sulfonamide, and *N,N,N',N'*-Tetramethyl-*O*-(1*H*-benzotriazol-1-yl)uronium
4
5 hexafluorophosphate, *O*-(benzotriazol-1-yl)-*N,N,N',N'*-tetramethyluronium
6
7 hexafluorophosphate (HBTU). Similarly, carboxamide (\pm)-**100** was synthesized from acid
8
9 (\pm)-**44** and ammonium chloride using HBTU. *N*-methyl amide analogue (\pm)-**101** was
10
11 prepared from (\pm)-**44** and methyl amine hydrochloride using T3P. Cyclopropyl amide (\pm)-
12
13 **102** was synthesized in a similar manner as carboxamide (\pm)-**100** but with
14
15
16
17
18 cyclopropylamine.

19
20
21
22
23 **Scheme 14^a**



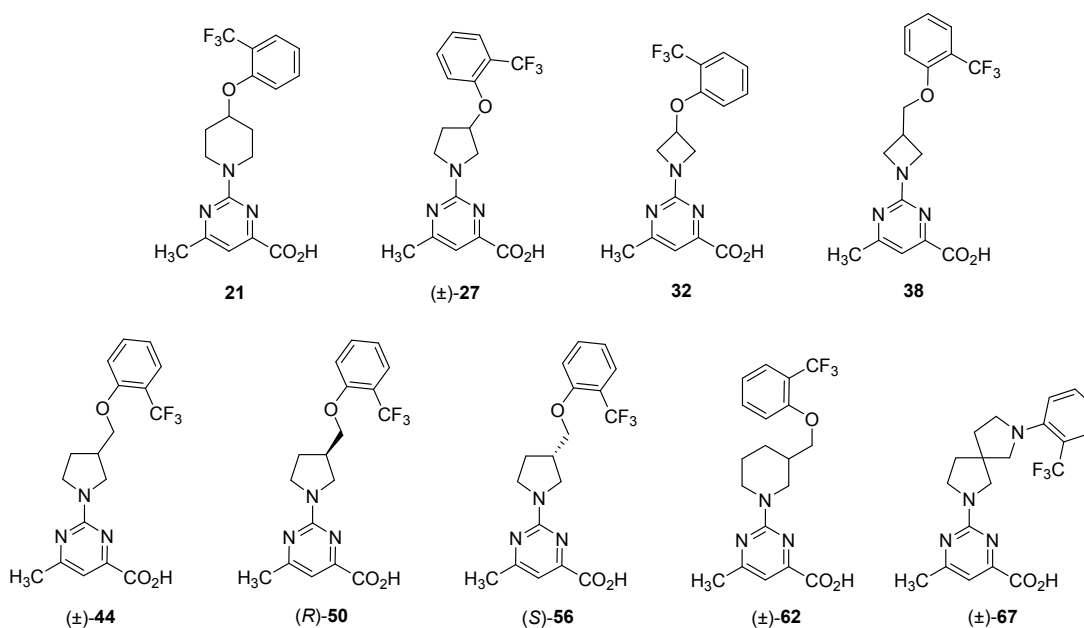
51 ^aReagents and conditions: (a) methane sulfonamide, HBTU, *i*-Pr₂NEt, DMF, rt, 18 h; (b) NH₄Cl,
52 HBTU, *i*-Pr₂NEt, DMF, rt, 18 h; (c) NHCH₃-HCl, T3P, *i*-Pr₂NEt, DMF, rt, 18 h; (d) cyclopropyl amine,
53 HBTU, *i*-Pr₂NEt, DMF, rt, 18 h.

1
2
3 (\pm)-**44** ((*R*)-**50** RBP4 SPA IC₅₀ = 65.0 nM; (*S*)-**56** RBP4 SPA IC₅₀ = 150.0 nM), however there
4
5 was no delineation between the enantiomers with regard to RBP4-TTR HTRF or TTR FP
6
7 activity. The remaining analogues of this sample set demonstrated diminished potency
8
9 for RBP4, TTR, or both targets. In light of these findings, the pyrrolidin-3-ylmethanol core
10
11 scaffold of (\pm)-**44** was selected for subsequent SAR exploration.
12
13

14
15 In the absence of docking models for both targets, we can only speculate as to why
16
17 the pyrrolidin-3-ylmethanol core scaffold of (\pm)-**44** provided the best balance of potency
18
19 for both target proteins. Firstly, the pyrrolidin-3-ylmethanol core scaffold of (\pm)-**44** shares
20
21 length and shape complementarity with the core linker of **8**, which previous RBP4 docking
22
23 models revealed was favorably aligned within the all-*trans*-retinol binding site.¹⁹ Previous
24
25 docking models depict the carboxylic acid of **8** engaged in key H-bond and electrostatic
26
27 interactions near the binding site opening as the core linker extends through the β -barrel
28
29 channel projecting the aryl head group deep into the inner cavity.¹⁹ We hypothesize (\pm)-
30
31 **44** similarly projects the aryl head group ring deep into the inner hydrophobic cavity,
32
33 however the additional rotational freedom of its pyrrolidin-3-ylmethanol core may impart
34
35 entropic penalties that lead to the observed slight reduction in potency relative to
36
37 rotationally constricted **8**. Thus, it is possible that the core scaffolds of analogues **21-38**
38
39 are either too long (i.e., **21**), too short (i.e., **32**) or of less than optimal geometry (i.e., (\pm)-
40
41 **27** and **38**) to achieve a desirable level of potency. The core scaffolds of analogues (\pm)-**62**
42
43 and (\pm)-**67** do present geometries that are of somewhat better alignment with **8** and (\pm)-
44
45 **44** in terms of length and geometry, which may explain the observed improved potencies
46
47 for them relative to **21-38**. Of this sample set, (\pm)-**44**-(\pm)-**67** also present the best potency
48
49
50
51
52
53
54
55
56
57
58
59
60

1
2
3 at TTR. Although these novel analogues do not present the biphenyl ether motif present
4
5
6 in T4, they do share some pharmacophoric similarity with the endogenous TTR ligand. It
7
8 is anticipated that the pyrimidine acid appendages of (\pm)-**44**-(\pm)-**67** engage in electrostatic
9
10 binding interactions with Lys15 and Glu54. Furthermore, (\pm)-**44**-(\pm)-**67** are of similar
11
12 length to T4 and can confer an orthogonal orientation among the head group and bottom
13
14 length to T4 and can confer an orthogonal orientation among the head group and bottom
15
16 group appendages that T4 adopts upon binding to TTR. We postulate that the B-region
17
18 aryl head groups of (\pm)-**44**-(\pm)-**67** are capable of projecting into the T4 inner binding site
19
20 where they are within proximity to position their respective *ortho*-trifluoromethyl groups
21
22 to potentially occupy resident HBP2 or HBP3 pockets. Future X-ray crystallographic
23
24 studies will determine if our proposed binding orientations of (\pm)-**44** at both proteins are
25
26 indeed accurate.
27
28
29
30
31

32 **Table 1.** *In vitro* RBP4 and TTR data for A-region scaffold hopping core analogues.
33
34
35
36
37



38

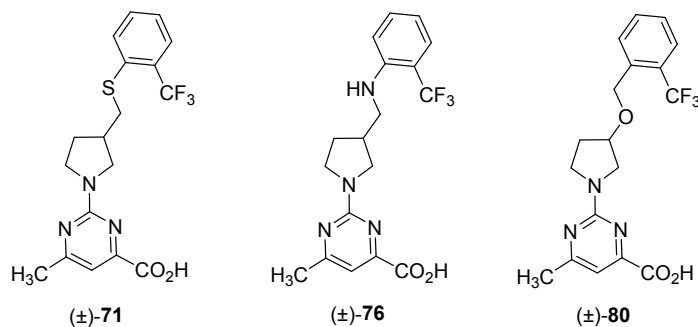
Compound	RBP4 SPA ^a IC ₅₀ (μM) ^d	RBP4-TTR HTRF ^b IC ₅₀ (μM) ^d	TTR FP ^c IC ₅₀ (μM) ^d
21	2.44	18.7	4.0
(±)- 27	>3	ND	8.8
32	>3	ND	13.5
38	0.8	6.5	26
(±)- 44	0.08	0.25	2.85
(<i>R</i>)- 50	0.065	0.24	3.2
(<i>S</i>)- 56	0.15	0.75	3.9
(±)- 62	0.48	15	1.1
(±)- 67	0.26	ND	1.6

^aIC₅₀ values for the SPA assay obtained in the presence of a fixed, 10 nM concentration of [³H]-all-*trans*-retinol. ^bIC₅₀ values for the HTRF assay obtained in the presence of 1 μM concentration of all-*trans*-retinol. ^cIC₅₀ values for the FP assay obtained in the presence of a fixed, 25 μM concentration of fluorescein isothiocyanate (FITC)-coupled TTR FP probe. ^dIC₅₀ data is represented as the mean ± standard deviation or compounds tested more than twice the IC₅₀ or as the mean of two independent experiments if only run twice. ND = Not determined.

Prior to exploring aromatic head group B-region SAR, we first explored the effects of either replacing the ether oxygen that connects the aromatic head group with the

1
2
3 pyrrolidine core of (\pm)-**44** with other heteroatoms or by repositioning the ether oxygen
4
5 connectivity from the aromatic ring to the pyrrolidine ring (Table 2). Interestingly,
6
7 replacing the (\pm)-**44** ether oxygen with sulfur or NH led to significantly diminished potency
8
9 for either RBP4 or TTR (or both). Furthermore, repositioning the ether oxygen to give (\pm)-
10
11 **80** led to complete loss of activity at RBP4 with a concomitant precipitous drop in TTR
12
13 potency. The requirement for an ether linker with the oxygen connectivity presented by
14
15 (\pm)-**44** may be due to the following factors (or a combination thereof): 1) the oxygen of
16
17 (\pm)-**44** is better able to optimally modulate electron density of the aromatic head group
18
19 for potential π - π interactions in the Phe-rich RBP4 β -ionone cavity relative to thioether
20
21 (\pm)-**71**, aniline (\pm)-**76**, and alkoxymethyl analogue (\pm)-**80**, 2) loss of potency for aniline (\pm)-
22
23 **76** may be attributed to a more polar, H-bond donating NH group residing in a lipophilic
24
25 area of both binding pockets, leading to unfavorable interactions and incurred
26
27 desolvation penalties, 3) the repositioning of the oxygen atom in (\pm)-**80** may also
28
29 adversely affect hydrogen bond accepting (HBA) binding interactions of the
30
31 aminopyrimidine fragment via the inductive effect, and 4) the ether oxygen of (\pm)-**44** may
32
33 stereoelectronically stabilize the bioactive conformation of the aromatic head group for
34
35 binding at RBP4 and TTR. The results obtained from this focused probe led to (\pm)-**44** B-
36
37 region SAR exploring similarly ether-linked aromatic head groups.
38
39
40
41
42
43
44
45
46
47
48
49
50
51
52
53
54
55
56
57
58
59
60

Table 2. *In vitro* RBP4 and TTR data for (±)-**44** analogues bearing alternative linkers to the 2-trifluoromethylphenyl aromatic head group.



Compound	RBP4 SPA ^a IC ₅₀ (μM) ^d	RBP4-TTR HTRF ^b IC ₅₀ (μM) ^d	TTR FP ^c IC ₅₀ (μM) ^d
(±)-71	0.23	1.3	10.5
(±)-76	0.9	7.5	3.5
(±)-80	>3	ND	13

^aIC₅₀ values for the SPA assay obtained in the presence of a fixed, 10 nM concentration of [³H]-all-*trans*-retinol. ^bIC₅₀ values for the HTRF assay obtained in the presence of 1 μM concentration of all-*trans*-retinol. ^cIC₅₀ values for the FP assay obtained in the presence of a fixed, 25 μM concentration of fluorescein isothiocyanate (FITC)-coupled TTR FP probe. ^dIC₅₀ data is represented as the mean ± standard deviation or compounds tested more than twice the IC₅₀ or as the mean of two independent experiments if only run twice. ND = Not determined.

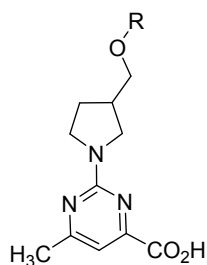
B-Region aromatic head group SAR exploration for analogue (±)-**44** was conducted with a set of varyingly substituted phenyl-bearing analogues ((±)-**83**-(±)-**93**) (Table 3). The

1
2
3 focused sample set was designed to explore how accommodative the inner binding
4
5 cavities of both binding sites would be to analogues presenting multiple aromatic
6
7 appendages of varying steric and electronic characteristics. Previously reported SAR by us
8
9 and others has shown that large and lipophilic groups are required at the *ortho* position
10
11 of the aromatic head group for any appreciable activity at RBP4. Specifically, the
12
13 trifluoromethyl (CF₃) group has served as an excellent moiety for generating potent RBP4
14
15 antagonists, which is attributed to its size (Hansch parameter $E_s = -2.4$) and lipophilicity
16
17 (Hansch parameter $\pi = 0.88$), which appears to be optimally suited for β -ionone pocket
18
19 occupancy. Replacement of the *ortho*-trifluoromethyl group with other groups that are
20
21 sterically smaller in size or are less lipophilic (i.e., Cl, CH₃) can result in a significant loss in
22
23 potency at RBP4 (data not shown). Similarly, varying the substitution pattern of the CF₃
24
25 group can also have an undesirable effect on RBP4 potency. It is for these reasons that
26
27 we largely maintained an *ortho*-substitution pattern for many of our B-region analogues
28
29 and that any alternative *ortho*-substituents explored were typically larger and more
30
31 lipophilic than CF₃. Thus, our initial set of analogues replaced the *ortho*-trifluoromethyl
32
33 group with large, lipophilic alkyl and cycloalkyl appendages ((\pm)-**83**-(\pm)-**85**). These
34
35 analogues were approximately 2-fold less potent than (\pm)-**44** in the RBP4 SPA binding
36
37 assay and were inactive at TTR. These results indicate that the RBP4 β -ionone is more
38
39 vacuous than the inner T4 binding cavity and that the sterically encumbered substituents
40
41 of analogues (\pm)-**83**-(\pm)-**85** may simply have been too large for the inner HBPs to
42
43 accommodate. The data also suggests that there is a limit to the size of the *ortho*-
44
45 substituent and that the CF₃ was optimal for further SAR exploration. We next probed
46
47
48
49
50
51
52
53
54
55
56
57
58
59
60

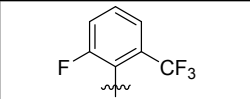
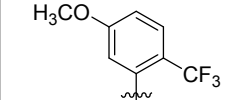
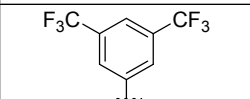
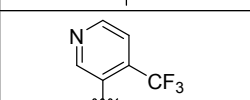
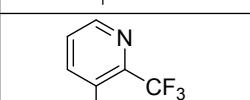
1
2
3 various halogenated aromatic head groups bearing a CF₃ group *ortho* the ether oxygen
4
5 ((±)-**86**-(±)-**89**) with the goal of identifying a substitution pattern that may better interact
6
7
8 with the inner T4 HBPs while more fully occupying the RBP4 β-ionone cavity. These
9
10 halogenated analogues did demonstrate activity for TTR. Interestingly, the positioning of
11
12 fluorine had a significant impact on TTR potency as analogue (±)-**88** was 6-fold less potent
13
14 than (±)-**89** ((±)-**88** TTR FP IC₅₀ = 13 μM; (±)-**89** TTR FP IC₅₀ = 1.9 μM). This may be
15
16 attributed to the CF₃ group and the fluorine of (±)-**89** together occupying HBPs, whereas
17
18 the positioning of fluorine in (±)-**88** is suboptimal and does not permit it to efficiently
19
20 occupy an inner HBP and/or does not allow the CF₃ group to do so. Notably, analogue (±)-
21
22 **89** may be poised for replacement of its fluorine with an iodine atom. Such an iodo
23
24 analogue may better occupy the inner HBPs of TTR (in a similar manner as T4) as well as
25
26 position the iodine for a σ-hole halogen binding interaction with the sulfur atom of Met73
27
28 residing in close proximity to the RBP4 β-ionone pocket. The 3,5-bis-CF₃ analogue (±)-**91**
29
30 mimics the bis-iodine substitution pattern of the aromatic head group of **4**. However, the
31
32 compound neither improved affinity for RBP4 nor was it active at TTR. It is for this reason
33
34 that the 3,5-bis-iodo congener that would more closely mimic T4 was not explored. Lastly,
35
36 we explored the effects of incorporating H-bond accepting groups in the B-region ((±)-**90**,
37
38 (±)-**92**, and (±)-**93**) that could potentially 1) engage in H-bond interactions with the Ser117
39
40 and Ser117' residues buried deep within the inner T4 binding cavity, and 2) engage in a
41
42 potential H-bond interaction with the His104 residue located with the RBP4 β-ionone
43
44 pocket. Anisole (±)-**90** was inactive at both targets and while pyridyl analogues (±)-**92**, and
45
46 (±)-**93** did exhibit moderate potency at RBP4 ((±)-**92** RBP4 SPA IC₅₀ = 0.52 μM; (±)-**93** RBP4
47
48
49
50
51
52
53
54
55
56
57
58
59
60

SPA IC_{50} = 0.66 μ M), they too were inactive at TTR. None of the B-region analogues showed improved potency for both targets relative to parent (\pm)-**44**, thus the C-region aromatic carboxylic acid bottom group SAR campaign was conducted using the (\pm)-3-((2-(trifluoromethyl)phenoxy)methyl)pyrrolidine core scaffold intact.

Table 3. *In vitro* RBP4 and TTR data for (\pm)-**44** B-region analogues bearing alternative substituted aryl head groups.



Compound	Aryl Head Group (R)	RBP4 SPA ^a IC_{50} (μ M) ^d	RBP4-TTR HTRF ^b IC_{50} (μ M) ^d	TTR FP ^c IC_{50} (μ M) ^d
(\pm)- 83		0.13	0.45	>30
(\pm)- 84		0.16	0.54	>30
(\pm)- 85		0.21	ND	>30
(\pm)- 86		0.18	ND	3.9
(\pm)- 87		0.24	0.87	3.9
(\pm)- 88		0.13	0.3	13

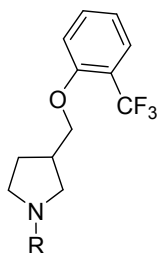
(±)- 89		0.3	1	1.9
(±)- 90		>3	ND	>30
(±)- 91		1.6	ND	>30
(±)- 92		0.52	3.7	>30
(±)- 93		0.66	ND	>30

^aIC₅₀ values for the SPA assay obtained in the presence of a fixed, 10 nM concentration of [³H]-all-*trans*-retinol. ^bIC₅₀ values for the HTRF assay obtained in the presence of 1 μM concentration of all-*trans*-retinol. ^cIC₅₀ values for the FP assay obtained in the presence of a fixed, 25 μM concentration of fluorescein isothiocyanate (FITC)-coupled TTR FP probe. ^dIC₅₀ data is represented as the mean ± standard deviation or compounds tested more than twice the IC₅₀ or as the mean of two independent experiments if only run twice. ND = Not determined.

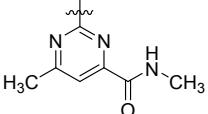
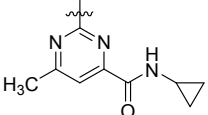
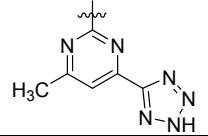
The SAR effects of pyrimidine-4-carboxylic acid, picolinic, nicotinic, and benzoic acid moieties used to replace the pyrimidine ring of (±)-**44** are provided in Table 4. Removal of the pyrimidine 6-methyl group had a deleterious effect for both targets as the des-methyl analogue ((±)-**94**) demonstrated a significant loss in RBP4 potency and a ~5-fold loss in TTR potency relative to (±)-**44** (RBP4 SPA IC₅₀ = 1.67 μM; TTR FP IC₅₀ = 11 μM). Selective removal of a pyrimidine nitrogen ((±)-**95** and (±)-**96**) or repositioning the carboxylic acid adjacent to the pyrrolidine core ((±)-**97**) did not yield analogues with improved binding profiles relative to (±)-**44**. We also explored the fluorinated benzoic acid appendage

1
2
3 featured in TTR ligand **12**. X-ray crystallographic data of **12** bound to TTR (PDB 4HIQ)
4
5 shows the fluorine projecting into HBP1.³³ Incorporation of this appendage ((±)-**98**) did
6
7 yield a slight improvement in TTR potency relative to (±)-**44** (TTR FP IC₅₀ = 1.88 μM),
8
9 however, the improvement in TTR potency came at the expense of RBP4 (RBP4 SPA IC₅₀
10
11 = 2.35 μM). Lastly, we also pursued isosteric replacements of the (±)-**44** carboxylic acid
12
13 with an acyl sulfonamide ((±)-**99**) as well as replacing the acid with carboxamides ((±)-**100**-
14
15 (±)-**102**). Collectively, these analogues provided compounds that were equipotent to (±)-
16
17 **44** for RBP4, however, they were either moderately less potent or inactive at TTR.
18
19 Interestingly, replacement of the carboxylic acid with a tetrazole isostere ((±)-**103**) did
20
21 furnish an analogue that was equipotent to (±)-**44** in the RBP4 SPA binding assay (RBP4
22
23 SPA IC₅₀ = 86.0 nM) and ~2-fold more potent in the TTR FP assay (TTR FP IC₅₀ = 1.26 μM).
24
25 However, (±)-**103** was approximately significantly less potent for RBP4 functional activity
26
27 than (±)-**44** ((±)-**103** RBP4-TTR HTRF IC₅₀ = 1.6 μM).
28
29
30
31
32
33
34
35
36
37
38
39
40
41
42
43
44
45
46
47
48
49
50
51
52
53
54
55
56
57
58
59
60

Table 4. *In vitro* RBP4 and TTR data for (±)-**44** analogues bearing alternative C-region bottom group aromatic carboxylic acids appendages, carboxylic acid isosteres, and carboxamides.



Compound	Aryl Head Group (R)	RBP4 SPA ^a IC ₅₀ (μM) ^d	RBP4-TTR HTRF ^b IC ₅₀ (μM) ^d	TTR FP ^c IC ₅₀ (μM) ^d
(±)- 94		1.67	ND	11
(±)- 95		0.13	0.54	7.4
(±)- 96		>3	ND	25
(±)- 97		0.68	1.3	4.9
(±)- 98		2.35	ND	1.88
(±)- 99		0.081	0.7	4.2
(±)- 100		0.062	2.3	>30

(±)- 101		0.089	>30	>30
(±)- 102		0.062	19	4.1
(±)- 103		0.086	1.6	1.26

^aIC₅₀ values for the SPA assay obtained in the presence of a fixed, 10 nM concentration of [³H]-all-*trans*-retinol. ^bIC₅₀ values for the HTRF assay obtained in the presence of 1 μM concentration of all-*trans*-retinol. ^cIC₅₀ values for the FP assay obtained in the presence of a fixed, 25 μM concentration of fluorescein isothiocyanate (FITC)-coupled TTR FP probe. ^dIC₅₀ data is represented as the mean ± standard deviation or compounds tested more than twice the IC₅₀ or as the mean of two independent experiments if only run twice. ND = Not determined.

Analogue (±)-**44** emerged as a lead upon completion of our SAR campaign and was further profiled (Table 5). Compound (±)-**44** possesses very good kinetic solubility in and robust microsomal stability as evidenced by the very low intrinsic clearance (CL_{int}) values. The compound is highly protein bound and lacks limiting inhibitory activity in a standard cytochrome P450 (CYP) panel and at the human ether-a-go-go (hERG) channel. Importantly, unlike **8**, which possesses ancillary PPARγ agonist activity, (±)-**44** was found to be devoid of such activity.

Table 5. ADME Profile obtained for advanced analogue (\pm)-**44**.

Solubility ^a	Microsomal CL _{int} (μ L/min/mg) ^b				Liver Microsomal Stability (% remaining at 30 min) ^c				CYP Inhibition (% inhibition at 10 μ M) 2C9, 2C19, 2D6, 3A4	hERG ^d (IC ₅₀)	PPAR γ (IC ₅₀)	%PPB ^e		
	H	R	M	cyno	HLM	RLM	MLM	cyno LM				H	R	M
187.4 μ M	<0.0231				105	93	95	103	2C9 – 0% 2C19 – (-)8% 2D6 – 18.1% 3A4 – (-)12.2%	>30 μ M	>100 μ M	99.8	96	96

^aKinetic solubility measured in PBR (pH= 7.4). ^bMicrosomal intrinsic clearance (CL_{int}); H = human; R = rat; M = mouse; cyno = cynomolgus monkey. ^cLiver microsomal metabolic stability, % of parent drug remaining after a 30 minute incubation in the presence of the microsomes; HLM = human liver microsomes; RLM = rat liver microsomes; MLM = mouse liver microsomes; cyno LM = cynomolgus monkey liver microsomes. ^dCiPA hERG QPatch Assay; compounds were tested (n = 2) in a five-point concentration-response study. ^e%PPB = plasma protein binding; H = human, R = rat, M = mouse.

(\pm)-44 PK Characteristics in CD-1 male mice. (\pm)-**44** was dosed IV (2 mg/kg) and PO (5 mg/kg) in CD-1 male mice and the calculated PK parameters are given in Table 6. Compound (\pm)-**44** was found to be relatively stable (CL_{int} = 0.0499 L/hr/kg) with a long half-life of 9.9 h. Significant absorption was achieved (C_{max} of 3033 ng/ml) relatively rapidly (T_{max} = 0.83 h). High levels of exposure were attained (AUC_{INF} was 52439 hr·ng/mL) and the estimated %F was 52%.

Table 6. (\pm)-**44** PK data with CD-1 male mice.

Route	Dose	C ₀ ^a (ng/ml)	CL ^b (L/hr/kg)	t _{1/2} ^c (h)	V _{ss} ^d (L/kg)	AUC _{last} ^e (hr·ng/mL)	AUC _{INF} ^f (hr·ng/mL)	%F ⁱ
IV	2 mg/kg	9129 (661)	0.0499 (0.005)	8.6 (1.15)	0.518 (0.069)	39523 (3665)	40336 (4021)	NA
Route	Dose	C _{max} ^g (ng/ml)	T _{max} ^h (h)	t _{1/2} ^c (h)	V _{ss} ^d (mL/kg)	AUC _{last} ^e (hr·ng/mL)	AUC _{INF} ^f (hr·ng/mL)	%F ⁱ
PO	5 mg/kg	3033 (692)	0.83 (0.29)	9.9 (2.0)	NA	50400 (5898)	52439 (7214)	52.0 (7.15)

Data are represented as the mean with standard deviation in parentheses (mean (SD)). Dosing groups consisted of three drug naïve adult male CD-1 mice. IV administration: Test article was administered at the 2 mg/kg dose; test article vehicle = 3% DMA/45% PEG300/12% Ethanol/40% Sterile water; PO administration: test article was administered at the 5 mg/kg dose, vehicle = 2 % Tween 80 in 0.9% saline. ^aObserved initial concentration of compound in blood at time zero. ^bTotal body clearance. ^cApparent half-life of the terminal phase of elimination of compound from blood. ^dVolume of distribution at steady state. ^eArea under the blood concentration versus time curve from 0 to the last time point that compound was quantifiable in blood. ^fArea under the blood concentration versus time curve from 0 to infinity. ^gMaximum observed concentration of compound in blood. ^hTime of maximum observed concentration of compound in blood. ⁱBioavailability; $F = (AUC_{INFpo} \times Dose_{iv}) \div AUC_{INFiv} \times Dose_{po}$.

(\pm)-44 PK-PD correlations in mouse. Confirmation of target engagement for (\pm)-**44** was assessed by measuring serum RBP4 level dynamics in mice after a single oral dose. A maximum of the 81% reduction in murine serum RBP4 levels was observed 6 h post oral administration of 25 mg/kg of (\pm)-**44** (Figure 10, A). Effects on serum TTR levels were not observed (data not shown). The dynamics of the *in vivo* serum RBP4 reduction correlated

with (\pm)-**44** systemic exposures after oral dosing (Figure 10, B) and a reduction in serum RBP4 (Figure 10, A). The observed maximal reduction (81%) and duration of effect (64% reduction observed at 24 h) correlate well with (\pm)-**44** PK properties such as high C_{max} , long exposure and slow clearance (Table 6). This data supports a conclusion on a generally good correlation between PK characteristics and PD effects between (\pm)-**44** exposures and degree of RBP4 lowering in mice.

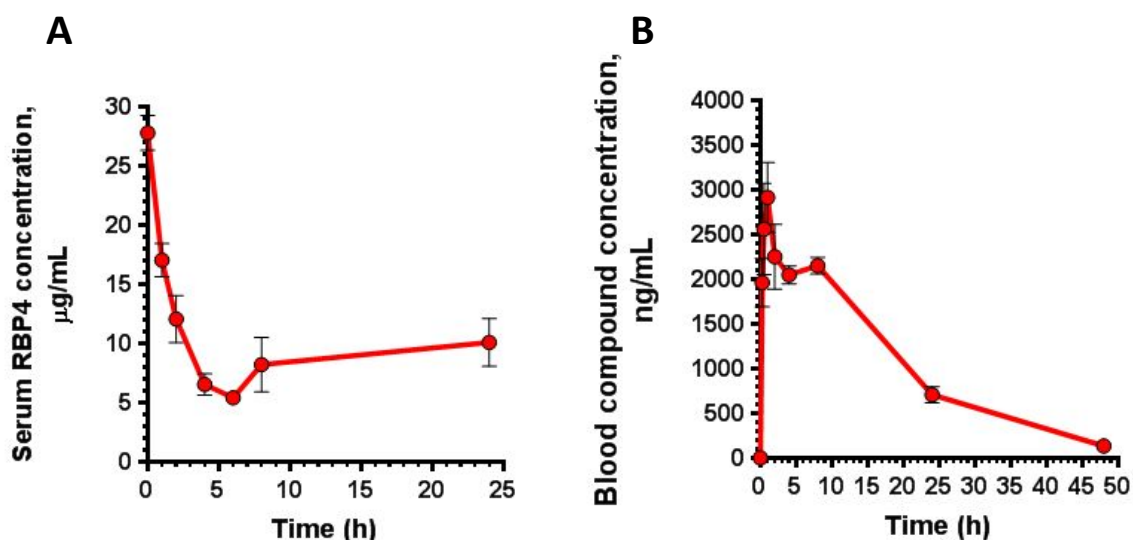


Figure 10. Murine PK-PD correlations of (\pm)-44**.** (A) Serum RBP4 levels following a single 25 mg/kg oral administration of (\pm)-**44**. (B) Blood compound levels following administration of a single oral 5 mg/kg dose of (\pm)-**44**. Data represented as the mean \pm SD. Three mice per treatment group were used in the study.

A very good correlation has been previously established between the ability of RBP4 antagonists from different classes to induce serum RBP4 lowering and preclinical efficacy

1
2
3 in the *Abca4*^{-/-} mouse model.^{11a, 13, 14} Based on its very good RBP4 lowering activity, it
4
5 seems reasonable to expect (±)-**44** to be efficacious in reducing the formation of cytotoxic
6
7 lipofuscin retinoids in the retina.
8
9

10
11
12 **Analogue (±)-44 attenuates formation of high molecular forms of TTR.** Inhibition of the
13
14 acid-induced TTR aggregation *in vitro* is a well-established approach to characterization
15
16 of TTR tetramer kinetic stabilizers.^{45, 46} Long-term 72-h incubation of TTR at 37 °C in acidic
17
18 conditions leads to the tetramer destabilization and dissociation followed by partial
19
20 monomer misfolding and oligomerization into amyloid fibrils and other high molecular
21
22 weight aggregates.⁴⁷ To explore the activity of the bispecific analogue (±)-**44** as a TTR
23
24 tetramer kinetic stabilizer, we evaluated the ability of this compound to prevent acid-
25
26 mediated TTR aggregate formation using modifications of the previously published
27
28 protocol.^{48, 49} Two compounds were used as a positive control in the aggregation
29
30 experiments, tafamidis and benzbromarone. Tafamidis (**11**) is a potent TTR tetramer
31
32 kinetic stabilizer approved as a therapy for familial amyloid polyneuropathy while
33
34 benzbromarone (structure not shown), a uricosuric drug, was found in our prior
35
36 experiments to be a potent TTR ligand with IC₅₀ of 293 nM in the FP TTR binding assay
37
38 which is on par with the reported potency of **11** in this assay.^{35a} Following 72 h of
39
40 incubation with DMSO at pH 4.0 the high molecular forms of TTR were significantly
41
42 increased while no such forms were observed after a similar incubation period at neutral
43
44 pH (Figure 11, A). Similar to the activity of two potent TTR ligands, **11** and benzbromarone,
45
46 (±)-**44** significantly reduced the formation of high molecular weight TTR species (Figure
47
48
49
50
51
52
53
54
55
56
57
58
59
60

11, A) indicating that it can act as a TTR tetramer kinetic stabilizer. Higher intensities of the TTR monomer bands in samples treated with **11**, benzbromarone, and (\pm)-**44** in comparison to DMSO reflected a corresponding decrease in TTR aggregation conferred by **11**, benzbromarone, and (\pm)-**44**. Quantitative analysis of band intensity revealed a 3.6-, 5.6-, and 4.7-fold reduction in formation of high molecular weight aggregates induced by tafamidis, benzbromarone, and (\pm)-**44**, respectively (Figure 11, B). Significant increase in the TTR monomer band intensities associated with the decrease in aggregate formations were evident in samples treated with **11**, benzbromarone, and (\pm)-**44** (Figure 11, C). Overall, the results of the aggregation experiments established that bispecific analogue (\pm)-**44** can act as a TTR tetramer kinetic stabilizer.

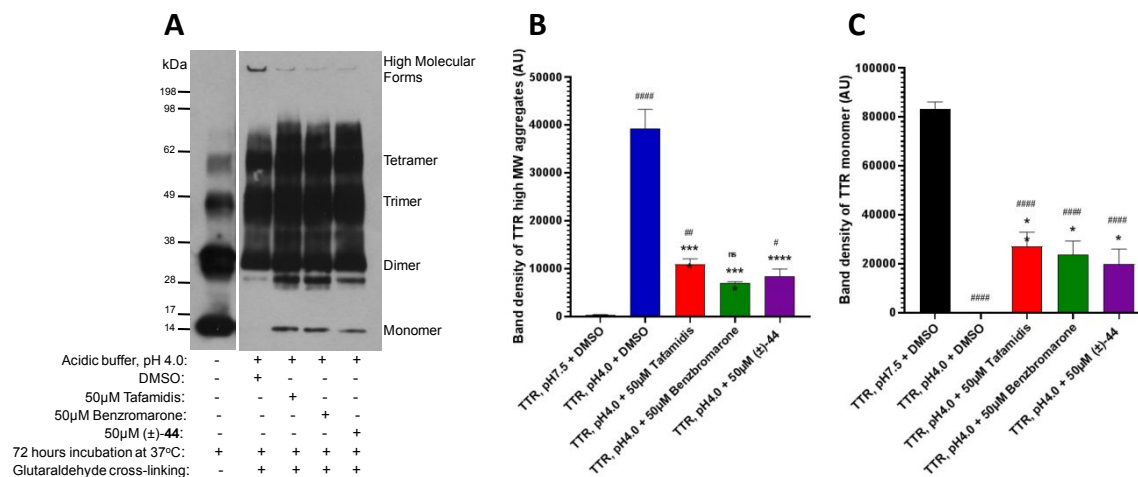


Figure 11. Analogue (\pm)-44 reduces the formation of high molecular weight TTR forms in the acid-induced aggregation assay. (A), TTR protein (5 μ g) was aggregated by using acetate buffer (pH 4.0) and incubated for 72 h at 37°C. After incubation in the presence of 50 μ M **11**, 50 μ M benzbromarone, and 50 μ M (\pm)-**44**, samples were cross-linked and subjected to SDS-PAGE

1
2
3 followed by western blotting with TTR antibodies. The representative blot of at least three
4 independent experiments is presented. (B, C), Bar graphs represent pixel volumes of TTR high
5 molecular weight aggregates (B) and monomers (C). The vertical axes represent the ratio of pixel
6 volume means \pm S.D. of the scanned bands on the immunoblots in arbitrary units. Statistical
7 significance was determined by one-way ANOVA with Holm-Sidak *post hoc* test; *, $p \leq 0.05$; **, p
8 ≤ 0.01 ; ***, $p \leq 0.001$; ****, $p \leq 0.0001$ compare to TTR aggregation (pH 4.0) + DMSO group, #, p
9 ≤ 0.05 ; ##, $p \leq 0.01$; ###, $p \leq 0.001$; ####, $p \leq 0.0001$ compare to TTR without aggregation (pH 7.5) group.
10
11
12
13
14
15
16
17
18
19
20

21 CONCLUSIONS

22
23
24 AMD is the most common cause of blindness in developed nations that generally
25 afflicts people of 60 years of age or older.⁵⁰ In the Caucasian population over the age of
26 80 the frequency of all forms of AMD is 90% in males and 16.4% in females.⁵¹ Currently,
27 there are no FDA-approve pharmacotherapies available for the most prevalent dry form
28 of AMD, which affects 90% of AMD patients. SSA is a common late-onset disease
29 associated with accumulation of wild-type TTR amyloid deposits in extracellular
30 compartments of different tissues and organs. The heart is usually the dominant site of
31 involvement.^{30a} SSA is recognized as a major cause of severe cardiac dysfunction in the
32 elderly, which includes congestive heart failure and cardiac death.⁵² SSA affects
33 approximately 25% of patients over the age of 80.⁵² The number of people with AMD is
34 projected to increase to 288 million in 2040.⁵³ The high rate of comorbidity between dry
35 AMD and SSA is expected based on the high population frequency of both conditions in
36 older individuals. In recent years, we identified and characterized different structural
37 classes of RBP4 antagonists as a potential treatment for macular degeneration and
38
39
40
41
42
43
44
45
46
47
48
49
50
51
52
53
54
55
56
57

1
2
3 NAFLD.^{14, 18-20, 26} We showed that selective RBP4 antagonists can induce a desired drop in
4
5 serum RBP4^{18, 19, 26} partially decreasing the concentration of visual cycle retinoids in the
6
7 retina and significantly inhibiting cytotoxic A2E biosynthesis in *Abca4*^{-/-} mice, a model that
8
9 recapitulates the Stargardt disease phenotype.¹⁴ However, long-term use of selective
10
11 RBP4 antagonists in AMD patients who also have SSA may not be optimal. It is known
12
13 that holo-RBP4-TTR interaction stabilizes TTR tetramers and prevents formation of TTR
14
15 amyloid fibrils. Selective RBP4 antagonists release the unliganded TTR tetramer from the
16
17 holo-RBP4-TTR complex in circulation and the release of the unliganded TTR may be
18
19 associated with destabilization of TTR tetramers and, potentially, with the TTR amyloid
20
21 fibril formation in a fraction of susceptible individuals prone to developing TTR
22
23 amyloidosis, such as SSA patients. We sought to identify novel RBP4 antagonists that also
24
25 exhibited TTR tetramer stabilizing capability. We utilized previously reported SAR for **8**
26
27 and reported X-ray crystallographic data for ligands bound to RBP4 (PDB 3FMZ)⁸ and TTR
28
29 (PDB 2ROX)^{5c} to enable our structure-based drug design campaign. Our premise was to
30
31 identify compounds with suitable RBP4 antagonistic potency that could provide adequate
32
33 TTR tetramer kinetic stabilization. We initially investigated a series of alternative core
34
35 linker analogues via a scaffold hopping approach starting from **8**, which ultimately lead to
36
37 the discovery of (±)-**44**. Compound (±)-**44** possesses a favorable balance of *in vitro*
38
39 potency for both targets, desirable ADME properties, and excellent PK characteristics in
40
41 mouse (Table 6). In addition, the compound lowered serum RBP4 levels upon oral dosing
42
43 in mice (>80%) (Figure 10) and significantly decreased TTR high molecular weight
44
45 aggregates in an *in vitro* TTR aggregate assay (Figure 11). These data suggest that (±)-**44**
46
47
48
49
50
51
52
53
54
55
56
57
58
59
60

1
2
3 shows potential as an oral treatment for RBP4-related indications while preventing
4 possible TTR amyloid fibril formation and ATTR comorbidities such as SSA or hereditary
5 TTR amyloidosis. One general safety concern for the novel class of bispecific compounds
6 relates to their effect on traffic and delivery of thyroxine and vitamin A.
7
8
9
10
11

12 Binding of compounds like (\pm)-**44** to TTR is not expected to significantly affect
13 thyroxine metabolism and function given that less than 1% of circulating TTR carries
14 thyroxine while another serum protein, TBG, functions as the primary T4 carrier in the
15 blood. TTR knock-out mice are phenotypically normal with no signs of growth or
16 developmental abnormalities.⁵⁴ Similarly, serum RBP4 lowering by bispecific compounds
17 is unlikely to promote systemic vitamin A deficiency symptoms given the ability of
18 alternative RBP4/TTR-independent pathways to provide retinoids to tissues, including the
19 retina.⁵⁵⁻⁶¹ *Rbp4*^{-/-} mice present no systemic abnormalities⁵⁵⁻⁵⁷ or retinal degeneration.⁵⁶
20
21
22
23
24
25
26
27
28
29
30
31
32 It is hopeful that the class of bispecific compounds exemplified by (\pm)-**44** will be safe and
33 efficacious as an orally administered pharmacotherapeutic for the dry AMD-SSA
34 comorbidity.
35
36
37
38
39
40
41

42 EXPERIMENTAL SECTION

43
44
45 ***In vitro* binding of compounds to RBP4.** Compound binding to RBP4 was assessed in
46 the radiometric scintillation proximity (SPA) assay that was previously described.^{18, 19, 26}
47
48
49
50 The assay measured competitive displacement of radiolabeled [³H]-all-*trans*-retinol from
51 native RBP4 purified from human urine (Fitzgerald, 30R-AR022L). The protein was
52 biotinylated using the EZ-link Sulfo-NHS-LC-Biotinylation kit from ThermoFisher (Cat
53
54
55
56
57
58
59
60

1
2
3 #21335) as recommended by the manufacturer. Binding assays were implemented in a
4
5 final volume of 100 μ L in SPA buffer (1 \times PBR, pH 7.4, 1 mM EDTA, 0.1% BRA, 0.5% CHAPS).
6
7
8 The assay reaction included a radioligand, 10 nM [3 H]-all-*trans*-retinol (48.7 Ci/mmol;
9
10 PerkinElmer, Waltham, MA), along with the 0.3 mg/well Streptavidin-PVT beads
11
12 (PerkinElmer, RPNQ0006) and 50 nM biotinylated human RBP4. Unlabeled retinol (Sigma,
13
14 cat # 95144) at 20 μ M was added to control wells to assess a nonspecific binding.
15
16
17 Radioactivity counts were measured using CHAMELEON plate reader (Hidex Oy, Turku,
18
19 Finland) after 16 h of incubation at rt with mild shaking.
20
21
22

23 **Assessment of antagonistic activity in the HTRF RBP4-TTR interaction assay.** The
24
25 ability of analogues to act as antagonists of all-*trans*-retinol-dependent RBP4-TTR
26
27 interaction was measured in the HTRF (Homogenous Time-Resolved Fluorescence) assay
28
29 as we described previously.^{18, 19, 26} Untagged TTR (Calbiochem, cat #529577) and Maltose-
30
31 Binding Protein-tagged RBP4 expressed in *E. coli* were used in this assay. HTRF Cryptate
32
33 labeling kit from CisBio (Cisbio, cat #62EUSPEA, Bedford, MA) was used to label TTR with
34
35 Eu³⁺ Cryptate. The assay was performed in a final assay volume of 16 μ L in the buffer that
36
37 contained 10 mM Tris-HCl pH 7.5, 1 mM DTT, 0.05% NP-40, 0.05% Prionex, 6% glycerol,
38
39 and 400 mM KF. Other components of the reaction mix included 60 nM MBP-RBP4, 5 nM
40
41 TTR-Eu, 26.7 nM of anti-MBP antibody conjugated with d2 (Cisbio, cat #61MBPDAA), and
42
43 1 μ M all-*trans* retinol (Sigma, cat # 95144). All of the reactions were performed under dim
44
45 red light in the dark. The plates were read in the SpectraMax M5e Multimode Plate
46
47 Reader (Molecular Devices, Sunnyvale, CA) after the overnight incubation at 4 $^{\circ}$ C.
48
49
50 Fluorescence was excited at 337 nm; emission was measured at 668 and 620 nm with 75
51
52
53
54
55
56
57
58
59
60

1
2
3 μs counting delay. The HTRF signal was expressed as the ratio of fluorescence intensity:
4
5
6 $\text{Flu}_{668}/\text{Flu}_{620} \times 10,000$.

7
8 **Fluorescence Polarization TTR Tetramer Binding Assay.** Compound binding to TTR
9
10 was assessed in the fluorescence polarization assay. The assay measured competitive
11
12 displacement of the fluorescent probe, FITC-diclofenac, from TTR isolated from human
13
14 plasma (Clabiochem-Millipore, cat. No. 52957). FITC-diclofenac was synthesized at
15
16 LeadGen Labr, LLC following the published procedure.⁵⁹ Each well contained 200 nM TTR
17
18 and 100 nM FITC-diclofenac in the FP buffer (10 mM Tris-HCl pH 7.5, 150 mM NaCl, 0.01%
19
20 CHAPS, 0.01%Prionex) along with test compounds. Nonspecific binding was determined
21
22 in the presence of 500 μM unlabeled diclofenac (Sigma-Aldrich). Reactions with test
23
24 compounds were incubated overnight at 4 $^{\circ}\text{C}$ and FP was measured on SpectramaxM5e
25
26 plate reader (Molecular Devices).
27
28
29
30
31

32 **TTR Aggregation Assay.** The ability of test compounds to prevent TTR aggregation was
33
34 evaluated under the acidic conditions that favor TTR aggregation and fibril formation. A 2
35
36 μl solution of 167 μM human TTR (ACRO Biosystems #H5223) was incubated with 7 μl 50
37
38 mM sodium acetate pH 4.0 (Sigma # S7545), 100 mM KCl (Sigma # S5405) in the presence
39
40 or absence of 1 μl TTR inhibitor for 72 h at 37 $^{\circ}\text{C}$. At the end of the incubation, 3.5 μl 500
41
42 mM sodium phosphate (Sigma #S5136) buffer pH=8.0 was added to each sample for
43
44 neutralization and 0.6 μl 5% CHAPS (Sigma #C5070) as a detergent to prevent
45
46 reassociation of protein. The cross-linking was performed by adding 1.5 μl 5%
47
48 glutaraldehyde solution (Sigma# G6257). After 4 min, the reaction was stopped by the
49
50 addition of 2.5 μl freshly made 5% NaBH_4 . Samples were subjected to TTR western
51
52
53
54
55
56
57
58
59
60

1
2
3 blotting with prealbumin antibodies (1:500; Dako #A0002). Band intensity for TTR
4
5 monomer and TTR aggregates was quantified from scanned images of the blots.
6
7

8 **General Chemistry.** All reactions were performed under a dry atmosphere of nitrogen
9
10 unless otherwise specified. Indicated reaction temperatures refer to the reaction bath,
11
12 while room temperature (rt) is noted as 25 °C. Commercial grade reagents and anhydrous
13
14 solvents were used as received from vendors and no attempts were made to purify or dry
15
16 these components further. Removal of solvents under reduced pressure was
17
18 accomplished with a Buchi rotary evaporator at approximately 28 mm Hg pressure using
19
20 a Teflon-linked KNF vacuum pump. Thin layer chromatography was performed using 1" x
21
22 3" AnalTech No. 02521 silica gel plates with fluorescent indicator. Visualization of TLC
23
24 plates was made by observation with either short wave UV light (254 nm lamp), 10%
25
26 phosphomolybdic acid in ethanol or in iodine vapors. Preparative thin layer
27
28 chromatography was performed using Analtech, 20 × 20 cm, 1000 micron preparative TLC
29
30 plates. Flash column chromatography was carried out using a Teledyne Isco CombiFlash
31
32 Companion Unit and a Biotage® Selekt System with Teledyne Isco RediSep Rf and Biotage
33
34 Sfar silica gel columns. If needed, products were purified by reverse phase
35
36 chromatography, using a Teledyne Isco CombiFlash Companion Unit and a Biotage® Selekt
37
38 System with a RediSep Gold C18 reverse phase column. Proton NMR spectra were
39
40 obtained on a 400 MHz Varian nuclear magnetic resonance spectrometer. Chemical shifts
41
42 (δ) are reported in parts per million (ppm) and coupling constant (J) values are given in
43
44 Hz, with the following spectral pattern designations: s, singlet; d, doublet; t, triplet, q,
45
46 quartet; quint, quintet; m, multiplet; dd, doublet of doublets; dt, doublet of triplets; dq;
47
48
49
50
51
52
53
54
55
56
57

1
2
3 doublet of quartets; br, broad signal. Tetramethylsilane was used as an internal reference.
4
5
6 Peak listing, multiplicity designations, and coupling constant calculations were conducted
7
8 using Mnova v.14 software (Mestrelab Research). Carbon NMR spectra were obtained on
9
10 a 500 MHz Bruker AV III nuclear magnetic resonance spectrometer and tetramethylsilane
11
12 was used as an internal reference. Fluorine NMR spectra were obtained on a 400 MHz
13
14 Bruker AV III nuclear magnetic resonance spectrometer. Any melting points provided are
15
16 uncorrected and were obtained using a Stanford Research Systems OptiMelt melting
17
18 point apparatus (MPA100) with an automated melting point system. Mass spectroscopic
19
20 analyses were performed using ESI ionization on a Waters AQUITY UPLC MS triple
21
22 quadrapole mass spectrometer. High pressure liquid chromatography (HPLC) purity
23
24 analysis was performed using a Waters Breeze2 HPLC system with a binary solvent system
25
26 A and B using a gradient elution [A, H₂O with 0.1% formic acid; B, CH₃CN with 0.1% formic
27
28 acid] and flow rate = 0.5 mL/min, with UV detection at 254 nm (system equipped with a
29
30 photodiode array (PDA) detector). An ACQUITY UPLC BEH C18 column, 130 Å, 1.7 μm, 2.1
31
32 mm × 50 mm was used. High resolution mass spectrometry (HRMS) analysis was was
33
34 performed using an Agilent 6530 Accurate-Mass Q-TOF. All final compounds tested for *in*
35
36 *vitro* and *in vivo* biological testing were purified to ≥95% purity, and these purity levels
37
38 were measured by both ¹H NMR and HPLC.
39
40
41
42
43
44
45
46
47
48
49

50 *6-Methyl-2-(4-(2-(trifluoromethyl)phenoxy)piperidin-1-yl)pyrimidine-4-carboxylic*

51
52 *Acid (21)*. Step A: To a 0 °C cooled solution of *tert*-butyl 4-oxopiperidine-1-carboxylate
53
54 (**15**, 5.0 g, 25.1 mmol) in CH₃OH (50 mL) at was added NaBH₄ (1.14 g, 30.1 mmol). The
55
56
57
58
59
60

1
2
3 mixture stirred for 8 h while gradually warming to rt. The mixture was concentrated under
4 reduced pressure and the resulting residue was diluted with H₂O (100 mL) and extracted
5 with CH₂Cl₂ (2 × 100 mL). The combined organic extracts were dried over Na₂SO₄, filtered,
6 and evaporated under reduced pressure to give *tert*-butyl 4-hydroxypiperidine-1-
7 carboxylate (**16**) as a white solid (4.5 g, 89%): ¹H NMR (400 MHz, CDCl₃): δ 3.91-3.75 (m,
8 3H), 3.05-2.96 (m, 2H), 1.90-1.79 (m, 2H), 1.49-1.40 (m, 11H); ES MS: *m/z* 224 [M + Na]⁺.
9
10
11
12
13
14
15
16
17

18 Step B: To a 0 °C cooled solution of *tert*-butyl 4-hydroxypiperidine-1-carboxylate (**16**,
19 4.5 g, 22.3 mmol) in CH₂Cl₂ (50 mL) were added Et₃N (4.7 ml, 33.5 mmol) and DMAP (0.127
20 g, 1.10 mmol) followed by the addition of TsCl (5.10 g, 26.8 mmol). The resulting solution
21 was stirred for 16 h while gradually warming to rt under an atmosphere of N₂. The mixture
22 was diluted with saturated aqueous NaOH (50 mL) and extracted with EtOAc (3 × 100 mL).
23 The combined organic extracts were washed with H₂O (100 mL), brine (100 mL), dried
24 over Na₂SO₄, filtered, and concentrated under reduced pressure. The resulting residue
25 was chromatographed over silica gel (0% to 50% EtOAc in hexanes) to give *tert*-butyl 4-
26 (tosyloxy)piperidine-1-carboxylate (**17**) as a colorless liquid (6.6 g, 84%): ¹H NMR (400
27 MHz, CDCl₃) δ 7.82 (m, 2H), 7.49 (m, 2H), 4.69 (br, 1H), 3.49 (m, 2H), 3.15 (m, 2H), 2.43
28 (br, 3H), 1.70 (m, 2H), 1.51 (m, 2H), 1.38 (s, 9H); ESI MS *m/z* 356 [M + H]⁺.
29
30
31
32
33
34
35
36
37
38
39
40
41
42
43
44

45 Step C: To a solution of *tert*-butyl 4-(tosyloxy)piperidine-1-carboxylate (**17**, 0.250 g,
46 0.703 mmol) in anhydrous DMF (4 mL) were added Cs₂CO₃ (0.450 g, 1.38 mmol) and 2-
47 (trifluoromethyl)phenol (95.0 mg, 0.586 mmol) and the resulting solution was stirred at
48 80 °C for 16 h under an atmosphere of N₂. The mixture was allowed to cool to rt and then
49 diluted with H₂O (20 mL). The aqueous mixture was extracted with EtOAc (3 × 25 mL) and
50
51
52
53
54
55
56
57
58
59
60

1
2
3 the combined organic extracts were washed with H₂O (3 × 25 mL), brine (25 mL), dried
4
5 over Na₂SO₄, filtered, and concentrated under reduced pressure. The resulting residue
6
7 was chromatographed over silica gel (0% to 30% EtOAc in hexanes) to give *tert*-butyl 4-
8
9 (2-(trifluoromethyl)phenoxy)piperidine-1-carboxylate (**18**) as a white solid (0.118 g, 56%):
10
11 ¹H NMR (400 MHz, acetone-*d*₆) δ 7.65-7.55 (m, 2H), 7.30 (d, *J* = 8.0 Hz, 1H), 7.08 (t, *J* = 7.6
12
13 Hz, 1H), 4.92-4.82 (m, 1H), 3.67-3.57 (m, 2H), 3.50-3.40 (m, 2H), 2.0-1.90 (m, 2H), 1.80-
14
15 1.70 (m, 2H), 1.45 (s, 9H); ESI MS *m/z* 346 [M + H]⁺.
16
17
18
19

20 Step D: To a 0 °C cooled solution of *tert*-butyl 4-(2-
21
22 (trifluoromethyl)phenoxy)piperidine-1-carboxylate (**18**, 0.118 g, 0.341 mmol) in CH₂Cl₂
23
24 (10 mL) was added TFA (0.33 mL, 4.31 mmol) and the resulting solution was stirred for 16
25
26 h while gradually warming to rt. The mixture was neutralized by being carefully poured
27
28 into a solution of saturated aqueous NaHCO₃ (10 mL). The biphasic mixture was separated
29
30 and the aqueous layer was further extracted with CH₂Cl₂ (3 × 20 mL). The combined
31
32 organic extracts were washed with brine (20 mL), dried over Na₂SO₄, filtered, and
33
34 concentrated under reduced pressure to give 4-(2-(trifluoromethyl)phenoxy)piperidine
35
36 (**19**) as a white solid (80.0 mg, 95%): ¹H NMR (400 MHz, acetone-*d*₆) δ 7.70-7.60 (m, 2H),
37
38 7.37 (d, *J* = 6.0 Hz, 1H), 7.14 (t, *J* = 7.6 Hz, 1H), 5.10-5.03 (m, 1H), 3.50-3.40 (m, 4H), 2.47-
39
40 2.37 (m, 2H), 2.21-2.11 (m, 2H); ESI MS *m/z* 246 [M + H]⁺.
41
42
43
44
45
46

47 Step E: A mixture of 4-(2-(trifluoromethyl)phenoxy)piperidine (**19**, 0.100 g, 0.408
48
49 mmol), methyl 2-chloro-6-methylpyrimidine-4-carboxylate (76.1 mg, 0.408 mmol), and *i*-
50
51 Pr₂NEt (0.21 mL, 1.22 mmol) in THF (10 mL) was heated at reflux for 16 h under an
52
53 atmosphere of N₂. The reaction was concentrated under reduced pressure and the
54
55
56
57

1
2
3 resulting residue was chromatographed over silica gel (0% to 100% EtOAc in hexanes) to
4
5 give methyl 6-methyl-2-(4-(2-(trifluoromethyl)phenoxy)piperidin-1-yl)pyrimidine-4-
6
7 carboxylate (**20**) as an off-white solid (0.140 g, 87%): MS (ESI+) m/z 396 [M + H]⁺.
8
9

10 Step F: A solution of methyl 6-methyl-2-(4-(2-(trifluoromethyl)phenoxy)piperidin-1-
11
12 yl)pyrimidine-4-carboxylate (**20**, 0.100 g, 0.253 mmol) and LiOH (18.1 mg, 0.758 mmol) in
13
14 CH₃OH (5 mL), THF (5 mL), and H₂O (5 mL) stirred at rt for 16 h. The mixture was acidified
15
16 to pH = 5 with 2 N aqueous HCl and extracted with CH₂Cl₂ (3 × 10 mL). The combined
17
18 organic extracts were washed with brine (20 mL), dried over Na₂SO₄, filtered, and
19
20 concentrated under reduced pressure to give 6-methyl-2-(4-(2-
21
22 (trifluoromethyl)phenoxy)piperidin-1-yl)pyrimidine-4-carboxylic acid (**21**) as an off-white
23
24 solid (87.8 mg, 91%): ¹H NMR (400 MHz, CDCl₃) δ 7.56-7.53 (m, 2H), 7.22 (d, *J* = 6.0 Hz,
25
26 2H), 7.02-7.51 (m, 1H), 4.86 (br, 1H), 3.99-3.85 (m, 4H), 2.37 (s, 3H), 2.05-1.95 (m, 2H),
27
28 1.81-1.80 (m, 2H); ESI MS m/z 382 [M + H]⁺; HPLC >99% (AUC), *t*_R = 16.8 min.
29
30
31
32
33
34

35 (*±*)-6-Methyl-2-(3-(2-(trifluoromethyl)phenoxy)pyrrolidin-1-yl)pyrimidine-4-carboxylic
36
37 Acid ((*±*)-**27**). Step A: To a 0 °C cooled solution of (*±*)-*tert*-butyl 3-hydroxypyrrolidine-1-
38
39 carboxylate ((*±*)-**22**, 1.00 g, 5.34 mmol) in CH₂Cl₂ (20 mL) were added Et₃N (1.1 mL, 8.02
40
41 mmol) and DMAP (32.0 mg, 0.262 mmol) followed by the addition of TsCl (1.10 g, 5.88
42
43 mmol). The resulting solution was stirred for 16 h while gradually warming to rt under an
44
45 atmosphere of N₂. The mixture was diluted with saturated aqueous NaOH (20 mL) and
46
47 extracted with EtOAc (3 × 50 mL). The combined organic extracts were washed with H₂O
48
49 (50 mL) and brine (50 mL), dried over Na₂SO₄, filtered, and concentrated under reduced
50
51 pressure. The resulting residue was chromatographed over silica gel (0% to 50% EtOAc in
52
53
54
55
56
57
58
59
60

1
2
3 hexanes) to give (\pm)-*tert*-butyl 3-(tosyloxy)pyrrolidine-1-carboxylate ((\pm)-**23**) as a colorless
4
5 liquid (1.50 g, 82%): $^1\text{H NMR}$ (400 MHz, CDCl_3) δ 7.81 (d, J = 8.9 Hz, 2H), 7.34 (d, J = 7.8 Hz,
6
7 2H), 5.05 (br, 1H), 3.43 (m, 4H), 2.43 (br, 3H), 2.06 (m, 2H), 1.45 (s, 9H); ESI MS m/z 342
8
9 [M + H] $^+$.
10

11
12
13 Step B: To a solution of (\pm)-*tert*-butyl 3-(tosyloxy)pyrrolidine-1-carboxylate ((\pm)-**23**,
14
15 0.100 g 0.293 mmol) in DMF (4 mL) were added Cs_2CO_3 (0.290 g, 0.902 mmol) and 2-
16
17 (trifluoromethyl)phenol (73.0 mg, 0.450 mmol) and the resulting mixture was stirred at
18
19 80 °C for 16 h under an atmosphere of N_2 . The mixture was allowed to cool to rt and then
20
21 diluted with H_2O (20 mL). The aqueous mixture was extracted with EtOAc (3 \times 25 mL) and
22
23 the combined organic extracts were washed with H_2O (3 \times 25 mL), brine (25 mL), dried
24
25 over Na_2SO_4 , filtered, and concentrated under reduced pressure. The resulting residue
26
27 was chromatographed over silica gel (0% to 30% EtOAc in hexanes) to give (\pm)-*tert*-butyl
28
29 3-(2-(trifluoromethyl)phenoxy)pyrrolidine-1-carboxylate ((\pm)-**24**) as a white solid (80.0
30
31 mg, 83%): $^1\text{H NMR}$ (400 MHz, acetone- d_6) δ 7.62 (m, 2H), 7.34 (d, J = 8.0 Hz 1H), 7.15 (t, J
32
33 = 7.6 Hz, 1H), 5.20 (s, 1H), 3.65-3.40 (m, 4H), 2.19 (m, 2H), 1.44 (s, 9H); ESI MS m/z 332
34
35 [M + H] $^+$.
36
37
38
39
40
41

42 Step C: To a 0 °C cooled solution of (\pm)-*tert*-butyl 3-(2-
43
44 (trifluoromethyl)phenoxy)pyrrolidine-1-carboxylate ((\pm)-**24**, 80.0 mg, 0.241 mmol) in
45
46 CH_2Cl_2 (5 mL) was added TFA (0.18 mL, 2.41 mmol) and the resulting solution was stirred
47
48 at for 8 h while gradually warming to rt. The mixture was neutralized by carefully pouring
49
50 it into a solution of saturated aqueous NaHCO_3 (10 mL). The biphasic mixture was
51
52 separated and the aqueous layer was further extracted with CH_2Cl_2 (3 \times 20 mL). The
53
54
55
56
57

1
2
3 combined organic extracts were washed with brine (20 mL), dried over Na₂SO₄, filtered,
4
5 and concentrated under reduced pressure to give (±)-3-(2-
6 (trifluoromethyl)phenoxy)pyrrolidine ((±)-**25**) as a white solid (50.0 mg, 90%); ESI MS *m/z*
7
8 232 [M + H]⁺.
9
10

11
12
13 Step D: A mixture of (±)-3-(2-(trifluoromethyl)phenoxy)pyrrolidine ((±)-**25**, 0.100 g,
14
15 0.432 mmol), methyl 2-chloro-6-methylpyrimidine-4-carboxylate (80.6 mg, 0.432 mmol),
16
17 and *i*-Pr₂NEt (0.23 mL, 1.29 mmol) in THF (10 mL) was heated at reflux for 16 h under an
18
19 atmosphere of N₂. The reaction was allowed to cool to rt and then concentrated under
20
21 reduced pressure. The resulting residue was chromatographed over silica gel (0% to 100%
22
23 EtOAc in hexanes) to give (±)-methyl 6-methyl-2-(3-(2-
24 (trifluoromethyl)phenoxy)pyrrolidin-1-yl)pyrimidine-4-carboxylate ((±)-**26**) as an off-
25
26 white solid (0.145 g, 88%): ¹H NMR (400 MHz, CDCl₃) δ 7.52 (d, *J* = 8.0 Hz, 1H), 7.45 (t, *J* =
27
28 7.6 Hz, 1H), 7.00 (s, 1H), 6.98-6.95 (m, 2H), 5.10 (s, 1H), 4.00-3.86 (m, 3H), 3.89 (s, 3H),
29
30 3.76-3.74 (m, 2H), 2.38 (s, 3H), 2.22-2.19 (m, 1H); ESI MS *m/z* 382 [M + H]⁺.
31
32
33
34
35
36

37
38 Step E: A solution of (±)-methyl 6-methyl-2-(3-(2-(trifluoromethyl)phenoxy)pyrrolidin-
39
40 1-yl)pyrimidine-4-carboxylate ((±)-**26**, 48.8 g, 0.128 mmol) and LiOH (9.21 mg, 0.384
41
42 mmol) in CH₃OH (5 mL), THF (5 mL), and H₂O (5 mL) was stirred at rt for 16 h. The mixture
43
44 was acidified to pH 5 with 2 N aqueous HCl and extracted with CH₂Cl₂ (3 × 10 mL). The
45
46 combined organic extracts were washed with brine, dried over Na₂SO₄, filtered, and
47
48 concentrated under reduced pressure to give (±)-6-methyl-2-(3-(2-
49
50 (trifluoromethyl)phenoxy)pyrrolidin-1-yl)pyrimidine-4-carboxylic acid ((±)-**27**) as an off-
51
52 white solid (0.043 g, 91%): ¹H NMR (400 MHz, DMSO-*d*₆) δ 7.61-7.54 (m, 2H), 7.34-7.33
53
54
55
56
57
58
59
60

1
2
3 (m, 1H), 7.00-6.93 (m, 2H), 5.31 (s, 1H), 3.77-3.86 (m, 3H), 3.50-3.48 (m, 1H), 2.30 (s, 3H),
4
5 2.29-2.20 (m, 2H); ESI MS m/z 368 [M + H]⁺; HPLC >99% (AUC), t_R = 14.5 min.

6
7
8 *6-Methyl-2-(3-(2-(trifluoromethyl)phenoxy)azetidin-1-yl)pyrimidine-4-carboxylic Acid*

9
10 **(32)**. Step A: To a solution of *tert*-butyl 3-(tosyloxy)azetidine-1-carboxylate (**28**, 0.500 g
11
12 1.52 mmol) in DMF (20 mL) were added Cs₂CO₃ (990 mg, 3.05 mmol) and 2-
13
14 (trifluoromethyl)phenol (0.272 g, 1.68 mmol) and the resulting solution was stirred at 80
15
16 °C for 16 h under an atmosphere of N₂. The mixture was allowed to cool to rt and then
17
18 diluted with H₂O (50 mL) and extracted with EtOAc (3 × 50 mL). The combined organic
19
20 extracts were washed with H₂O (3 × 50 mL), brine, dried over Na₂SO₄, filtered, and
21
22 concentrated under reduced pressure. The resulting residue was chromatographed over
23
24 silica gel (0% to 30% EtOAc in hexanes) to give *tert*-butyl 3-(2-
25
26 (trifluoromethyl)phenoxy)azetidine-1-carboxylate (**29**) as a colorless liquid (0.400 g, 82%):
27
28 ¹H NMR (400 MHz, CDCl₃) δ 7.59 (d, J = 7.3 Hz, 1H), 7.61-7.45 (m, 1H), 7.06-7.03 (m, 1H),
29
30 6.65 (d, J = 7.9 Hz, 1H), 4.99-4.91 (m, 1H), 4.35-4.30 (m, 2H), 4.10-4.05 (m, 2H), 1.44 (s,
31
32 9H); ESI MS m/z 318 [M + H]⁺.

33
34
35
36
37
38
39
40 Step B: To a 0 °C cooled solution of *tert*-butyl 3-(2-(trifluoromethyl)phenoxy)azetidine-
41
42 1-carboxylate (**29**, 0.400 g, 1.20 mmol) in CH₂Cl₂ (20 mL) was TFA (0.96 mL, 12.0 mmol)
43
44 and the resulting solution was stirred for 16 h while gradually warming to rt. The mixture
45
46 neutralized by carefully pouring it into a solution of saturated aqueous NaHCO₃ (10 mL).
47
48 The biphasic mixture was separated and the aqueous layer was further extracted with
49
50 CH₂Cl₂ (3 × 20 mL). The combined organic extracts were washed with brine (20 mL), dried
51
52 over Na₂SO₄, filtered, and concentrated under reduced pressure to give 3-(2-
53
54
55
56
57
58
59
60

(trifluoromethyl)phenoxy)azetidide (**30**) as a white solid (0.240 g, 87%): ESI MS m/z 218 [M + H]⁺.

Step C: A mixture of 3-(2-(trifluoromethyl)phenoxy)azetidide (**30**, 0.100 g, 0.460 mmol), methyl 2-chloro-6-methylpyrimidine-4-carboxylate (85.9 mg, 0.460 mmol), and *i*-Pr₂NEt (0.24 mL, 1.38 mmol) in THF (10 mL) was heated at reflux for 16 h under an atmosphere of N₂. The reaction was concentrated under reduced pressure and the resulting residue was chromatographed over silica gel (0% to 100% EtOAc in hexanes) to give methyl 6-methyl-2-(3-(2-(trifluoromethyl)phenoxy)azetidide-1-yl)pyrimidine-4-carboxylate (**31**) as an off-white solid (0.152 g, 90%): MS (ESI+) m/z [M + H]⁺.

Step D: A solution of methyl 6-methyl-2-(3-(2-(trifluoromethyl)phenoxy)azetidide-1-yl)pyrimidine-4-carboxylate (**31**, 0.100 g, 0.272 mmol) and LiOH (19.5 mg, 0.816 mmol) in CH₃OH (5 mL), THF (5 mL), and H₂O (5 mL) stirred at rt for 16 h. The mixture was acidified to pH 5 with 2 N aqueous HCl and extracted with CH₂Cl₂ (3 × 10 mL). The combined organic extracts were washed with brine (10 mL), dried over Na₂SO₄, filtered, and concentrated under reduced pressure to give 6-methyl-2-(3-(2-(trifluoromethyl)phenoxy)azetidide-1-yl)pyrimidine-4-carboxylic acid (**32**) as an off-white solid (83.6 mg, 87%): ¹H NMR (400 MHz, CDCl₃) δ 7.59-7.54 (m, 2H), 7.14 (s, 1H), 7.08 (t, *J* = 7.6 Hz, 1H), 6.94 (d, *J* = 8.0 Hz, 1H), 5.28 (m, 1H), 4.61-4.60 (m, 2H), 4.15-4.12 (m, 2H), 2.40 (s, 3H); ESI MS m/z 354 [M + H]⁺; ESI MS m/z 354 [M + H]⁺; HPLC >99% (AUC), *t*_R = 14.1 min.

6-Methyl-2-(3-((2-(trifluoromethyl)phenoxy)methyl)azetidide-1-yl)pyrimidine-4-carboxylic Acid (38). Step A: To a 0 °C cooled solution of *tert*-butyl 3-(hydroxymethyl)azetidide-1-carboxylate (**33**, 3.0 g, 16.0 mmol) in CH₂Cl₂ (50 mL) were

1
2
3 added Et₃N (4.5 ml, 32.0 mmol) and DMAP (97.0 mg, 0.736 mmol) followed by the
4
5 addition of TsCl (3.35 g, 17.6 mmol). The resulting solution was stirred for 16 h while
6
7 gradually warming to rt under an atmosphere of N₂. The mixture was diluted with
8
9 saturated solution of aqueous NaOH (50 mL) and was extracted with EtOAc (3 × 100 mL).
10
11 The combined organic extracts were washed with H₂O (50 mL) and brine (50 mL), dried
12
13 over Na₂SO₄, filtered, and concentrated under reduced pressure to give *tert*-butyl 3-
14
15 ((tosyloxy)methyl)azetidone-1-carboxylate (**34**) as a colorless liquid (5.0 g, 92%): ESI MS
16
17 *m/z* 342 [M + H]⁺.
18
19
20
21
22

23 Step B: To a solution of *tert*-butyl 3-((tosyloxy)methyl)azetidone-1-carboxylate (**34**, 5.0
24
25 g 14.6 mmol) in DMF (50 mL) were added Cs₂CO₃ (9.5 g, 29.32 mmol) and 2-
26
27 (trifluoromethyl)phenol (2.3 g, 14.6 mmol) and the resulting mixture was stirred at 80 °C
28
29 for 16 h under an atmosphere of N₂. The mixture was allowed to cool to rt and then
30
31 diluted with H₂O (100 mL) and extracted with EtOAc (3 × 50 mL). The combined organic
32
33 extracts were washed with H₂O (3 × 50 mL), brine (50 mL), dried over Na₂SO₄, filtered,
34
35 and concentrated under reduced pressure to give crude *tert*-butyl 3-((2-
36
37 (trifluoromethyl)phenoxy)methyl)azetidone-1-carboxylate (**35**) as a brown liquid (4.5 g,
38
39 93%): ESI MS *m/z* 332 [M + H]⁺.
40
41
42
43
44

45 Step C: To a 0 °C cooled solution of *tert*-butyl 3-((2-
46
47 (trifluoromethyl)phenoxy)methyl)azetidone-1-carboxylate (**35**, 4.50 g, 13.59 mmol) in
48
49 CH₂Cl₂ (50 mL) was added TFA (10.3 mL, 135 mmol) and the resulting solution was stirred
50
51 at for 8 h while gradually warming to rt. The mixture was neutralized by carefully pouring
52
53 it into a solution of saturated aqueous NaHCO₃ (10 mL). The biphasic mixture was
54
55
56
57
58
59
60

1
2
3 separated and the aqueous layer was further extracted with CH₂Cl₂ (3 × 20 mL). The
4
5 combined organic extracts were washed with brine (20 mL), dried over Na₂SO₄, filtered,
6
7 and concentrated under reduced pressure to give 3-((2-
8
9 (trifluoromethyl)phenoxy)methyl)piperidine (**36**) as a white solid (2.8 g, 90% crude): ESI
10
11 MS *m/z* 232 [M + H]⁺.
12
13

14
15 Step D: A mixture of 3-((2-(trifluoromethyl)phenoxy)methyl)azetidine (**36**, 1.0 g, 4.32
16
17 mmol), methyl 2-chloro-6-methylpyrimidine-4-carboxylate (0.807 g, 4.32 mmol), and *i*-
18
19 Pr₂NEt (2.25 mL, 12.9 mmol) in THF (20 mL) was heated at reflux for 16 h under an
20
21 atmosphere of N₂. The reaction was concentrated under reduced pressure and the
22
23 resulting residue was chromatographed over silica gel (0% to 100% EtOAc in hexanes) to
24
25 give methyl 6-methyl-2-(3-((2-(trifluoromethyl)phenoxy)methyl)azetid-1-yl)pyrimidine-
26
27 4-carboxylate (**37**) as an off-white solid (1.64 g, 86%): ¹H NMR (400 MHz, CDCl₃) δ 7.52 (d,
28
29 *J* = 7.6 Hz, 1H), 7.45 (t, *J* = 7.6 Hz, 1H), 7.05 (s, 1H), 7.00-6.95 (m, 2H), 4.33 (t, *J* = 8.8 Hz,
30
31 2H), 4.22-4.21 (m, 2H), 4.08-4.04 (m, 2H), 3.91 (s, 3H), 3.18-3.16 (m, 1H), 2.40 (s, 3H); ESI
32
33 MS *m/z* 382 [M + H]⁺.
34
35
36
37
38

39
40 Step E: A solution of methyl 6-methyl-2-(3-((2-
41
42 (trifluoromethyl)phenoxy)methyl)azetid-1-yl)pyrimidine-4-carboxylate (**37**, 1.0 g, 2.62
43
44 mmol) and LiOH (0.188 g, 7.86 mmol) in CH₃OH (10 mL), THF (10 mL), and H₂O (10 mL)
45
46 was stirred at rt for 16 h. The mixture was acidified to pH = 5 with 2 N aqueous HCl and
47
48 extracted with CH₂Cl₂ (3 × 10 mL). The combined organic extracts were washed with brine
49
50 (10 mL), dried over Na₂SO₄, filtered, and concentrated under reduced pressure to give 6-
51
52 methyl-2-(3-((2-(trifluoromethyl)phenoxy)methyl)azetid-1-yl)pyrimidine-4-carboxylic
53
54
55
56
57

1
2
3 acid (**38**) as an off-white solid (0.914 g, 95%): $^1\text{H NMR}$ (400 MHz, CDCl_3) δ 7.51 (d, $J = 7.6$
4 Hz, 1H), 7.46 (t, $J = 7.6$ Hz, 1H), 7.00 (s, 1H), 7.00-6.94 (m, 2H), 4.33 (t, $J = 8.4$ Hz, 2H), 4.24-
5 4.22 (m, 2H), 4.07-4.03 (m, 2H), 3.17-3.15 (m, 1H), 2.42 (s, 3H); ESI MS m/z 368 $[\text{M} + \text{H}]^+$;
6
7 HPLC 98.2% (AUC), $t_R = 13.5$ min.

8
9
10
11
12
13 *(±)*-6-Methyl-2-(3-((2-(trifluoromethyl)phenoxy)methyl)pyrrolidin-1-yl)pyrimidine-4-
14
15 *carboxylic Acid ((±)-44)*. Step A: To a 0 °C solution of (*±*)-*tert*-butyl 3-
16 (hydroxymethyl)pyrrolidine-1-carboxylate ((*±*)-**39**, 2.0 g, 9.93 mmol), Et_3N (2.8 ml, 83.7
17 mmol), and DMAP (60.4 mg, 0.494 mmol) in CH_2Cl_2 (50 mL) was added TsCl (2.27 g, 11.9
18 mmol). The resulting mixture was stirred for 16 h while gradually warming to rt under an
19 atmosphere of N_2 . The mixture was diluted with saturated aqueous NaOH solution (50
20 mL) and then extracted with EtOAc (3 × 100 mL). The combined organic extracts were
21 washed with H_2O (50 mL), brine (50 mL), dried over Na_2SO_4 , filtered, and concentrated
22 under reduced pressure. The resulting residue was chromatographed over silica gel (0–
23 30% EtOAc in hexanes) to give (*±*)-*tert*-butyl 3-((tosyloxy)methyl)pyrrolidine-1-
24 carboxylate ((*±*)-**40**) as a white solid (3.1g, 88%): $^1\text{H NMR}$ (400 MHz, $\text{DMSO}-d_6$) δ 7.76 (d, J
25 = 8.4 Hz, 2H), 7.46 (d, $J = 8.4$ Hz, 2H), 3.97 (d, $J = 6.8$ Hz, 2H), 3.28-3.25 (m, 1H), 3.24-3.19
26 (m, 2H), 3.13-3.10 (m, 1H), 2.85-2.81 (m, 1H), 2.39 (s, 3H), 1.82-1.81 (m, 1H), 1.49-1.47
27 (m, 1H), 1.33 (s, 9H); ESI MS m/z 356 $[\text{M} + \text{H}]^+$.

28
29
30
31
32
33
34
35
36
37
38
39
40
41
42
43
44
45
46
47 Step B: To a solution of (*±*)-*tert*-butyl 3-((tosyloxy)methyl)pyrrolidine-1-carboxylate
48 ((*±*)-**40**, 1.0 g 2.81 mmol) in DMF (10 mL) were added Cs_2CO_3 (2.74 g, 8.41 mmol) and 2-
49 (trifluoromethyl)phenol (0.410 g, 2.53 mmol) and the resulting mixture was stirred at 80
50 °C for 16 h under an atmosphere of N_2 . The mixture was allowed to cool to rt and then
51
52
53
54
55
56
57

1
2
3 diluted with H₂O (30 mL). The aqueous mixture was extracted with EtOAc (3 × 50 mL) and
4
5 the combined organic extracts were washed with H₂O (3 × 50 mL), brine (50 mL), dried
6
7 over Na₂SO₄, filtered, and concentrated under reduced pressure. The resulting residue
8
9 was chromatographed over silica gel (0% to 30% EtOAc in hexanes) to give (±)-*tert*-butyl
10
11 3-((2-(trifluoromethyl)phenoxy)methyl)pyrrolidine-1-carboxylate ((±)-**41**) as a white solid
12
13 (0.816 g, 84%): ¹H NMR (400 MHz, DMSO-*d*₆) δ 7.61-7.56 (m, 2H), 7.22 (d, *J* = 8.8 Hz, 1H),
14
15 7.06 (t, *J* = 7.6 Hz, 1H), 4.09-4.02 (m, 2H), 3.44-3.35 (m, 1H), 3.36-3.33 (m, 1H), 3.25-3.19
16
17 (m, 1H), 3.11-3.01 (m, 1H), 2.62-2.55 (m, 1H), 1.97 (br, 1H), 1.96-1.64 (m, 1H), 1.35 (s, 9H);
18
19 ESI MS *m/z* 346 [M + H]⁺.
20
21
22
23

24
25 Step C: To a 0 °C solution of (±)-*tert*-butyl 3-((2-
26
27 (trifluoromethyl)phenoxy)methyl)pyrrolidine-1-carboxylate ((±)-**41**, 0.800 g 2.32 mmol) in
28
29 CH₂Cl₂ (10 mL) was added TFA (3.5 mL, 46.3 mmol) and the resulting mixture was stirred
30
31 for 16 h while gradually warming to rt under an atmosphere of N₂. The mixture was
32
33 neutralized by carefully pouring it into a solution of saturated aqueous NaHCO₃ (50 mL)
34
35 and the resulting biphasic mixture was separated. The aqueous layer was further
36
37 extracted with CH₂Cl₂ (3 × 50 mL) and the combined organic extracts were washed with
38
39 brine (50 mL), dried over Na₂SO₄, filtered, and concentrated under reduced pressure to
40
41 give (±)-3-((2-(trifluoromethyl)phenoxy)methyl)pyrrolidine ((±)-**42**) as a white solid (0.520
42
43 g, 90%): ¹H NMR (400 MHz, DMSO-*d*₆) δ 9.25 (br, 1H), 7.62-7.57 (m, 2H), 7.22 (d, *J* = 8.4
44
45 Hz, 1H), 7.07 (t, *J* = 7.6 Hz, 1H), 4.16-4.05 (m, 2H), 3.38-3.33 (m, 1H), 3.28-3.16 (m, 2H),
46
47 2.98 (t, *J* = 8.0 Hz, 1H), 2.77-2.69 (m, 1H), 2.11-2.03 (m, 1H), 1.78-1.69 (m, 1H); ESI MS *m/z*
48
49 346 [M + H]⁺; ESI MS *m/z* 246 [M + H]⁺.
50
51
52
53
54
55
56
57
58
59
60

1
2
3 Step D: To a solution of (\pm)-*tert*-butyl 3-((2-
4 (trifluoromethyl)phenoxy)methyl)pyrrolidine-1-carboxylate ((\pm)-**42**, 0.265 g 1.08 mmol) in
5 THF (5 mL) were added *i*-Pr₂NEt (0.6 mL, 3.24 mmol) and methyl 2-chloro-6-
6 methylpyrimidine-4-carboxylate (0.242 g, 1.29 mmol) and the resulting mixture stirred at
7 reflux for 16 h. The mixture was allowed to cool to rt and then concentrated under
8 reduced pressure. The resulting residue was chromatographed over silica gel (0% to 50%
9 EtOAc in hexanes) to give (\pm)-methyl 6-methyl-2-(3-((2-
10 (trifluoromethyl)phenoxy)methyl)pyrrolidin-1-yl)pyrimidine-4-carboxylate ((\pm)-**43**) as a
11 white solid (0.362 g, 85%): ¹H NMR (400 MHz, CDCl₃) δ 7.54 (d, *J* = 7.6 Hz, 1H), 7.44 (t, *J* =
12 7.6 Hz, 1H), 6.99 (s, 1H), 6.97-6.92 (m, 2H), 4.10-4.06 (m, 1H), 4.00-3.96 (m, 1H), 3.91 (s,
13 3H), 3.89-3.86 (m, 1H), 3.79-3.76 (m, 1H), 3.66-3.61 (m, 1H), 3.51-3.47 (m, 1H), 2.86-2.82
14 (m, 1H), 2.39 (s, 3H), 2.24-2.20 (m, 1H), 1.99-1.94 (m, 1H); ESI MS *m/z* 396 [M + H]⁺.

15
16
17
18
19
20
21
22
23
24
25
26
27
28
29
30
31
32 Step E: To a solution of (\pm)-methyl 6-methyl-2-(3-((2-
33 (trifluoromethyl)phenoxy)methyl)pyrrolidin-1-yl)pyrimidine-4-carboxylate ((\pm)-**43**, 0.250
34 g, 0.632 mmol) in CH₃OH (4 mL), THF (4 mL), and H₂O (2 mL) was added LiOH (0.151 g,
35 6.32 mmol) and the mixture stirred at rt for 16 h. The mixture was concentrated under
36 reduced pressure to remove the volatile solvents and the resulting aqueous mixture was
37 diluted with additional H₂O (10 mL) and acidified with 2 N aqueous HCl to pH = 3. The
38 acidified mixture was extracted with EtOAc (3 \times 50 mL) and the combined organic extracts
39 were washed with brine (50 mL), dried over Na₂SO₄, filtered, and concentrated under
40 reduced pressure to give (\pm)-1-(4-(2-(trifluoromethyl)phenyl)piperidine-1-
41 carbonyl)pyrrolidine-2-carboxylic acid ((\pm)-**44**) as a white solid (0.160 g, 66%): Mp = 105 -
42
43
44
45
46
47
48
49
50
51
52
53
54
55
56
57
58
59
60

1
2
3 106 °C; ¹H NMR (400 MHz, DMSO-*d*₆) δ 7.59 (m, 2H, H₁ and H₃), 7.28 (d, *J* = 8.4 Hz, 1H, H₄),
4
5 7.09 (t, *J* = 7.6 Hz, 1H, H₂), 6.97 (s, 1H, H₅), 4.16-4.11 (dq, *J* = 16.1, 9.2 Hz, 2H, H₆ and H₇),
6
7 3.77 (dd, *J* = 11.4, 7.5 Hz, 1H, H₈), 3.70 (m, 1H, H₉), 3.52 (dt, *J* = 11.3, 7.6 Hz, 1H, H₁₀), 3.39
8
9 (dt, *J* = 9.2, 7.2 Hz, 1H, H₁₁), 2.76 (quint, *J* = 7.1 Hz, 1H, H₁₄), 2.35 (s, 3H, 3 × H₁₅), 2.19-2.09
10
11 (m, 1H, H₁₂), 1.87 (dq, *J* = 12.3, 8.0 Hz, 1H, H₁₃); ¹³C NMR (500 MHz, DMSO-*d*₆) δ 169.46,
12
13 166.28, 160.16, 156.37, 134.29, 126.74, 124.95, 122.79, 120.33, 116.88, 113.57, 107.71,
14
15 69.75, 49.00, 45.82, 27.54, 24.06; ¹⁹F NMR (400 MHz, DMSO-*d*₆) δ -59.98 (s, CF₃); ESI MS
16
17 *m/z* 382 [M + H]⁺; HRMS (ESI⁺) C₁₈H₁₈F₃N₃O₃ calculated [M + H]⁺ = 382.1379, observed [M
18
19 + H]⁺ = 382.1380; combustion analysis (%CHN): calculated for C₁₈H₁₈F₃N₃O₃•0.25H₂O: %C
20
21 = 56.03; %H = 4.83; %N = 10.89; found: %C = 56.04; %H = 4.89; %N = 10.86; HPLC 98.7%
22
23 (AUC), *t*_R = 14.5 min.

24
25
26
27
28
29
30
31 *(R)*-6-Methyl-2-(3-((2-(trifluoromethyl)phenoxy)methyl)pyrrolidin-1-yl)pyrimidine-4-
32
33 *carboxylic Acid ((R)*-**50**). Compound *(R)*-**50** was prepared from *tert*-butyl *(R)*-3-
34
35 (hydroxymethyl)pyrrolidine-1-carboxylate (*(R)*-**45**) according to a similar procedure
36
37 described for the synthesis of (±)-**44**: ¹H NMR (400 MHz, CDCl₃) δ 7.55 (d, *J* = 7.6 Hz, 1H),
38
39 7.45 (t, *J* = 7.6 Hz, 1H), 7.12 (s, 1H), 7.01-6.94 (m, 2H), 4.07-4.06 (m, 2H), 3.86-3.77 (m,
40
41 2H), 3.62-3.51 (m, 2H), 2.89-2.86 (m, 1H), 2.43 (s, 3H), 2.27-2.23 (m, 1H), 2.14-2.01 (m,
42
43 1H); ESI MS *m/z* 382 [M + H]⁺; HPLC >99% (AUC), *t*_R = 14.5 min.

44
45
46
47
48
49
50
51 *(S)*-6-Methyl-2-(3-((2-(trifluoromethyl)phenoxy)methyl)pyrrolidin-1-yl)pyrimidine-4-
52
53 *carboxylic Acid ((S)*-**56**). Compound *(S)*-**56** was prepared from *tert*-butyl *(S)*-3-
54
55 (hydroxymethyl)pyrrolidine-1-carboxylate (*(S)*-**51**) according to a similar procedure
56
57 described for the synthesis of (±)-**44**: ¹H NMR (400 MHz, CDCl₃) δ 7.56 (d, *J* = 8.0 Hz, 1H),
58
59
60

1
2
3 7.46 (t, $J = 8.4$ Hz, 1H), 7.12 (s, 1H), 7.01-6.94 (m, 2H), 4.07-4.06 (m, 2H), 3.86-3.77 (m,
4
5 2H), 3.62-3.51 (m, 2H), 2.90-2.85 (m, 1H), 2.44 (s, 3H), 2.26-2.24 (m, 1H), 2.14-2.01 (m,
6
7 1H); ESI MS m/z 382 [M + H]⁺; HPLC >99% (AUC), $t_R = 14.5$ min.
8
9

10 (*±*)-6-Methyl-2-(3-((2-(trifluoromethyl)phenoxy)methyl)piperidin-1-yl)pyrimidine-4-
11
12 *carboxylic Acid* ((*±*)-**62**). Step A: To a 0 °C solution of (*±*)-*tert*-butyl 3-
13
14 (hydroxymethyl)piperidine-1-carboxylate ((*±*)-**57**, 1.0 g, 4.65 mmol) in CH₂Cl₂ (20 mL)
15
16 were added Et₃N (0.81 ml, 5.80 mmol) and DMAP (52.0 mg, 0.426 mmol) followed by the
17
18 addition of TsCl (0.883 g, 4.65 mmol). The resulting solution was stirred for 16 h while
19
20 gradually warming to rt. The reaction mixture was diluted with saturated aqueous NaOH
21
22 solution (50 mL) and was extracted with EtOAc (3 × 100 mL). The combined organic
23
24 extracts were washed with H₂O (100 mL) and brine (100 mL), dried over Na₂SO₄, filtered,
25
26 and concentrated under reduced pressure to give (*±*)-*tert*-butyl 3-
27
28 ((tosyloxy)methyl)piperidine-1-carboxylate ((*±*)-**58**) as a colorless liquid (1.6 g, 94%): ESI
29
30 MS m/z 370 [M + H]⁺.
31
32
33
34
35
36

37 Step B: To a solution of (*±*)-*tert*-butyl 3-((tosyloxy)methyl)piperidine-1-carboxylate
38
39 ((*±*)-**58**, 0.500 g 1.35 mmol) in DMF (20 mL) were added Cs₂CO₃ (0.650 g, 2.00 mmol) and
40
41 2-(trifluoromethyl)phenol (0.219 g, 1.35 mmol) and the resulting mixture was stirred at
42
43 80 °C for 16 h under an atmosphere of N₂. The reaction mixture was allowed to cool to rt
44
45 and then diluted with H₂O (50 mL) and extracted with EtOAc (3 × 50 mL). The combined
46
47 organic extracts were washed with H₂O (3 × 50 mL), brine (50 mL), dried over Na₂SO₄,
48
49 filtered, and concentrated under reduced pressure to give (*±*)-*tert*-butyl 3-((2-
50
51
52
53
54
55
56
57
58
59
60

(trifluoromethyl)phenoxy)methyl)piperidine-1-carboxylate ((±)-**59**) as a brown oil (0.400 g, 82%): ESI MS m/z 360 [M + H]⁺.

Step C: To a 0 °C solution of (±)-*tert*-butyl 3-((2-(trifluoromethyl)phenoxy)methyl)piperidine-1-carboxylate ((±)-**59**, 0.400 g, 1.11 mmol) in CH₂Cl₂ (20 mL) was added TFA (0.85 mL, 11.1 mmol) and the resulting solution was stirred for 8 h while gradually warming to rt. The mixture was neutralized by carefully pouring it into a solution of saturated aqueous NaHCO₃ (10 mL). The biphasic mixture was separated and the aqueous layer was further extracted with CH₂Cl₂ (3 × 20 mL). The combined organic extracts were washed with brine (20 mL), dried over Na₂SO₄, filtered, and concentrated under reduced pressure to give (±)-3-((2-(trifluoromethyl)phenoxy)methyl)piperidine ((±)-**60**) as a white solid (0.250 g, 86%): ESI MS m/z 260 [M + H]⁺.

Step D: To a solution of (±)-3-((2-(trifluoromethyl)phenoxy)methyl)piperidine ((±)-**60**, 0.100 g, 0.385 mmol) in THF (5 mL) were added *i*-Pr₂NEt (0.20 mL, 1.16 mmol) and methyl 2-chloro-6-methylpyrimidine-4-carboxylate (71.8 mg, 0.385 mmol) and the resulting mixture stirred at reflux for 16 h under an atmosphere of N₂. The mixture was allowed to cool to rt and then concentrated under reduced pressure. The resulting residue was chromatographed over silica gel (0% to 50% EtOAc in hexanes) to give (±)-methyl 6-methyl-2-(3-((2-(trifluoromethyl)phenoxy)methyl)piperidin-1-yl)pyrimidine-4-carboxylate ((±)-**61**) as a white solid (0.137 g, 87%): ¹H NMR (400 MHz, DMSO-*d*₆) δ 7.59-7.55 (m, 2H), 7.22 (d, *J* = 8.4 Hz, 1H), 7.05 (t, *J* = 7.6 Hz, 1H), 6.94 (s, 1H), 4.79 (d, *J* = 12.8

1
2
3 Hz, 1H), 4.55 (d, $J = 12.8$ Hz, 1H), 4.04-3.96 (m, 2H), 3.80 (s, 3H), 2.93-2.83 (m, 3H), 2.29
4
5 (s, 3H), 1.85-1.71 (m, 4H); ESI MS m/z 410 $[M + H]^+$.
6

7
8 Step E: To a solution of (\pm)-methyl 6-methyl-2-(3-((2-
9
10 (trifluoromethyl)phenoxy)methyl)piperidin-1-yl)pyrimidine-4-carboxylate ((\pm)-**61**, 0.100
11
12 g, 0.244 mmol) in CH₃OH (4 mL), THF (4 mL), and H₂O (2 mL) was added LiOH (58.4 mg,
13
14 2.44 mmol) and the mixture stirred at rt for 16 h. The mixture was concentrated under
15
16 reduced pressure to remove the volatile solvents and the resulting aqueous mixture was
17
18 diluted with additional H₂O (10 mL) and acidified with 2 N aqueous HCl to pH = 3. The
19
20 acidified mixture was extracted with EtOAc (3 \times 50 mL) and the combined organic extracts
21
22 were washed with brine (50 mL), dried over Na₂SO₄, filtered, and concentrated under
23
24 reduced pressure to give (\pm)-6-methyl-2-(3-((2-
25
26 (trifluoromethyl)phenoxy)methyl)piperidin-1-yl)pyrimidine-4-carboxylic acid ((\pm)-**62**) as a
27
28 white solid (96.4 mg, 66%): ¹H NMR (400 MHz, DMSO-*d*₆) δ 7.60-7.56 (m, 2H), 7.23 (d, $J =$
29
30 8.8 Hz, 1H), 7.06 (t, $J = 8.0$ Hz, 1H), 6.91 (s, 1H), 4.77 (d, $J = 10.4$ Hz, 1H), 4.57 (d, $J = 13.2$
31
32 Hz, 1H), 4.02-4.00 (m, 2H), 2.92-2.84 (m, 3H), 2.29 (s, 3H), 1.93-1.71 (m, 4H), 1.41-1.39
33
34 (m, 2H); ESI MS m/z 396 $[M + H]^+$; HPLC >99% (AUC), $t_R = 16.2$ min.
35
36
37
38
39
40
41

42 (\pm)-6-Methyl-2-(7-(2-(trifluoromethyl)phenyl)-2,7-diazaspiro[4.4]nonan-2-
43
44 yl)pyrimidine-4-carboxylic Acid ((\pm)-**67**). Step A: A mixture of (\pm)-*tert*-butyl 2,7-
45
46 diazaspiro[4.4]nonane-2-carboxylate ((\pm)-**63**, 0.250 g, 1.11 mmol) and 1-bromo-2-
47
48 (trifluoromethyl)benzene (0.273 g, 1.22 mmol) in 1,4-dioxane was degassed with N₂ for 5
49
50 min followed by the addition of Cs₂CO₃ (1.08 g, 3.31 mmol), X-Phos (0.105 mg, 0.223
51
52 mmol) and Pd₂(dba)₃ (0.101 g, 0.112 mmol). The reaction mixture was stirred at 110 °C
53
54
55
56
57
58
59
60

1
2
3 for 16 h in a sealed vessel. The mixture was then allowed to cool to rt and concentrated
4
5 under reduced pressure. The resulting residue was chromatographed over silica gel (0%
6
7 to 30% EtOAc in hexane) to give (\pm)-methyl *tert*-butyl 7-(2-(trifluoromethyl)phenyl)-2,7-
8
9 diazaspiro[4.4]nonane-2-carboxylate ((\pm)-**64**) as an off-white amorphous solid (0.230 g,
10
11 56%): ESI MS m/z 371 [M + H]⁺.
12
13
14

15 Step B: To a 0 °C solution of (\pm)-methyl *tert*-butyl 7-(2-(trifluoromethyl)phenyl)-2,7-
16
17 diazaspiro[4.4]nonane-2-carboxylate ((\pm)-**64**, 0.100 g, 2.69 mmol) in CH₂Cl₂ (5 mL) was
18
19 added TFA (0.20 mL, 2.61 mmol) and the resulting solution was stirred for 8 h while
20
21 gradually warming to rt. The mixture was neutralized by carefully pouring it into a solution
22
23 of saturated aqueous NaHCO₃ (10 mL). The biphasic mixture was separated and the
24
25 aqueous layer was further extracted with CH₂Cl₂ (3 × 20 mL). The combined organic
26
27 extracts were washed with brine (20 mL), dried over Na₂SO₄, filtered, and concentrated
28
29 under reduced pressure to give (\pm)-2-(2-(trifluoromethyl)phenyl)-2,7-
30
31 diazaspiro[4.4]nonane ((\pm)-**65**) as a white solid (65.0 mg, 90%): ESI MS m/z 271 [M + H]⁺.
32
33
34
35
36

37 Step C: To a solution of (\pm)-2-(2-(trifluoromethyl)phenyl)-2,7-diazaspiro[4.4]nonane
38
39 ((\pm)-**65**, 0.150 g, 0.554 mmol) in THF (5 mL) were added *i*-Pr₂NEt (0.29 mL, 1.66 mmol) and
40
41 methyl 2-chloro-6-methylpyrimidine-4-carboxylate (0.103 g, 0.554 mmol) and the
42
43 resulting mixture stirred at reflux for 16 h under an atmosphere of N₂. The mixture was
44
45 allowed to cool to rt and then concentrated under reduced pressure. The resulting residue
46
47 was chromatographed over silica gel (0% to 50% EtOAc in hexanes) to give (\pm)-methyl 6-
48
49 methyl-2-(7-(2-(trifluoromethyl)phenyl)-2,7-diazaspiro[4.4]nonan-2-yl)pyrimidine-4-
50
51 carboxylate ((\pm)-**66**) as a white solid (0.205 g, 88%): ¹H NMR (400 MHz, CDCl₃) δ 7.55 (d, *J*
52
53
54
55
56
57
58
59
60

1
2
3 = 6.4 Hz, 1H), 7.35 (t, $J = 7.6$ Hz, 1H), 7.00 (s, 1H), 6.95 (d, $J = 8.4$ Hz, 1H), 6.87 (t, $J = 7.6$
4 Hz, 1H), 3.91 (s, 3H), 3.74-3.61 (m, 4H), 3.47-3.44 (m, 2H), 3.30 (s, 2H), 2.39 (s, 3H), 2.08-
5 1.93 (m, 4H); ESI MS m/z 421 $[M + H]^+$.
6
7
8
9

10 Step D: To a solution of (\pm)-methyl 6-methyl-2-(7-(2-(trifluoromethyl)phenyl)-2,7-
11 diazaspiro[4.4]nonan-2-yl)pyrimidine-4-carboxylate ((\pm)-**66**, 0.100 g, 0.237 mmol) in
12 CH₃OH (4 mL), THF (4 mL), and H₂O (2 mL) was added LiOH (56.9 mg, 2.37 mmol) and the
13 mixture stirred at rt for 16 h. The mixture was concentrated under reduced pressure to
14 remove the volatile solvents and the resulting aqueous mixture was diluted with
15 additional H₂O (10 mL) and acidified with 2 N aqueous HCl to pH = 3. The acidified mixture
16 was extracted with EtOAc (3 \times 50 mL) and the combined organic extracts were washed
17 with brine (50 mL), dried over Na₂SO₄, filtered, and concentrated under reduced pressure
18 to give (\pm)-6-methyl-2-(7-(2-(trifluoromethyl)phenyl)-2,7-diazaspiro[4.4]nonan-2-
19 yl)pyrimidine-4-carboxylic acid ((\pm)-**67**) as a white solid (65.5 mg, 68%): ¹H NMR (400 MHz,
20 CDCl₃) δ 7.56 (d, $J = 8.0$ Hz, 1H), 7.37 (t, $J = 7.6$ Hz, 1H), 7.13 (s, 1H), 7.01-6.99 (m, 1H),
21 6.93-6.88 (m, 1H), 3.67-3.55 (m, 4H), 3.46 (t, $J = 6.8$ Hz, 2H), 3.31-3.26 (m, 2H), 2.44 (s,
22 3H), 2.10-1.97 (m, 4H); ESI MS m/z 407 $[M + H]^+$; HPLC 98.4% (AUC), $t_R = 15.5$ min.
23
24
25
26
27
28
29
30
31
32
33
34
35
36
37
38
39
40
41

42 (*(\pm)*-6-Methyl-2-(3-(((2-(trifluoromethyl)phenyl)thio)methyl)pyrrolidin-1-yl)pyrimidine-
43 4-carboxylic Acid ((\pm)-**71**). Compound (\pm)-**71** was prepared from (\pm)-*tert*-butyl 3-
44 ((tosyloxy)methyl)pyrrolidine-1-carboxylate ((\pm)-**40**) and 2-(trifluoromethyl)benzenethiol
45 according to a similar procedure described for the synthesis of (\pm)-**44**: ¹H NMR (400 MHz,
46 acetone-*d*₆) δ 7.72 (t, $J = 7.2$ Hz, 2H), 7.61 (t, $J = 7.2$ Hz, 1H), 7.40 (t, $J = 8.0$ Hz, 1H), 7.05
47 (s, 1H), 3.89-3.70 (m, 2H), 3.59-3.55 (m, 1H), 3.42-3.74 (m, 1H), 3.25 (d, $J = 7.2$ Hz, 2H),
48
49
50
51
52
53
54
55
56
57
58
59
60

1
2
3 2.64–2.62 (m, 1H), 2.40 (s, 3H), 2.27-2.24 (m, 1H), 1.92-1.87 (m, 1H); ESI MS m/z 398 [M
4 + H]⁺; HPLC 97.1% (AUC), t_R = 14.9 min.
5
6

7
8 *(±)-6-Methyl-2-(3-(((2-(trifluoromethyl)phenyl)amino)methyl)pyrrolidin-1-*
9 *yl)pyrimidine-4-carboxylic Acid ((±)-76)*. Step A: To a solution of *(±)-tert-butyl 3-*
10 *formylpyrrolidine-1-carboxylate ((±)-72*, 0.300 g, 1.51 mmol) and 2-
11 *(trifluoromethyl)aniline* (0.242 g, 1.51 mmol) in CH₂Cl₂ (10 mL) was added NaBH(OAc)₃
12 (0.960 g, 4.53 mmol) and the mixture stirred at rt for 16h. The mixture was washed with
13 saturated aqueous NaHCO₃ solution (5 mL), brine (5mL), dried over Na₂SO₄, filtered, and
14 concentrated under reduced pressure to give crude *(±)-tert-butyl 3-(((2-*
15 *(trifluoromethyl)phenyl)amino)methyl)pyrrolidine-1-carboxylate ((±)-73)* as an oil, which
16 was used as is in the next step (0.400 g, 77% crude yield): ESI MS m/z 345 [M + H]⁺.
17
18
19
20
21
22
23
24
25
26
27
28
29

30 Step B: Step B: To a 0 °C solution of *(±)-tert-butyl 3-(((2-*
31 *(trifluoromethyl)phenyl)amino)methyl)pyrrolidine-1-carboxylate ((±)-73*, 0.400 g, 1.16
32 mmol) in CH₂Cl₂ (5 mL) was added TFA (0.89 mL, 11.6 mmol) and the resulting solution
33 was stirred for 12 h while gradually warming to rt. The mixture was neutralized by
34 carefully pouring it into a solution of saturated aqueous NaHCO₃ (10 mL). The biphasic
35 mixture was separated and the aqueous layer was further extracted with CH₂Cl₂ (3 × 20
36 mL). The combined organic extracts were washed with brine (20 mL), dried over Na₂SO₄,
37 filtered, and concentrated under reduced pressure to give *(±)-N-(pyrrolidin-3-ylmethyl)-*
38 *2-(trifluoromethyl)aniline ((±)-74)* as a yellow oil and used as is in the next step (0.360 g):
39
40
41
42
43
44
45
46
47
48
49
50
51
52 ESI MS m/z 245 [M + H]⁺.
53
54
55
56
57
58
59
60

1
2
3 Step C: To a solution of ((±)-*N*-(pyrrolidin-3-ylmethyl)-2-(trifluoromethyl)aniline ((±)-
4 **74**, 0.360 g, 1.16 mmol) in THF (5 mL) were added *i*-Pr₂NEt (0.61 mL, 3.48 mmol) and
5 methyl 2-chloro-6-methylpyrimidine-4-carboxylate (0.216 g, 1.16 mmol) and the resulting
6 mixture stirred at reflux for 16 h under an atmosphere of N₂. The mixture was allowed to
7 cool to rt and then concentrated under reduced pressure. The resulting residue was
8 chromatographed over silica gel (0% to 50% EtOAc in hexanes) to give (±)-methyl 6-
9 methyl-2-(3-(((2-(trifluoromethyl)phenyl)amino)methyl)pyrrolidin-1-yl)pyrimidine-4-
10 carboxylate ((±)-**75**) as a white solid (0.290 g, 63%): ¹H NMR (400 MHz, CDCl₃) δ 7.43-7.40
11 (m, 1H), 7.35-7.31 (m, 1H), 7.00 (s, 1H), 6.71-6.68 (m, 2H), 4.40 (br, 1H), 3.91 (s, 3H), 3.90-
12 3.86 (m, 1H), 3.79-3.58 (m, 1H), 3.41-3.19 (m, 4H), 2.68-2.62 (m, 1H), 2.40 (s, 3H), 2.22-
13 2.16 (m, 1H), 1.82-1.77 (m, 1H) ; ESI MS *m/z* 395 [M + H]⁺.

14
15
16
17
18
19
20
21
22
23
24
25
26
27
28
29
30 Step D: To a solution of (±)-methyl 6-methyl-2-(3-(((2-
31 (trifluoromethyl)phenyl)amino)methyl)pyrrolidin-1-yl)pyrimidine-4-carboxylate ((±)-**75**,
32 0.110 g, 0.278 mmol) in CH₃OH (4 mL), THF (4 mL), and H₂O (2 mL) was added LiOH (56.9
33 mg, 2.37 mmol) and the mixture stirred at rt for 16 h. The mixture was concentrated under
34 reduced pressure to remove the volatile solvents and the resulting aqueous mixture was
35 diluted with additional H₂O (10 mL) and acidified with 2 N aqueous HCl to pH = 3. The
36 acidified mixture was extracted with EtOAc (3 × 50 mL) and the combined organic extracts
37 were washed with brine (50 mL), dried over Na₂SO₄, filtered, and concentrated under
38 reduced pressure to give (±)-6-methyl-2-(3-(((2-
39 (trifluoromethyl)phenyl)amino)methyl)pyrrolidin-1-yl)pyrimidine-4-carboxylic acid ((±)-
40 **76**) as a white solid (90.0 mg, 68%): ¹H NMR (400 MHz, DMSO-*d*₆) δ 7.36-7.32 (m, 2H),
41
42
43
44
45
46
47
48
49
50
51
52
53
54
55
56
57
58
59
60

1
2
3 6.84-6.79 (m, 2H), 6.20 (t, $J = 7.6$ Hz, 1H), 5.53 (br, 1H), 3.63-3.58 (m, 2H), 3.41-3.39 (m,
4
5 1H), 3.25-3.17 (m, 3H), 2.58-2.57 (m, 1H), 2.23 (s, 3H), 1.98-1.95 (m, 1H), 1.70-1.67 (m,
6
7 1H) ; ESI MS m/z 381 [M + H]⁺; HPLC >99% (AUC), $t_R = 14.5$ min.
8
9

10
11 (\pm)-6-Methyl-2-(3-((2-(trifluoromethyl)benzyl)oxy)pyrrolidin-1-yl)pyrimidine-4-
12
13 *carboxylic Acid* ((\pm)-**80**). Step A: To a 0 °C cooled solution of *tert*-butyl 3-
14
15 hydroxypyrrrolidine-1-carboxylate ((\pm)-**22**, 0.500 g, 2.67 mmol) in DMF (5 mL) was added
16
17 NaH (0.267 g, 6.68 mmol). The mixture stirred at 0 °C under an atmosphere of N₂ for 30
18
19 min, then 1-(bromomethyl)-2-(trifluoromethyl)benzene (0.766 g, 3.20 mmol) was added
20
21 and the resulting mixture stirred for 16 h while gradually warming to rt. The mixture was
22
23 cooled back to 0 °C and carefully quenched via dilution with H₂O (20 mL). The aqueous
24
25 mixture was extracted with EtOAc (3 × 30 mL) and the combined organic extracts were
26
27 washed with H₂O (3 × 30 mL) and brine (30 mL), dried over Na₂SO₄, filtered, and
28
29 concentrated under reduced pressure to give (\pm)-*tert*-butyl 3-((2-
30
31 (trifluoromethyl)benzyl)oxy)pyrrolidine-1-carboxylate ((\pm)-**77**) as an off-white solid (0.900
32
33 g, 97% crude yield), which was used as is in the next step: ESI MS m/z 346 [M + H]⁺.
34
35
36
37
38
39

40 Step B: To a 0 °C cooled solution of (\pm)-*tert*-butyl 3-((2-
41
42 (trifluoromethyl)benzyl)oxy)pyrrolidine-1-carboxylate ((\pm)-**77**, 0.900 g 2.61 mmol) in
43
44 CH₂Cl₂ (5 mL) was added TFA (2.0 mL, 26.0 mmol) and the resulting solution stirred for 8
45
46 h. while gradually warming to rt. The mixture was neutralized by carefully pouring it into
47
48 aqueous saturated NaHCO₃ solution (30 mL). The biphasic mixture was separated and the
49
50 aqueous layer was further extracted with CH₂Cl₂ (3 × 30 mL). The combined organic
51
52 extracts were washed with brine (30 mL), dried over Na₂SO₄, filtered, and concentrated
53
54
55
56
57
58
59
60

1
2
3 under reduced pressure to give (\pm)-3-((2-(trifluoromethyl)benzyl)oxy)pyrrolidine ((\pm)-**78**)
4
5 as a white solid (0.450 g, 70% crude yield): ESI MS m/z 246[M + H]⁺.
6
7

8 Step C: To a solution of (\pm)-3-((2-(trifluoromethyl)benzyl)oxy)pyrrolidine ((\pm)-**78**, 0.100
9
10 g, 0.407 mmol) in THF (5 mL) were added *i*-Pr₂NEt (0.25 mL, 1.23 mmol) and methyl 2-
11
12 chloro-6-methylpyrimidine-4-carboxylate (76.2 mg, 0.408 mmol) and the resulting
13
14 solution was stirred at 80 °C for 16 h under an atmosphere of N₂. The mixture was allowed
15
16 to cool to rt and then concentrated under reduced pressure. The resulting residue was
17
18 chromatographed over silica gel (0% to 50% EtOAc in hexanes) to give (\pm)-methyl 6-
19
20 methyl-2-(3-((2-(trifluoromethyl)benzyl)oxy)pyrrolidin-1-yl)pyrimidine-4-carboxylate
21
22 ((\pm)-**79**) as a white solid (0.110 g, 68%): ¹H NMR (400 MHz, acetone-*d*₆) δ 7.75-7.68 (m,
23
24 2H), 7.62 (t, *J* = 7.2 Hz, 1H), 7.47 (t, *J* = 7.6 Hz, 1H), 6.97 (s, 1H), 4.78-4.76 (m, 2H), 4.41-
25
26 4.39 (m, 1H), 3.85 (s, 3H), 3.74-3.66 (m, 4H), 2.36 (s, 3H), 2.31-2.04 (m, 2H); ESI MS m/z
27
28 396 [M + H]⁺.
29
30
31
32
33

34
35 Step D: To a solution of (\pm)-methyl 6-methyl-2-(3-((2-
36
37 (trifluoromethyl)benzyl)oxy)pyrrolidin-1-yl)pyrimidine-4-carboxylate ((\pm)-**79**, 90.0 mg,
38
39 0.228 mmol) in CH₃OH (4 mL), THF (4 mL) and H₂O (2 mL) was added LiOH (54.5 mg, 2.28
40
41 mmol) and the mixture stirred at rt for 16 h. the mixture was and concentrated under
42
43 reduced pressure to remove the volatile solvents and the resulting aqueous layer was
44
45 diluted with additional H₂O (10 mL) and acidified with 2 N aqueous HCl to pH = 3. The
46
47 mixture was extracted with EtOAc (3 × 30 mL) and the combined organic extracts were
48
49 washed with brine (30 mL), dried over Na₂SO₄, filtered, and concentrated under reduced
50
51 pressure to give (\pm)-6-methyl-2-(3-((2-(trifluoromethyl)benzyl)oxy)pyrrolidin-1-
52
53
54
55
56
57

1
2
3 yl)pyrimidine-4-carboxylic acid ((±)-**80**) as a white solid (60.0 mg, 85%): ¹H NMR (400 MHz,
4 DMSO-*d*₆) δ 7.67-7.59 (m, 3H), 7.47-7.45 (m, 1H), 6.90 (s, 1H), 4.64-4.58 (m, 2H), 4.28-4.23
5 (m, 1H), 3.66-3.46 (m, 4H), 2.25 (s, 3H), 2.05-1.98 (m, 2H); ESI MS *m/z* 382 [M + H]⁺; HPLC
6
7
8 98.1% (AUC), *t*_R = 14.4 min.

9
10
11
12
13 *(±)*-2-(3-((2-(*Tert*-butyl)phenoxy)methyl)pyrrolidin-1-yl)-6-methylpyrimidine-4-
14
15 *carboxylic Acid* ((±)-**83**). Compound (±)-**83** was prepared from 2-(*tert*-butyl)phenol and
16
17 (±)-*tert*-butyl 3-((tosyloxy)methyl)pyrrolidine-1-carboxylate ((±)-**40**) according to a similar
18
19 procedure described for the synthesis of (±)-**44**: ¹H NMR (400 MHz, CDCl₃) δ 7.28 (d, *J* =
20
21 8.0 Hz, 1H), 7.17-7.12 (m, 2H), 6.91-6.82 (m, 2H), 4.06-4.00 (m, 3H), 3.93-3.82 (s, 1H),
22
23 3.63-3.51 (m, 2H), 2.93-2.90 (m, 1H), 2.44 (s, 3H), 2.31-2.28 (m, 1H), 2.00-1.98 (m, 1H),
24
25 1.38 (s, 9H); ESI MS *m/z* 370 [M + H]⁺; HPLC 96.4% (AUC), *t*_R = 16.2 min.

26
27
28
29
30
31 *(±)*-2-(3-((2-Cyclopentylphenoxy)methyl)pyrrolidin-1-yl)-6-methylpyrimidine-4-
32
33 *carboxylic Acid* ((±)-**84**). Compound (±)-**84** was prepared from 2-cyclopentylphenol and
34
35 (±)-*tert*-butyl 3-((tosyloxy)methyl)pyrrolidine-1-carboxylate ((±)-**40**) according to a similar
36
37 procedure described for the synthesis of (±)-**44**: ¹H NMR (400 MHz, DMSO-*d*₆) δ 7.16-7.07
38
39 (m, *J* = 8.0 Hz, 2H), 6.94 (s, 1H), 6.90 (d, *J* = 7.6 Hz, 1H), 6.83 (t, *J* = 7.2 Hz, 1H), 3.98 (d, *J* =
40
41 6.4 Hz, 2H), 3.76-3.63 (m, 2H), 3.53-3.39 (m, 2H), 3.22-3.15 (m, 1H), 2.77-2.71 (m, 1H),
42
43 2.32 (s, 3H), 2.17-2.11 (m, 1H), 1.90-1.83 (m, 3H), 1.68-1.66 (m, 2H), 1.61-1.44 (m, 4H);
44
45 ESI MS *m/z* 382 [M + H]⁺; HPLC 95.2% (AUC), *t*_R = 16.4 min.

46
47
48
49
50
51 *(±)*-2-(3-((2-Cyclohexylphenoxy)methyl)pyrrolidin-1-yl)-6-methylpyrimidine-4-
52
53 *carboxylic Acid* ((±)-**85**). Compound (±)-**85** was prepared from 2-cyclohexylphenol and (±)-
54
55 *tert*-butyl 3-((tosyloxy)methyl)pyrrolidine-1-carboxylate ((±)-**40**) according to a similar
56
57

1
2
3 procedure described for the synthesis of (\pm)-**44**: $^1\text{H NMR}$ (400 MHz, $\text{DMSO-}d_6$) $^1\text{H NMR}$
4 (400 MHz, CDCl_3) δ 7.17-7.15 (m, 1H), 7.13-7.11 (m, 1H), 7.12 (s, 1H), 6.92-6.88 (m, 1H),
5
6 6.82 (d, $J = 8.4$ Hz, 1H), 4.01-3.93 (m, 2H), 3.87-3.80 (m, 2H), 3.69-3.48 (m, 2H), 2.89-2.84
7
8 (m, 2H), 2.43 (s, 3H), 2.26-2.15 (m, 1H), 1.99-1.96 (m, 1H), 1.83-1.69 (m, 5H), 1.41-1.22
9
10 (m, 5H); ESI MS m/z 396 $[\text{M} + \text{H}]^+$; HPLC 98.3% (AUC), $t_R = 17.1$ min.

11
12
13 (\pm)-2-(3-((3-Chloro-2-(trifluoromethyl)phenoxy)methyl)pyrrolidin-1-yl)-6-
14
15 methylpyrimidine-4-carboxylic Acid ((\pm)-**86**). Compound (\pm)-**86** was prepared from 3-
16
17 chloro-2-(trifluoromethyl)phenol and (\pm)-*tert*-butyl 3-((tosyloxy)methyl)pyrrolidine-1-
18
19 carboxylate ((\pm)-**40**) according to a similar procedure described for the synthesis of (\pm)-
20
21 **44**: $^1\text{H NMR}$ (400 MHz, $\text{DMSO-}d_6$) δ 7.56 (d, $J = 8.4$ Hz, 1H), 7.26 (d, $J = 8.4$ Hz, 1H), 7.19 (d,
22
23 $J = 7.6$ Hz, 1H), 6.94 (s, 1H), 4.19-4.10 (m, 2H), 3.76-3.63 (m, 2H), 3.51-3.44 (m, 1H), 3.33-
24
25 3.32 (m, 1H), 2.77-2.70 (m, 1H), 2.32 (s, 3H), 2.15-2.07 (m, 1H), 1.87-1.79 (m, 1H); ESI MS
26
27 m/z 416 $[\text{M} + \text{H}]^+$; HPLC 99.0% (AUC), $t_R = 15.1$ min.

28
29
30 (\pm)-2-(3-((4-Fluoro-2-(trifluoromethyl)phenoxy)methyl)pyrrolidin-1-yl)-6-
31
32 methylpyrimidine-4-carboxylic Acid ((\pm)-**87**). Compound (\pm)-**87** was prepared from 4-
33
34 fluoro-2-(trifluoromethyl)phenol and (\pm)-*tert*-butyl 3-((tosyloxy)methyl)pyrrolidine-1-
35
36 carboxylate ((\pm)-**40**) according to a similar procedure described for the synthesis of (\pm)-
37
38 **44**: $^1\text{H NMR}$ (400 MHz, $\text{DMSO-}d_6$) δ 7.48-7.44 (m, 2H), 7.28-7.25 (m, 1H), 6.92 (s, 1H), 4.12-
39
40 4.08 (m, 2H), 3.72-3.68 (m, 1H), 3.64-3.60 (m, 1H), 3.47-3.42 (m, 1H), 3.33-3.29 (m, 1H),
41
42 2.71-2.68 (m, 1H), 2.32 (s, 3H), 2.10-2.06 (m, 1H), 1.83-1.78 (m, 1H); ESI MS m/z 400 $[\text{M} +$
43
44 $\text{H}]^+$; HPLC 98.7% (AUC), $t_R = 14.8$ min.

1
2
3 *(±)-2-(3-((5-Fluoro-2-(trifluoromethyl)phenoxy)methyl)pyrrolidin-1-yl)-6-*

4
5
6 *methylpyrimidine-4-carboxylic Acid ((±)-88)*. Compound (±)-**88** was prepared from 5-
7
8 fluoro-2-(trifluoromethyl)phenol and (±)-*tert*-butyl 3-((tosyloxy)methyl)pyrrolidine-1-
9
10 carboxylate ((±)-**40**) according to a similar procedure described for the synthesis of (±)-
11
12 **44**: ¹H NMR (400 MHz, DMSO-*d*₆) δ 7.66-7.62 (m, 1H), 7.20 (d, *J* = 11.2 Hz, 1H), 6.93 (s,
13
14 1H), 6.91-6.86 (m, 1H), 4.18-4.10 (m, 2H), 3.73-3.63 (m, 2H), 3.51-3.44 (m, 1H), 3.35-3.32
15
16 (m, 1H), 2.76-2.69 (m, 1H), 2.31 (s, 3H), 2.14-2.06 (m, 1H), 1.87-1.79 (m, 1H); ESI MS *m/z*
17
18 400 [M + H]⁺; HPLC 98.0% (AUC), *t*_R = 14.7 min.

19
20
21
22 *(±)-2-(3-((2-Fluoro-6-(trifluoromethyl)phenoxy)methyl)pyrrolidin-1-yl)-6-*

23
24
25 *methylpyrimidine-4-carboxylic Acid ((±)-89)*. Compound (±)-**89** was prepared from 2-
26
27 fluoro-6-(trifluoromethyl)phenol and (±)-*tert*-butyl 3-((tosyloxy)methyl)pyrrolidine-1-
28
29 carboxylate ((±)-**40**) according to a similar procedure described for the synthesis of (±)-
30
31 **44**: ¹H NMR (400 MHz, DMSO-*d*₆) δ 7.64-7.60 (m, 1H), 7.48 (d, *J* = 8.0 Hz, 1H), 7.29-7.24
32
33 (m, 1H), 6.94 (s, 1H), 4.19-4.13 (m, 2H), 3.77-3.73 (m, 1H), 3.67-3.61 (m, 1H), 3.51-3.45
34
35 (m, 1H), 3.34-3.34 (m, 1H), 2.77-2.72 (m, 1H), 2.32 (s, 3H), 2.13-2.09 (m, 1H), 1.89-1.82
36
37 (m, 1H); ESI MS *m/z* 400 [M + H]⁺; HPLC 96.7% (AUC), *t*_R = 14.8 min.

38
39
40
41
42 *(±)-2-(3-((5-Methoxy-2-(trifluoromethyl)phenoxy)methyl)pyrrolidin-1-yl)-6-*

43
44
45 *methylpyrimidine-4-carboxylic Acid ((±)-90)*. Compound (±)-**90** was prepared from 5-
46
47 methoxy-2-(trifluoromethyl)phenol and (±)-*tert*-butyl 3-((tosyloxy)methyl)pyrrolidine-1-
48
49 carboxylate ((±)-**40**) according to a similar procedure described for the synthesis of (±)-
50
51 **44**: ¹H NMR (400 MHz, CDCl₃) δ 7.47 (d, *J* = 8.8 Hz, 1H), 6.94 (s, 1H), 6.75 (s, 1H), 6.58 (d, *J*
52
53 = 8.4 Hz, 1H), 4.13-4.07 (m, 2H), 3.79 (s, 3H), 3.74-3.64 (m, 2H), 3.51-3.45(m, 1H), 3.36-
54
55
56
57
58
59
60

3.31 (m, 1H), 2.73-2.70 (m, 1H), 2.31 (s, 3H), 2.12-2.08 (m, 1H), 1.87-1.80 (m, 1H); ESI MS m/z 412 [M + H]⁺; HPLC >99% (AUC), t_R = 14.6 min.

(±)-2-(3-((3,5-Bis(trifluoromethyl)phenoxy)methyl)pyrrolidin-1-yl)-6-methylpyrimidine-4-carboxylic Acid ((±)-**91**). Compound (±)-**91** was prepared from 3,5-bis(trifluoromethyl)phenol and (±)-*tert*-butyl 3-((tosyloxy)methyl)pyrrolidine-1-carboxylate ((±)-**40**) according to a similar procedure described for the synthesis of (±)-**44**: ¹H NMR (400 MHz, DMSO-*d*₆) δ 7.61-7.59 (m, 3H), 6.94 (s, 1H), 4.23-4.14 (m, 2H), 3.76-3.71 (m, 1H), 3.69-3.63 (m, 1H), 3.53-3.47 (m, 1H), 3.42-3.38 (m, 1H), 2.78-2.71 (m, 1H), 2.32 (s, 3H), 2.16-2.08 (m, 1H), 1.89-1.81 (m, 1H); ESI MS m/z 450 [M + H]⁺; HPLC 97.0% (AUC), t_R = 16.0 min.

(±)-6-Methyl-2-(3-(((4-(trifluoromethyl)pyridin-3-yl)oxy)methyl)pyrrolidin-1-yl)pyrimidine-4-carboxylic Acid ((±)-**92**). Compound (±)-**92** was prepared from 4-(trifluoromethyl)pyridin-3-ol and (±)-*tert*-butyl 3-((tosyloxy)methyl)pyrrolidine-1-carboxylate ((±)-**40**) according to a similar procedure described for the synthesis of (±)-**44**: ¹H NMR (400 MHz, CDCl₃) δ 8.44 (s, 1H), 8.37 (d, *J* = 4.8 Hz, 1H), 7.43 (d, *J* = 4.8 Hz, 1H), 7.13 (s, 1H), 4.21-4.20 (m, 2H), 3.87-3.78 (m, 2H), 3.65-3.64 (m, 1H), 3.54-3.49 (m, 1H), 2.93-2.86 (m, 1H), 2.44 (s, 3H), 2.29-2.24 (m, 1H), 2.02-1.97 (m, 1H); ESI MS m/z 383 [M + H]⁺; HPLC >99% (AUC), t_R = 12.6 min.

(±)-6-Methyl-2-(3-(((2-(trifluoromethyl)pyridin-3-yl)oxy)methyl)pyrrolidin-1-yl)pyrimidine-4-carboxylic Acid ((±)-**93**). Compound (±)-**93** was prepared from 2-(trifluoromethyl)pyridin-3-ol and (±)-*tert*-butyl 3-((tosyloxy)methyl)pyrrolidine-1-carboxylate ((±)-**40**) according to a similar procedure described for the synthesis of (±)-

1
2
3 **44**: ^1H NMR (400 MHz, CDCl_3) δ 8.26 (d, $J = 4.4$ Hz, 1H), 7.45-7.42 (m, 1H), 7.34 (d, $J = 8.4$
4 Hz, 1H), 7.13 (s, 1H), 4.11-4.07 (m, 2H), 3.86-3.85 (m, 2H), 3.63-3.61 (m, 1H), 3.51-3.47
5 (m, 1H), 2.91-2.84 (m, 1H), 2.44 (s, 3H), 2.28-2.25 (m, 1H), 2.00-1.97 (m, 1H); ESI MS m/z
6 383 $[\text{M} + \text{H}]^+$; HPLC 99.0% (AUC), $t_R = 12.7$ min.
7
8
9
10

11
12
13 *(\pm)*-2-(3-((2-(Trifluoromethyl)phenoxy)methyl)pyrrolidin-1-yl)pyrimidine-4-carboxylic
14 Acid (*(\pm)*-**94**). Compound (*(\pm)*-**94**) was prepared from methyl 2-chloropyrimidine-4-
15 carboxylate and (*(\pm)*-3-((2-(trifluoromethyl)phenoxy)methyl)pyrrolidine (*(\pm)*-**42**) according
16 to a similar procedure described for the synthesis of (*(\pm)*-**44**: ^1H NMR (400 MHz, $\text{DMSO}-d_6$)
17 δ 8.50 (d, $J = 4.8$ Hz, 1H), 7.61-7.57 (m, 2H), 7.26 (d, $J = 8.4$ Hz, 1H), 7.06 (t, $J = 7.6$ Hz, 1H),
18 7.00 (d, $J = 5.2$ Hz, 1H), 4.15 (br, 2H), 3.77-3.63 (m, 2H), 3.53-3.47 (m, 1H), 3.37-3.33 (m,
19 1H), 2.79-2.72 (m, 1H), 2.17-2.09 (m, 1H), 1.90-1.83 (m, 1H); ESI MS m/z 368 $[\text{M} + \text{H}]^+$;
20 HPLC >99% (AUC), $t_R = 14.3$ min.
21
22
23
24
25
26
27
28
29
30
31

32
33 *(\pm)*-4-Methyl-6-(3-((2-(trifluoromethyl)phenoxy)methyl)pyrrolidin-1-yl)picolinic Acid
34 (*(\pm)*-**95**). Step A: To a mixture of (*(\pm)*-3-((2-(trifluoromethyl)phenoxy)methyl)pyrrolidine
35 (*(\pm)*-**42**, 0.200 g, 0.815 mmol), methyl 6-chloro-4-methylpicolinate (0.151 g, 0.815 mmol),
36 and Cs_2CO_3 (0.796 g, 2.44 mmol) in N_2 degassed anhydrous 1,4-dioxane (10 mL) was
37 added XantPhos (0.153 g, 0.265 mmol) and $\text{Pd}_2(\text{dba})_3$ (74.6 mg, 0.082 mmol). The mixture
38 was heated at 80 °C in a sealed vessel for 16 h. The reaction mixture was allowed to cool
39 to rt and then diluted with H_2O (30 mL) and extracted with EtOAc (3 \times 50 mL). The
40 combined organic extracts were washed with H_2O (3 \times 50 mL), brine (50 mL), dried over
41 Na_2SO_4 , filtered, and concentrated under reduced pressure. The resulting residue was
42 chromatographed over silica gel (0% to 50% EtOAc in hexanes) to give (*(\pm)*-methyl 4-
43
44
45
46
47
48
49
50
51
52
53
54
55
56
57
58
59
60

1
2
3 methyl-6-(3-((2-(trifluoromethyl)phenoxy)methyl)pyrrolidin-1-yl)picolinate as an off-
4
5 white solid (0.180 g, 56%): $^1\text{H NMR}$ (400 MHz, CDCl_3) δ 7.54 (d, $J = 7.6$ Hz, 1H), 7.44 (t, $J =$
6
7 8.0 Hz, 1H), 7.23-7.20 (m, 1H), 7.00-6.92 (m, 2H), 6.34 (s, 1H), 4.08-3.99 (m, 2H), 3.89 (s,
8
9 3H), 3.76-3.72 (m, 1H), 3.69-3.63 (m, 1H), 3.55-3.49 (m, 1H), 3.40-3.36 (m, 1H), 2.89-2.82
10
11 (m, 1H), 2.27 (s, 3H), 2.25-2.18 (m, 1H), 2.00-1.93 (m, 1H); ESI MS m/z 395 $[\text{M} + \text{H}]^+$.

12
13
14
15 Step B: To a solution of (\pm)-methyl 4-methyl-6-(3-((2-
16
17 (trifluoromethyl)phenoxy)methyl)pyrrolidin-1-yl)picolinate (0.190 g, 0.481 mmol) in
18
19 CH_3OH (6 mL), THF (6 mL), and H_2O (3 mL) was added LiOH (0.115 g, 4.81 mmol) and the
20
21 mixture stirred at rt for 16 h. The mixture was concentrated under reduced pressure to
22
23 remove the volatile solvents and the resulting aqueous mixture was diluted with
24
25 additional H_2O (10 mL) and acidified with 2 N aqueous HCl to pH = 3. The acidified mixture
26
27 was extracted with EtOAc (3 \times 20 mL) and the combined organic extracts were washed
28
29 with brine (20 mL), dried over Na_2SO_4 , filtered, and concentrated under reduced pressure
30
31 to give (\pm)-2-(3-((2-(trifluoromethyl)phenoxy)methyl)pyrrolidin-1-yl)pyrimidine-4-
32
33 carboxylic acid ((\pm)-**95**) as a white solid (0.136 g, 77%): $^1\text{H NMR}$ (400 MHz, $\text{DMSO}-d_6$)
34
35 δ 7.57-7.54 (m, 2H), 7.15 (d, $J = 8.4$ Hz, 1H), 7.05-7.01 (m, 2H), 6.18 (s, 1H), 4.02-3.92 (m,
36
37 2H), 3.68-3.46 (m, 3H), 3.34-3.32 (m, 1H), 2.64-2.61 (m, 1H), 2.13 (s, 3H), 2.10-2.01 (m,
38
39 1H), 1.81-1.68 (m, 1H); ESI MS m/z 381 $[\text{M} + \text{H}]^+$; HPLC >99% (AUC), $t_R = 12.8$ min.

40
41
42
43
44
45
46
47 (\pm)-6-(3-((2-(Trifluoromethyl)phenoxy)methyl)pyrrolidin-1-yl)picolinic acid ((\pm)-**96**).

48
49 Compound (\pm)-**96** was prepared from methyl 6-chloropicolinate and (\pm)-3-((2-
50
51 (trifluoromethyl)phenoxy)methyl)pyrrolidine ((\pm)-**42**) according to a similar procedure
52
53 described for the synthesis of (\pm)-**95**: $^1\text{H NMR}$ (400 MHz, CDCl_3) δ 7.63-7.54 (m, 2H), 7.46-
54
55
56
57

1
2
3 7.42 (m, 2H), 7.00-6.95 (m, 2H), 6.62-6.60 (m, 1H), 4.10-4.04 (m, 2H), 3.77-3.60 (m, 2H),
4
5 3.51-3.39 (m, 2H), 2.92-2.80 (m, 1H), 2.25-2.22 (m, 1H), 2.08-1.96 (m, 1H); ESI MS m/z 367
6
7
8 $[M + H]^+$; HPLC 95.8% (AUC), $t_R = 12.7$ min.
9

10 *(±)-2-(3-((2-(Trifluoromethyl)phenoxy)methyl)pyrrolidin-1-yl)nicotinic Acid ((±)-97).*

11
12 Compound **(±)-97** was prepared from methyl 2-chloronicotinate and **(±)-3-((2-**
13 **(trifluoromethyl)phenoxy)methyl)pyrrolidine ((±)-42)** according to a similar procedure
14
15 described for the synthesis of **(±)-95**: ^1H NMR (400 MHz, CDCl_3) δ 8.40 (d, $J = 4.4$ Hz, 1H),
16
17 8.23 (d, $J = 7.6$ Hz, 1H), 7.52 (d, $J = 7.6$ Hz, 1H), 7.47-7.43 (m, 1H), 7.00-6.91 (m, 3H), 4.10-
18
19 4.02 (m, 2H), 3.61-3.37 (m, 4H), 2.93-2.86 (m, 1H), 2.29-2.21 (m, 1H), 1.98-1.89 (m, 1 H);
20
21 ESI MS m/z 367 $[M + H]^+$; HPLC 98.3% (AUC), $t_R = 12.0$ min.
22
23
24
25
26

27 *(±)-4-Fluoro-3-(3-((2-(trifluoromethyl)phenoxy)methyl)pyrrolidin-1-yl)benzoic Acid*
28 **((±)-98)**. Step A: To a mixture of **(±)-3-((2-(trifluoromethyl)phenoxy)methyl)pyrrolidine**
29 **((±)-42**, 0.300 g, 1.22 mmol) and methyl 3-bromo-4-fluorobenzoate (0.342 g, 1.47 mmol)
30
31 in N_2 degassed 1,4-dioxane was added Cs_2CO_3 (1.2 g, 3.66 mmol), XPhos (58.1 mg, 0.12
32
33 mmol), and $\text{Pd}_2(\text{dba})_3$ (37.9 mg, 0.037 mmol). The mixture was stirred at 110 °C in a sealed
34
35 vessel for 16 h and then allowed to cool to rt. The mixture was concentrated under
36
37 reduced pressure and the resulting residue was chromatographed over silica gel (0% to
38
39 40% EtOAc in hexanes) to give methyl 4-fluoro-3-(3-((2-
40
41 (trifluoromethyl)phenoxy)methyl)pyrrolidin-1-yl)benzoate as a white solid (0.198 mg,
42
43 41%): ^1H NMR (400 MHz, CDCl_3) δ 7.54 (d, $J = 7.6$ Hz, 1H), 7.45 (t, $J = 7.6$ Hz, 1H), 7.37-7.32
44
45 (m, 2H), 7.00-6.95 (m, 3H), 4.04 (d, $J = 7.2$ Hz, 2H), 3.85 (s, 3H), 3.64-3.59 (m, 1H), 3.52-
46
47
48
49
50
51
52
53
54
55
56
57
58
59
60

3.46 (m, 2H), 3.40-3.35 (m, 1H), 2.85-2.81 (m, 1H), 2.22-2.17 (m, 1H), 1.93-1.88 (m, 1H);

ESI MS m/z 398 [M + H]⁺.

Step B: To a solution of methyl 4-fluoro-3-(3-((2-(trifluoromethyl)phenoxy)methyl)pyrrolidin-1-yl)benzoate (0.120 g, 0.63 mmol) in a mixture of CH₃OH (4 mL), THF (4 mL), and H₂O (2 mL) was added LiOH (0.144 g, 6.04 mmol). The mixture stirred at rt for 16 h and was concentrated under reduced pressure to remove the volatile solvents. The resulting aqueous layer was diluted with H₂O (50 mL) and acidified with 2 N aqueous HCl to pH = 3. The aqueous mixture was extracted with EtOAc (3 × 50 mL) and the combined organic extracts were washed with brine, dried over Na₂SO₄, filtered, and concentrated under reduced pressure to give 4-fluoro-3-(3-((2-(trifluoromethyl)phenoxy)methyl)pyrrolidin-1-yl)benzoic acid ((±)-**98**) as a white solid (78.0 mg, 67%): δ 7.59-7.55 (d, J = 7.6 Hz, 2H), 7.24-7.20 (m, 3H), 7.13-7.02 (m, 2H), 4.13-4.07 (m, 2H), 3.52-3.48 (m, 1H), 3.39 (br, 2H), 3.29-3.25 (m, 1H), 2.73-2.70 (m, 1H), 2.11-2.08 (m, 1H), 1.81-1.76 (m, 1H); ESI MS m/z 384 [M + H]⁺; HPLC 98.5% (AUC), t_R = 16.1 min.

((±)-6-Methyl-N-(methanesulfonyl)-2-(3-((2-(trifluoromethyl)phenoxy)methyl)pyrrolidin-1-yl)pyrimidine-4-carboxamide ((±)-**99**). Step A: To a mixture of 6-methyl-2-(3-((2-(trifluoromethyl)phenoxy)methyl)pyrrolidin-1-yl)pyrimidine-4-carboxylic acid ((±)-**44**, 50.0 mg, 0.131 mmol), HBTU (74.5 mg, 0.197 mmol), and *i*-Pr₂NEt (0.08 mL, 0.393 mmol) in DMF (4 mL) was added methanesulfonamide (19.1 mg, 0.197 mmol). The resulting solution was stirred at rt for 18 h under an atmosphere of N₂. The mixture was diluted with H₂O (10 mL) and extracted with EtOAc (3 × 20 mL). The combined organic extracts

1
2
3 were washed with H₂O (3 × 20 mL) and brine, dried over Na₂SO₄, filtered, and
4
5 concentrated under reduced pressure. The resulting crude residue was chromatographed
6
7 over silica gel (0% to 80% EtOAc in hexanes) to give 6-methyl-*N*-(methylsulfonyl)-2-(3-((2-
8
9 (trifluoromethyl)phenoxy)methyl)pyrrolidin-1-yl)pyrimidine-4-carboxamide ((±)-**99**) as a
10
11 white solid (30.0 mg, 50%): ¹H NMR (400 MHz, acetone-*d*₆) δ 10.36 (br, 1H), 7.61-7.57 (m,
12
13 2H), 7.27-7.25 (m, 1H), 7.10-7.06 (m, 2H), 4.23 (br, 2H), 3.92-3.82 (m, 2H), 3.65-3.49 (m,
14
15 2H), 3.34 (s, 3H), 2.92-2.82 (m, 2H), 2.42 (s, 3H), 2.25-2.22 (m, 1H); ESI MS *m/z* 459 [M +
16
17 H]⁺; HPLC 98.4% (AUC), *t*_R = 15.9 min.

18
19
20
21
22
23 *(±)*-6-Methyl-2-(3-((2-(trifluoromethyl)phenoxy)methyl)pyrrolidin-1-yl)pyrimidine-4-
24
25 carboxamide ((±)-**100**). Compound (±)-**100** was prepared from NH₄Cl and 6-methyl-2-(3-
26
27 ((2-(trifluoromethyl)phenoxy)methyl)pyrrolidin-1-yl)pyrimidine-4-carboxylic acid ((±)-**44**
28
29 according to a similar procedure described for the synthesis of (±)-**99**: ¹H NMR (400 MHz,
30
31 CDCl₃) δ 7.71 (br, 1H), 7.55 (d, *J* = 8.0 Hz, 1H), 7.45 (t, *J* = 7.6 Hz, 1H), 7.14 (s, 1H), 7.00-
32
33 6.94 (m, 2H), 5.57 (br, 1H), 4.06-4.02 (m, 2H), 3.88-3.83 (m, 1H), 3.79-3.73 (m, 1H), 3.63-
34
35 3.57 (m, 1H), 3.51-3.47 (m, 1H), 2.89-2.84 (m, 1H), 2.40 (s, 3H), 2.26-2.19 (m, 1H), 1.99-
36
37 1.94 (m, 1H); ESI MS *m/z* 381 [M + H]⁺; HPLC >99% (AUC), *t*_R = 14.3 min.

38
39
40
41
42
43 *(±)*-*N*,6-dimethyl-2-(3-((2-(trifluoromethyl)phenoxy)methyl)pyrrolidin-1-yl)pyrimidine-
44
45 4-carboxamide ((±)-**101**). Step A: To a solution of 6-methyl-2-(3-((2-
46
47 (trifluoromethyl)phenoxy)methyl)pyrrolidin-1-yl)pyrimidine-4-carboxylic acid ((±)-**44**,
48
49 50.0 mg, 0.131 mmol), T₃P (50% w/w in CH₂Cl₂) (83.4 mg, 0.262 mmol), and *i*-Pr₂NEt (0.2
50
51 mL, 1.05 mmol) in CH₂Cl₂ (3 mL) was added methylamine hydrochloride (44.0 mg, 0.393
52
53 mmol). The mixture stirred at ambient temperature for 18 h and was then concentrated
54
55
56

1
2
3 under reduced pressure. The resulting residue was chromatographed over silica gel (0%
4 to 60% EtOAc in hexane) to give *N*,6-dimethyl-2-(3-((2-
5 (trifluoromethyl)phenoxy)methyl)pyrrolidin-1-yl)pyrimidine-4-carboxamide ((±)-**101**) as a
6 white solid (40.0 mg, 77%): ¹H NMR (400 MHz, acetone-*d*₆) δ 8.25 (br, 1H), 7.62-7.59 (m,
7 2H), 7.26 (d, *J* = 8.0 Hz, 1H), 7.08-7.05 (m, 2H), 4.23-4.19 (m, 2H), 3.88-3.83 (m, 1H), 3.79-
8 3.74 (m, 1H), 3.60-3.58 (m, 1H), 3.50-3.48 (m, 1H), 2.88 (s, 3H), 2.87-2.82 (m, 1H), 2.36 (s,
9 3H), 2.22-2.19 (m, 1H), 2.02-2.01 (m, 1H); ESI MS *m/z* 395 [M + H]⁺; HPLC >99% (AUC), *t*_R
10 = 14.7 min.

11
12
13
14
15
16
17
18
19
20
21
22
23 *(±)*-*N*-Cyclopropyl-6-methyl-2-(3-((2-(trifluoromethyl)phenoxy)methyl)pyrrolidin-1-
24 yl)pyrimidine-4-carboxamide ((±)-**102**). Compound (±)-**102** was prepared from
25 cyclopropylamine and 6-methyl-2-(3-((2-(trifluoromethyl)phenoxy)methyl)pyrrolidin-1-
26 yl)pyrimidine-4-carboxylic acid ((±)-**44** according to a similar procedure described for the
27 synthesis of (±)-**100**: ¹H NMR (400 MHz, acetone-*d*₆) δ 8.17 (br, 1H), 7.62-7.57 (m, 2H),
28 7.26 (d, *J* = 8.4 Hz, 1H), 7.10-7.04 (m, 2H), 4.21 (br, 2H), 3.87-3.82 (m, 1H), 3.76-3.72 (m,
29 1H), 3.58-3.55 (m, 1H), 3.49-3.44 (m, 1H), 2.88-2.78 (m, 2H), 2.36 (s, 3H), 2.23-2.13 (m,
30 1H), 2.02-1.95 (m, 1H), 0.75-0.73 (m, 2H), 0.58 (br, 2H); ESI MS *m/z* 421 [M + H]⁺; HPLC
31 >99% (AUC), *t*_R = 15.3 min.

32
33
34
35
36
37
38
39
40
41
42
43
44
45 *(±)*-4-Methyl-6-(2*H*-tetrazol-5-yl)-2-(3-((2-
46 (trifluoromethyl)phenoxy)methyl)pyrrolidin-1-yl)pyrimidine ((±)-**103**). Step A: A mixture of
47 6-methyl-2-(3-((2-(trifluoromethyl)phenoxy)methyl)pyrrolidin-1-yl)pyrimidine-4-
48 carboxamide ((±)-**100**, 0.200 g, 0.526 mmol), NaN₃ (0.142 g, 0.375 mmol), and
49 tetrachlorosilane (98.5 mg, 0.579 mmol) in CH₃CN (4 mL) stirred at 80 °C for 18 h in a
50
51
52
53
54
55
56
57
58
59
60

1
2
3 sealed vessel. The reaction mixture was allowed to cool to rt and diluted with saturated
4
5 NaHCO₃ (5 mL). The aqueous mixture was extracted with CHCl₃ (3 × 50 mL) and the
6
7 combined organic extracts were washed with brine (50 mL), dried over Na₂SO₄, filtered,
8
9 and concentrated under reduced pressure. The resulting residue was chromatographed
10
11 over silica gel (0% to 10% CH₃OH in CH₂Cl₂) to give 4-methyl-6-(2H-tetrazol-5-yl)-2-(3-((2-
12
13 (trifluoromethyl)phenoxy)methyl)pyrrolidin-1-yl)pyrimidine ((±)-**103**) as a white solid
14
15 (66.0 mg, 30%): ¹H NMR (400 MHz, acetone-*d*₆) δ 7.62-7.58 (m, 2H), 7.28-7.25 (m, 2H),
16
17 7.08 (t, *J* = 7.6 Hz, 1H), 4.28-4.21 (m, 3H), 3.91-3.86 (m, 1H), 3.80-3.74 (m, 1H), 3.65-3.58
18
19 (m, 1H), 3.52-3.47 (m, 1H), 2.92-2.85 (m, 1H), 2.42 (s, 3H), 2.27-2.21 (m, 1H); ESI MS *m/z*
20
21 406 [M + H]⁺; HPLC 97.4% (AUC), *t*_R = 14.6 min.
22
23
24
25
26
27
28
29

30 ASSOCIATED CONTENT

31 Supporting Information

32
33 The Supporting Information is available free of charge on the ACS publications website at
34
35 <http://pubr.acs.org>.
36
37

38
39 The Supporting Information contains the following:
40
41

42 RBP4 *in vitro* assay protocols, TTR *in vitro* assay protocols, mouse PK study
43
44 protocols, serum RBP4 collection and measurement protocols, *in vitro* ADME
45
46 assay protocols, general chemistry information, and spectroscopic and analytical
47
48 data for compound (±)-**44** (¹H NMR, ¹³C NMR, ¹⁹F NMR, MS, and HPLC), molecular
49
50 formula strings for biologically tested compounds (PDF);
51
52
53
54
55
56
57

1
2
3 Molecular formula strings for biologically tested compounds (CSV) is also
4
5 provided.
6
7
8
9

10 **AUTHOR INFORMATION**

11 **Corresponding Authors**

12
13
14
15
16 *Christopher L. Cioffi: phone, 518-694-7224; e-mail: christopher.cioffi@acphs.edu.

17
18 *Konstantin Petrukhin: phone, 212-305-9040; e-mail: kep4@cumc.columbia.edu.
19

20 **ORCID ID**

21
22
23 Christopher L. Cioffi: 0000-0003-0642-7905

24
25
26 Konstantin Petrukhin: 0000-0002-5545-6924
27

28 **Notes**

29
30 The authors declare the following competing financial interest(s): C.L.C., P. M., A.R., A.V.,
31
32 B.R., and K.P. are inventors on the patent applications for compounds disclosed in this
33
34 paper that are assigned to The Trustees of Columbia University in the City of New York
35
36 and Albany College of Pharmacy and Health Sciences.
37
38
39
40
41
42

43 **ACKNOWLEDGEMENTS**

44
45 Research reported in this publication was supported by the National Eye Institute of the
46
47 National Institutes of Health under Award Number R01EY028549. The content is solely
48
49 the responsibility of the authors and does not necessarily represent the official views of
50
51 the National Institutes of Health. This project has been funded in whole or in part with
52
53 Federal funds from the National Eye Institute, National Institutes of Health, Department
54
55
56
57

1
2
3 of Health and Human Services, NIH Grant R01EY028549 (to K.P. and C.L.C.). This study was
4
5 supported by NIH Grants P30 EY019007 (Core Support for Vision Research), and
6
7 unrestricted funds from Research to Prevent Blindness (New York, NY) to the Department
8
9 of Ophthalmology, Columbia University. The authors thank The Burch Family Foundation,
10
11 the Mary Jaharis-John Catsimatidis Scholarship Fund, the Kaplen Foundation, and the Eye
12
13 Surgery Fund for gifts supporting this study.
14
15
16
17
18
19

20 **ABBREVIATIONS**

21
22
23 A β , β -amyloid; *Abca4*, ATP-binding cassette, sub-family A (ABC1), member 4; ADME,
24
25 Absorption, Distribution, Metabolism, Elimination; AMD, age-related macular
26
27 degeneration; aq, aqueous; Arg, arginine; ATTR, transthyretin amyloidosis; ATTR-CM,
28
29 transthyretin amyloidosis cardiomyopathy; ATTR-PN, transthyretin amyloidosis
30
31 polyneuropathy; AUC, area under the curve; A2E, N-retinide-N-retinylidene
32
33 ethanolamine; Boc₂O, di-*tert*-butyl di-carbonate; CH₂Cl₂, dichloromethane; CH₃CN,
34
35 acetonitrile; CH₃OH, methyl alcohol; CL, clearance; CL_{int}, intrinsic clearance; Cs₂CO₃,
36
37 cesium carbonate; CF₃, trifluoromethyl; CSF, cerebral spinal fluid; CYP, cytochrome P450;
38
39 CYP2C9, cytochrome P450 2C9; CYP2C19, cytochrome P450 2C19; CYP2D6, cytochrome
40
41 P450 2D6; CYP3A4, cytochrome P450 3A4; DMAP, 1,4-dimethylaminopyridine; DME,
42
43 dimethoxyethane; DMF; *N,N*-dimethylformamide; Et₃N, triethylamine; Et₂O, diethyl
44
45 ether; EtOAc, ethyl acetate; EtOH, ethyl alcohol; %F, % oral bioavailability; fluorescein
46
47 isothiocyanate, FITC; FP, fluorescence polarization assay; Gln, glutamine; Glu, glutamic
48
49 acid; Gly, glycine; HBA, hydrogen bond acceptor; HBD, hydrogen bond donor; HBP,
50
51
52
53
54
55
56
57

1
2
3 halogen binding pocket; HBTU, (2-(1H-benzotriazol-1-yl)-1,1,3,3-tetramethyluronium
4
5 hexafluorophosphate; HCl, hydrochloric acid; hERG; human ether-a-go-go channel; HLM,
6
7 human liver microsomes; HOAc, acetic acid; HTRF, homogenous time resolved
8
9 fluorescence assay; HRMS, high resolution mass spectrometry; *i*-Pr₂NEt, *N,N*-
10
11 diisopropylethylamine; IV, intravenous; LiOH, lithium hydroxide; Leu, leucine; Lys, lysine;
12
13 Met, methionine; MLM, mouse liver microsomes; NAFLD, non-alcoholic fatty liver
14
15 disease; NaBH₄, sodium borohydride; NaBH(OAc)₃, sodium triacetoxyborohydride; NaN₃,
16
17 sodium azide; NH₄Cl, ammonium chloride; PBR, phosphate buffered saline; PD,
18
19 pharmacodynamics; PDB, Protein Data Bank; Pd₂(dba)₃,
20
21 tris(dibenzylideneacetone)dipalladium(0); Phe, phenylalanine; PK, pharmacokinetics; PO,
22
23 oral; PPAR γ , nuclear peroxisome proliferator-activated receptor-gamma; %PPB, % plasma
24
25 protein binding; RBP4, retinol binding protein-4; RLM, rat liver microsomes; RPE, retinal
26
27 pigment epithelium; SAR, structure-activity relationship; Ser, serine; S_N2, bimolecular
28
29 nucleophilic displacement; SPA, scintillation proximity assay; SSA, systemic senile
30
31 amyloidosis; STD-NMR, saturation transfer difference-NMR; TBG: thyroxine-binding
32
33 globulin; TFA, trifluoroacetic acid; THF, tetrahydrofuran; Thr, threonine; TTR,
34
35 transthyretin; TsCl; tosyl chloride; Tyr, tyrosine; T3P, Propanephosphonic acid anhydride;
36
37 T4, thyroxine; Val, valine; V_{ss}, volume of distribution at steady state; XantPhos, 4,5-
38
39 bis(diphenylphosphino)-9,9-dimethylxanthene; XPhos, 2-dicyclohexylphosphino-2',4',6'-
40
41 triisopropylbiphenyl.

REFERENCES

1. (a) Steinmetz, A. C.; Renaud, J. P.; Moras, D. Binding of ligands and activation of transcription by nuclear receptors. *Annu. Rev. Biophys. Biomol. Struct.* **2001**, *30*, 329-359; (b) Clagett-Dame, M.; DeLuca, H. F. The role of vitamin A in mammalian reproduction and embryonic development. *Annu. Rev. Nutr.* **2002**, *22*, 347-381; (c) Wolf, G., Multiple functions of vitamin A. *Physiological Rev.* **1984**, *64*, 873-937.
2. (a) Kiser, P. D.; Golczak, M.; Palczewski, K. Chemistry of the retinoid (visual) cycle. *Chem. Rev.* **2014**, *114*, 194-232; (b) Tsin, A.; Betts-Obregon, B.; Grigsby, J. Visual cycle proteins: structure, function, and roles in human retinal disease, *J. Biol. Chem.* **2018**, *293*, 13016-13021.
3. (a) Kanai, M.; Raz, A.; Goodman, D. S., Retinol-binding protein: the transport protein for vitamin A in human plasma. *J. Clin. Invest.* **1968**, *47*, 2025-2044; (b) Schlehuber, S.; Skerra, A. Lipocalins in drug discovery: from natural ligand-binding proteins to "anticalins". *Drug Discovery Today* **2005**, *10*, 23-33.
4. (a) Bobbert, T.; Raila, J.; Schwarz, F.; Mai, K.; Henze, A.; Pfeiffer, A. F. H.; Schweigert, F. J.; Spranger, J. Relation between retinol, retinol-binding protein 4, transthyretin and carotid intima media thickness. *Atherosclerosis* **2010**, *213*, 549-551; (b) Kawaguchi, R.; Zhong, M.; Kassai, M.; Ter-Stepanian, M.; Sun, H. Vitamin A transport mechanism of the multitransmembrane cell-surface receptor STRA6. *Membranes* **2015**, *5*, 425-453.
5. (a) Blake, C. C.; Geisow, M. J.; Oatley, S. J.; Rerat, B.; Rerat, C. Structure of prealbumin: secondary, tertiary and quaternary interactions determined by Fourier refinement at 1.8 Å. *J. Mol. Biol.* **1978**, *121*, 339-356; (b) Nilsson, S. F.; Rask, L.; Peterson, P. A. Studies

- 1
2
3 on thyroid hormone-binding proteins. II. Binding of thyroid hormones, retinol-binding
4 protein, and fluorescent probes to prealbumin and effects of thyroxine on prealbumin
5 subunit self-association. *J. Biol. Chem.* **1975**, *250*, 8554-8563; (c) Wojtczak, A.; Cody,
6 V.; Luft, J. R.; Pangborn, W. Structures of human transthyretin complexed with
7 thyroxine at 2.0 Å resolution and 3',5'-dinitro-N-acetyl-L-thyronine at 2.2 Å resolution.
8 *Acta. Crystallogr. D. Biol. Crystallogr.* **1996**, *52*, 758-765; (d) Hamilton, J. A.; Benson,
9 M. D. Transthyretin: a review from a structural perspective. *Cell. Mol. Life Sci.* **2001**,
10 *58*, 1491-1521. (e) Monaco, H. L.; Rizzi, M.; Coda, A. Structure of a complex of two
11 plasma proteins: transthyretin and retinol-binding protein. *Science* **1995**, *268*, 1039-
12 1041.
- 13
14
15
16
17
18
19
20
21
22
23
24
25
26
27
28 6. (a) Johnson, S. M.; Wiseman, R. L.; Sekijima, Y.; Green, N. S.; Adamski-Werner, S. L.;
29 Kelly, J. W. Native state kinetic stabilization as a strategy to ameliorate protein
30 misfolding diseases: a focus on the transthyretin amyloidoses. *Acc. Chem. Res.* **2005**,
31 *38*, 911-921; (b) Foss, T. R.; Wiseman, R. L.; Kelly, J. W. The pathway by which the
32 tetrameric protein transthyretin dissociates. *Biochemistry* **2005**, *44*, 15525-15533.
- 33
34
35
36
37
38
39
40 7. (a) Newcomer, M. E.; Jones, T. A.; Aqvist, J.; Sundelin, J.; Eriksson, U.; Rask, L.;
41 Peterson, P. A. The three-dimensional structure of retinol-binding protein. *EMBO J.*
42 **1984**, *3*, 1451-1454. (b) Cowan, S. W.; Newcomer, M. E.; Jones, T. A. Crystallographic
43 refinement of human serum retinol binding protein at 2 Å resolution. *Proteins* **1990**,
44 *8*, 44-61.
- 45
46
47
48
49
50
51
52 8. Motani, A.; Wang, Z.; Conn, M.; Siegler, K.; Zhang, Y.; Liu, Q.; Johnstone, S.; Xu, H.;
53 Thibault, S.; Wang, Y.; Fan, P.; Connors, R.; Le, H.; Xu, G.; Walker, N.; Shan, B.; Coward,

- 1
2
3 P. Identification and characterization of a non-retinoid ligand for retinol-binding
4 protein 4 which lowers serum retinol-binding protein 4 levels *in vivo*. *J. Biol. Chem.*
5
6
7
8 **2009**, *284*, 7673-7680.
9
- 10 9. Zanotti, G.; Folli, C.; Cendron, L.; Alfieri, B.; Nishida, S. K.; Gliubich, F.; Pasquato, N.;
11
12 Negro, A.; Berni, R. Structural and mutational analyses of protein-protein interactions
13 between transthyretin and retinol-binding protein. *FEBS J.* **2008**, *275*, 5841-5854.
14
15 Noy, N.; Slosberg, E.; Scarlata, S., Interactions of retinol with binding proteins: studies
16 with retinol-binding protein and with transthyretin. *Biochemistry* **1992**, *31*, 11118-
17
18 11124; (d) Noy, N.; Xu, Z. J., Interactions of retinol with binding proteins: implications
19 for the mechanism of uptake by cells. *Biochemistry* **1990**, *29*, 3878-3883; (e) Monaco,
20
21 H. L., The transthyretin-retinol-binding protein complex. *Biochim Biophys. Acta* **2000**,
22
23 *1482*, 65-72; (f) Monaco, H. L., Three-dimensional structure of the transthyretin-
24
25 retinol-binding protein complex. *Clin. Chem. Lab. Med.* **2002**, *40*, 1229-1236; (g)
26
27 Monaco, H. L.; Rizzi, M.; Coda, A., Structure of a complex of two plasma proteins:
28
29 transthyretin and retinol-binding protein. *Science* **1995**, *268*, 1039-1041.
30
31
32
33
34
35
36
37
38
39
- 40 10. Naylor, H. M.; Newcomer, M. E., The structure of human retinol-binding protein (RBP)
41
42 with its carrier protein transthyretin reveals an interaction with the carboxy terminus
43
44 of RBP. *Biochemistry* **1999**, *38*, 2647-2653.
45
46
- 47 11. (a) Radu, R. A.; Han, Y.; Bui, T. V.; Nusinowitz, S.; Bok, D.; Lichter, J.; Widder, K.; Travis,
48
49 G. H.; Mata, N. L., Reductions in serum vitamin A arrest accumulation of toxic retinal
50
51 fluorophores: a potential therapy for treatment of lipofuscin-based retinal diseases.
52
53
54
55
56
57
58
59
60

- 1
2
3 *Invest. Ophthalm. Vis. Sci.* **2005**, *46*, 4393-4401; (b) Palczewski, K., Retinoids for treatment
4 of retinal diseases. *Trends Pharmacol. Sci.* **2010**, *31*, 284-295.
5
6
7
8 12. (a) Petrukhin, K., Pharmacological inhibition of lipofuscin accumulation in the retina
9 as a therapeutic strategy for dry AMD treatment. *Drug Discov. Today Ther. Strateg.*
10 **2013**, *10*, e11-e20; (b) Petrukhin, K., New therapeutic targets in atrophic age-related
11 macular degeneration. *Expert Opin. Ther. Tar.* **2007**, *11*, 625-639.
12
13
14
15
16
17 13. Dobri, N.; Qin, Q.; Kong, J.; Yamamoto, K.; Liu, Z.; Moiseyev, G.; Ma, J.-X.; Allikmets,
18 R.; Sparrow, J. R.; Petrukhin, K., A1120, a nonretinoid RBP4 antagonist, inhibits
19 formation of cytotoxic bisretinoids in the animal model of enhanced retinal
20 lipofuscinogenesis. *Invest. Ophthalm. Vis. Sci.* **2013**, *54*, 85-95.
21
22
23
24
25
26
27 14. Racz, B.; Varadi, A.; Kong, J.; Allikmets, R.; Pearson, P. G.; Johnson, G.; Cioffi, C. L.;
28 Petrukhin, K. A non-retinoid antagonist of retinol-binding protein 4 rescues phenotype
29 in a model of Stargardt disease without inhibiting the visual cycle. *J. Biol. Chem.* **2018**,
30 *293*, 11574-11588.
31
32
33
34
35
36
37 15. (a) Young, R. W., Pathophysiology of age-related macular degeneration. *Surv*
38 *Ophthalmol.* **1987**, *31*, 291-306; (b) Dorey, C. K.; Wu, G.; Ebenstein, D.; Garsd, A.;
39 Weiter, J. J., Cell loss in the aging retina. Relationship to lipofuscin accumulation and
40 macular degeneration. *Invest. Ophthalm. Vis. Sci.* **1989**, *30*, 1691-1699; (c) Holz, F. G.;
41 Bellman, C.; Staudt, S.; Schutt, F.; Volcker, H. E., Fundus autofluorescence and
42 development of geographic atrophy in age-related macular degeneration. *Invest.*
43 *Ophthalm. Vis. Sci.* **2001**, *42*, 1051-1056; (d) Holz, F. G.; Bellmann, C.; Margaritidis, M.;
44 Schutt, F.; Otto, T. P.; Volcker, H. E., Patterns of increased in vivo fundus
45
46
47
48
49
50
51
52
53
54
55
56
57
58
59
60

1
2
3 autofluorescence in the junctional zone of geographic atrophy of the retinal pigment
4
5 epithelium associated with age-related macular degeneration. *Graefes Arch. Clin. Exp.*
6
7 *Ophthalmol.* **1999**, *237*, 145-152; (e) Holz, F. G.; Bindewald-Wittich, A.; Fleckenstein,
8
9 M.; Dreyhaupt, J.; Scholl, H. P.; Schmitz-Valckenberg, S., Progression of geographic
10
11 atrophy and impact of fundus autofluorescence patterns in age-related macular
12
13 degeneration. *Am. J. Ophthalmol.* **2007**, *143*, 463-472; (f) Schmitz-Valckenberg, S.;
14
15 Fleckenstein, M.; Scholl, H. P.; Holz, F. G., Fundus autofluorescence and progression
16
17 of age-related macular degeneration. *Surv. Ophthalmol.* **2009**, *54*, 96-117; (g)
18
19 Finnemann, S. C.; Leung, L. W.; Rodriguez-Boulan, E., The lipofuscin component A2E
20
21 selectively inhibits phagolysosomal degradation of photoreceptor phospholipid by the
22
23 retinal pigment epithelium. *Proc. Natl. Acad. Sci. U.S.A.* **2002**, *99*, 3842-3847; (h) Suter,
24
25 M.; Reme, C.; Grimm, C.; Wenzel, A.; Jaattela, M.; Esser, P.; Kociok, N.; Leist, M.;
26
27 Richter, C., Age-related macular degeneration. The lipofuscin component *N*-retinyl-*N*-
28
29 retinylidene ethanolamine detaches proapoptotic proteins from mitochondria and
30
31 induces apoptosis in mammalian retinal pigment epithelial cells. *J. Biol. Chem.* **2000**,
32
33 *275*, 39625-39630; (i) Sparrow, J. R.; Fishkin, N.; Zhou, J.; Cai, B.; Jang, Y. P.; Krane, S.;
34
35 Itagaki, Y.; Nakanishi, K., A2E, a byproduct of the visual cycle. *Vis. Res.* **2003**, *43*, 2983-
36
37 2990; (j) Sparrow, J. R.; Gregory-Roberts, E.; Yamamoto, K.; Blonska, A.; Ghosh, S. K.;
38
39 Ueda, K.; Zhou, J., The bisretinoids of retinal pigment epithelium. *Prog. Retin. Eye Res.*
40
41 **2012**, *31*, 121-135; (k) Delori, F. C., RPE lipofuscin in ageing and age-related macular
42
43 degeneration. In *Retinal Pigment Epithelium and Macular Disease (Documenta*
44
45
46
47
48
49
50
51
52
53
54
55
56
57
58
59
60

1
2
3 *Ophthalmologica*), G. Coscas, F. C. P., Ed. Kluwer Academic Publishers: Dordrecht, The
4
5 Netherlands 1995; Vol. 62, pp 37-45.
6
7

- 8 16.(a) Weng, J.; Mata, N. L.; Azarian, S. M.; Tzekov, R. T.; Birch, D. G.; Travis, G. H., Insights
9
10 into the function of Rim protein in photoreceptors and etiology of Stargardt's disease
11
12 from the phenotype in abcr knockout mice. *Cell* **1999**, *98*, 13-23; (b) Sparrow, J. R.;
13
14 Cai, B., Blue light-induced apoptosis of A2E-containing RPE: involvement of caspase-3
15
16 and protection by Bcl-2. *Invest. Opth. Vis. Sci.* **2001**, *42*, 1356-1362; (c) Bergmann,
17
18 M.; Schutt, F.; Holz, F. G.; Kopitz, J., Inhibition of the ATP-driven proton pump in RPE
19
20 lysosomes by the major lipofuscin fluorophore A2-E may contribute to the
21
22 pathogenesis of age-related macular degeneration. *FASEB J.* **2004**, *18*, 562-564; (d)
23
24 Sparrow, J. R.; Parish, C. A.; Hashimoto, M.; Nakanishi, K., A2E, a lipofuscin
25
26 fluorophore, in human retinal pigmented epithelial cells in culture. *Invest. Opth. Vis.*
27
28 *Sci.* **1999**, *40*, 2988-2995; (e) De, S.; Sakmar, T. P., Interaction of A2E with model
29
30 membranes. Implications to the pathogenesis of age-related macular degeneration. *J.*
31
32 *Gen. Physiol.* **2002**, *120*, 147-157; (f) Vives-Bauza, C.; Anand, M.; Shirazi, A. K.;
33
34 Magrane, J.; Gao, J.; Vollmer-Snarr, H. R.; Manfredi, G.; Finnemann, S. C., The age lipid
35
36 A2E and mitochondrial dysfunction synergistically impair phagocytosis by retinal
37
38 pigment epithelial cells. *J. Biol. Chem.* **2008**, *283*, 24770-24780; (g) Zhou, J.; Jang, Y.
39
40 P.; Kim, S. R.; Sparrow, J. R., Complement activation by photooxidation products of
41
42 A2E, a lipofuscin constituent of the retinal pigment epithelium. *Proc. Natl. Acad. Sci.*
43
44 *U.S.A.* **2006**, *103*, 16182-16187; (h) Radu, R. A.; Hu, J.; Yuan, Q.; Welch, D. L.;
45
46 Makshanoff, J.; Lloyd, M.; McMullen, S.; Travis, G. H.; Bok, D., Complement system
47
48
49
50
51
52
53
54
55
56
57

- dysregulation and inflammation in the retinal pigment epithelium of a mouse model for Stargardt macular degeneration. *J. Biol. Chem.* **2011**, *286*, 18593-18601; (i) Ben-Shabat, S.; Parish, C. A.; Vollmer, H. R.; Itagaki, Y.; Fishkin, N.; Nakanishi, K.; Sparrow, J. R., Biosynthetic studies of A2E, a major fluorophore of retinal pigment epithelial lipofuscin. *J. Biol. Chem.* **2002**, *277*, 7183-7190; (j) Rozanowska, M.; Jarvis-Evans, J.; Korytowski, W.; Boulton, M. E.; Burke, J. M.; Sarna, T., Blue light-induced reactivity of retinal age pigment. In vitro generation of oxygen-reactive species. *J. Biol. Chem.* **1995**, *270*, 18825-18830; (k) Sparrow, J. R.; Zhou, J.; Ben-Shabat, S.; Vollmer, H.; Itagaki, Y.; Nakanishi, K., Involvement of oxidative mechanisms in blue-light-induced damage to A2E-laden RPE. *Invest. Ophth. Vis. Sci.* **2002**, *43*, 1222-1227; (l) Dontsov, A. E.; Sakina, N. L.; Golubkov, A. M.; Ostrovsky, M. A., Light-induced release of A2E photooxidation toxic products from lipofuscin granules of human retinal pigment epithelium. *Dokl. Biochem. Biophys.* **2009**, *425*, 98-101.
17. (a) Berni, R.; Formelli, F., In vitro interaction of fenretinide with plasma retinol-binding protein and its functional consequences. *FEBS Lett.* **1992**, *308*, 43-45; (b) Adams, W. R.; Smith, J. E.; Green, M. H., Effects of N-(4-hydroxyphenyl)retinamide on vitamin A metabolism in rats. *Proc. Soc. Exp. Biol. Med.* **1995**, *208*, 178-185; (c) Mata, N. L.; Lichter, J. B.; Vogel, R.; Han, Y.; Bui, T. V.; Singerman, L. J., Investigation of oral fenretinide for treatment of geographic atrophy in age-related macular degeneration. *Retina* **2013**, *33*, 498-507.
18. Cioffi, C. L.; Dobri, N.; Freeman, E. E.; Conlon, M. P.; Chen, P.; Stafford, D. G.; Schwarz, D. M. C.; Golden, K. C.; Zhu, L.; Kitchen, D. B.; Barnes, K. D.; Racz, B.; Qin, Q.; Michelotti,

- 1
2
3 E.; Cywin, C. L.; Martin, W. H.; Pearson, P. G.; Johnson, G.; Petrukhin, K., Design,
4
5 synthesis, and evaluation of nonretinoid retinol binding protein 4 antagonists for the
6
7 potential treatment of atrophic age-related macular degeneration and Stargardt
8
9 disease. *J. Med. Chem.* **2014**, *57*, 7731-7757.
- 10
11
12
13 19. Cioffi, C. L.; Racz, B.; Freeman, E. E.; Conlon, M. P.; Chen, P.; Stafford, D. G.; Schwarz,
14
15 D. M.; Zhu, L.; Kitchen, D. B.; Barnes, K. D.; Dobri, N.; Michelotti, E.; Cywin, C. L.;
16
17 Martin, W. H.; Pearson, P. G.; Johnson, G.; Petrukhin, K. Bicyclic [3.3.0]-
18
19 octahydrocyclopenta[c]pyrrolo antagonists of retinol binding protein 4: potential
20
21 treatment of atrophic age-related macular degeneration and Stargardt disease. *J.*
22
23 *Med. Chem.* **2015**, *58*, 5863-5888.
- 24
25
26
27 20. Racz, B.; Varadi, A.; Pearson, P. G.; Petrukhin, K. Comparative pharmacokinetics and
28
29 pharmacodynamics of the advanced retinol-binding protein 4 antagonist in dog and
30
31 cynomolgus monkey. *PLoS One* **2020**, *15*, e0228291.
- 32
33
34
35 21. (a) Graham, T. E.; Yang, Q.; Bluher, M.; Hammarstedt, A.; Ciaraldi, T. P.; Henry, R. R.;
36
37 Wason, C. J.; Oberbach, A.; Jansson, P. A.; Smith, U.; Kahn, B. B. Retinol-binding
38
39 protein 4 and insulin resistance in lean, obese, and diabetic subjects. *N. Engl. J. Med.*
40
41 **2006**, *354*, 2552-2563; (b) Yang, Q.; Graham, T. E.; Mody, N.; Preitner, F.; Peroni, O.
42
43 D.; Zabolotny, J. M.; Kotani, K.; Quadro, L.; Kahn, B. B. Serum retinol binding protein 4
44
45 contributes to insulin resistance in obesity and type 2 diabetes. *Nature* **2005**, *436*,
46
47 356-362.
- 48
49
50
51
52 22. Aeberli, I.; Biebinger, R.; Lehmann, R.; L'Allemand, D.; Spinaz, G. A.; Zimmermann, M.
53
54 B. Serum retinol-binding protein 4 concentration and its ratio to serum retinol are
55
56
57
58
59
60

- 1
2
3 associated with obesity and metabolic syndrome components in children. *J. Clin.*
4
5 *Endocrinol. Metab.* **2007**, *92*, 4359-4365.
6
7
8 23. Kowalska, I.; Strackowski, M.; Adamska, A.; Nikolajuk, A.; Karczewska-Kupczewska,
9
10 M.; Otziomek, E.; Gorska, M. Serum retinol binding protein 4 is related to insulin
11
12 resistance and nonoxidative glucose metabolism in lean and obese women with
13
14 normal glucose tolerance. *J. Clin. Endocrinol. Metab.* **2008**, *93*, 2786-2789.
15
16
17 24. (a) Ingelsson, E.; Sundstrom, J.; Melhus, H.; Michaelsson, K.; Berne, C.; Vasan, R. S.;
18
19 Riserus, U.; Blomhoff, R.; Lind, L.; Arnlov, J. Circulating retinol-binding protein 4,
20
21 cardiovascular risk factors and prevalent cardiovascular disease in elderly.
22
23 *Atherosclerosis* **2009**, *206*, 239-244; (b) Qi, Q.; Yu, Z.; Ye, X.; Zhao, F.; Huang, P.; Hu, F.
24
25 B.; Franco, O. H.; Wang, J.; Li, H.; Liu, Y.; Lin, X. Elevated retinol-binding protein 4 levels
26
27 are associated with metabolic syndrome in Chinese people. *J. Clin. Endocrinol. Metab.*
28
29 **2007**, *92*, 4827-4834; (c) Norseen, J.; Hosooka, T.; Hammarstedt, A.; Yore, M. M.; Kant,
30
31 S.; Aryal, P.; Kiernan, U. A.; Phillips, D. A.; Maruyama, H.; Kraus, B. J.; Usheva, A.; Davis,
32
33 R. J.; Smith, U.; Kahn, B. B. Retinol-binding protein 4 inhibits insulin signaling in
34
35 adipocytes by inducing proinflammatory cytokines in macrophages through a c-Jun N-
36
37 terminal kinase- and toll-like receptor 4-dependent and retinol-independent
38
39 mechanism. *Mol. Cell. Biol.* **2012**, *32*, 2010-2019.
40
41
42 25. Lee, S. A.; Yuen, J. J.; Jiang, H.; Kahn, B. B.; Blaner, W. S., Adipocyte-specific
43
44 overexpression of retinol-binding protein 4 causes hepatic steatosis in mice.
45
46
47 *Hepatology* **2016**, *64*, 1534-1546.
48
49
50
51
52
53
54
55
56
57
58
59
60

- 1
2
3 26. Cioffi, C. L.; Racz, B.; Varadi, A.; Freeman, E. E.; Conlon, M. P.; Chen, P.; Zhu, L.; Kitchen,
4
5 D. B.; Barnes, K. D.; Martin, W. H.; Pearson, P. G.; Johnson, G.; Blaner, W. S.; Petrukhin,
6
7 K. Design, synthesis, and preclinical efficacy of novel nonretinoid antagonists of
8
9 retinol-binding protein 4 in the mouse model of hepatic steatosis. *J. Med. Chem.* **2019**
10
11 62, 5470-5500.
12
13
14
15 27. (a) Falk, R. H.; Comenzo, R. L.; Skinner, M. The systemic amyloidoses. *N. Engl. J. Med.*
16
17 **1997**, 337, 898-909; (b) Brunjes, D. L.; Castano, A.; Clemons, A.; Rubin, J.; Maurer, M.
18
19 S. Transthyretin cardiac amyloidosis in older Americans. *J. Card. Failure* **2016**, 22, 996-
20
21 1003; (c) Ton, V. K.; Mukherjee, M.; Judge, D. P. Transthyretin cardiac amyloidosis:
22
23 pathogenesis, treatments, and emerging role in heart failure with preserved ejection
24
25 fraction. *Clin. Med. Insights: Cardiol.* **2014**, 8s1, 39-44.
26
27
28
29
30 28. White, J. T.; Kelly, J. W. Support for the multigenic hypothesis of amyloidosis: the
31
32 binding stoichiometry of retinol-binding protein, vitamin A, and thyroid hormone
33
34 influences transthyretin amyloidogenicity in vitro. *Proc. Natl. Acad. Sci. U.S.A.* **2001**,
35
36 98, 13019-13024.
37
38
39
40 29. Hyung, S. J.; Deroo, S.; Robinson, C. V. Retinol and retinol-binding protein stabilize
41
42 transthyretin via formation of retinol transport complex. *ACS. Chem. Biol.* **2010**, 5,
43
44 1137-1146.
45
46
47 30. (a) Ruberg, F. L.; Berk, J. L. Transthyretin (TTR) cardiac amyloidosis. *Circulation* **2012**,
48
49 126, 1286-1300; (b) Connors, L. H.; Doros, G.; Sam, F.; Badiee, A.; Seldin, D. C.; Skinner,
50
51 M. Clinical features and survival in senile systemic amyloidosis: comparison to familial
52
53 transthyretin cardiomyopathy. *Amyloid* **2011**, 18, 157-159; (c) Westermark, P.;

- 1
2
3 Bergstrom, J.; Solomon, A.; Murphy, C.; Sletten, K. Transthyretin-derived senile
4 systemic amyloidosis: clinicopathologic and structural considerations. *Amyloid*. **2003**,
5
6 *10*, 48-54.
7
8
9
10
11 31. (a) Buxbaum, J. N.; Ruberg, F. L. Transthyretin V122I (pV142I)* cardiac amyloidosis: an
12 age-dependent autosomal dominant cardiomyopathy too common to be overlooked
13 as a cause of significant heart disease in elderly African Americans. *Genet. Med.* **2017**,
14 *19*, 733-742; (b) Alexander, K. M.; Falk, R. H. V122I TTR cardiac amyloidosis in patients
15 of African descent: recognizing a missed disease or the dog that didn't bark? *Circ.:*
16 *Heart Failure* **2016**, *9*, e003489.
17
18
19
20
21
22
23
24
25 32. Sekijima, Y.; Hammarström, P.; Matsumura, M.; Shimizu, Y.; Iwata, M.; Tokuda, T.;
26 Ikeda, S-I.; Kelly, J. W. Energetic Characteristics of the new transthyretin variant A25T
27 may explain its atypical central nervous system pathology *Lab. Investig.* **2003**, *83*, 409-
28
29
30
31
32
33
34
35 33. (a) Kerschen, P.; Plante-Bordeneuve, V. Current and future treatment approaches in
36 transthyretin familial amyloid polyneuropathy. *Curr. Treat. Options Neurol.* **2016**, *18*,
37
38
39
40
41
42
43
44
45
46
47
48
49
50
51
52
53
54
55
56
57
58
59
60

1
2
3 Adamski-Werner, S. L.; Kelly, J. W. Native state kinetic stabilization as a strategy to
4 ameliorate protein misfolding diseases: a focus on the transthyretin amyloidosis. *Acc.*
5
6 *Chem. Res.* **2005**, *38*, 911-921; (e) Nencetti, S.; Orlandini, E. TTR fibril formation
7
8 inhibitors: is there a SAR? *Curr. Med. Chem.* **2012**, *19*, 2356-2379; (f) Adams, D.;
9
10 Cauquil, C.; Labeyrie, C.; Beaudonnet, G.; Algalarrondo, V.; Théaudin, M. TTR kinetic
11
12 stabilizers and TTR gene silencing: a new era in therapy for familial amyloidotic
13
14 polyneuropathies. *Expert Opin. Pharmacother.* **2016**, *17*, 791-802.

15
16
17
18
19
20 34. (a) Coelho, T.; Merlini, G.; Bulawa, C. E.; Fleming, J. A.; Judge, D. P.; Kelly, J. W.; Maurer,
21
22 M. S.; Plante-Bordeneuve, V.; Labaudiniere, R.; Mundayat, R.; Riley, S.; Lombardo,
23
24 I.; Huertas, P. Mechanism of action and clinical application of tafamidis in hereditary
25
26 transthyretin amyloidosis. *Neurol. Ther.* **2016**, *5*, 1-25; (b) Nencetti, S.; Rossello, A.;
27
28 Orlandini, E. Tafamidis (Vyndaqel): A light for FAP patients. *ChemMedChem* **2013**, *8*,
29
30 1617-1619; (c) Lamb, Y. N.; Deeks, E. D. Tafamidis: A review in transthyretin
31
32 amyloidosis with polyneuropathy. *Drugs* **2019**, *79*, 863-874; (d) Bulawa, C. E.;
33
34 Connelly, S.; Devit, M.; Wang, L.; Weigel, C.; Fleming, J. A.; Packman, J.; Powers, E. T.;
35
36 Wiseman, R. L.; Foss, T. R.; Wilson, I. A.; Kelly, J. W.; Labaudiniere, R. Tafamidis, a
37
38 potent and selective transthyretin kinetic stabilizer that inhibits the amyloid cascade.
39
40
41
42
43
44
45 *Proc. Natl. Acad. Sci. U.S.A.* **2012**, *109*, 9629-9634.

46
47 35. (a) Penchala, S.C.; Connelly, S.; Wang, Y.; Park, M. S.; Zhao, L.; Baranczak, A.; Rappley,
48
49 I.; Vogel, H.; Liedtke, M.; Witteles, R. M.; Powers, E. T.; Reixach, N.; Chan, W. K.;
50
51 Wilson, I. A.; Kelly, J. W.; Graef, I. A.; Alhamadsheh, M. M. AG10 inhibits
52
53 amyloidogenesis and cellular toxicity of the familial amyloid cardiomyopathy-
54
55
56
57

- 1
2
3 associated V122I transthyretin. *Proc. Natl. Acad. Sci. U. S. A.* **2013**, *110*, 9992-9997;
4
5 (b) Miller, M.; Pal, A.; Albusairi, W.; Joo, H.; Pappas, B.; Haque Tuhin, M.T.; Liang, D.;
6
7 Jampala, R.; Liu, F.; Khan, J.; Faaij, M.; Park, M.; Chan, W.; Graef, I.; Zamboni, R.;
8
9 Kumar, N.; Fox, J.; Sinha, U.; Alhamadsheh, M. Enthalpy-driven stabilization of
10
11 transthyretin by AG10 mimics a naturally occurring genetic variant that protects from
12
13 transthyretin amyloidosis. *J. Med. Chem.* **2018**, *61*, 7862-7876.
14
15
16
17
18 36. Judge, D.P.; Heitner, S. B.; Falk, R. H.; Maurer, M. S.; Shah, S. J.; Witteles, R. M.;
19
20 Grogan, M.; Selby, V. N.; Jacoby, D.; Hanna, M.; Nativi-Nicolau, J.; Patel, J.; Rao, S.;
21
22 Sinha, U.; Turtle, C. W.; Fox, J. C. Transthyretin stabilization by AG10 in symptomatic
23
24 transthyretin amyloid cardiomyopathy. *J. Am. Coll. Cardiol.* **2019**, *74*, 285-295.
25
26
27
28 37. Berk, J. L.; Suhr, O. B.; Sekijima, Y.; Yamashita, T.; Heneghan, M.; Zeldenrust, S. R.;
29
30 Ando, Y.; Ikeda, S.; Gorevic, P.; Merlini, G.; Kelly, J. W.; Skinner, M.; Bisbee, A. B.; Dyck,
31
32 P. J.; Obici, L. Familial amyloidosis consortium. The diflunisal trial: study accrual and
33
34 drug tolerance. *Amyloid* **2012**, *19*, 37-38.
35
36
37
38 38. Sant'Anna, R.; Gallego, P.; Robinson, L. Z.; Pereira-Henriques, A.; Ferreira, N.; Pinheiro,
39
40 F.; Esperante, S.; Pallares, I.; Huertas, O.; Almeida, M. R.; Reixach, N.; Insa, R.;
41
42 Velazquez-Campoy, A.; Reverter, D.; Reig, N.; Ventura, S. Repositioning tolcapone as
43
44 a potent inhibitor of transthyretin amyloidogenesis and associated cellular toxicity.
45
46
47 *Nat. Commun.* **2016**, *7*, 10787.
48
49
50 39. Gimeno, A.; Santos, L. M.; Alemi, M.; Rivas, J.; Blasi, D.; Cotrina, E. Y.; Llop, J.; Valencia,
51
52 G.; Cardoso, I.; Quintana, J.; Arsequell, G.; Jiménez-Barbero. J. Insights on the
53
54
55
56
57
58
59
60

- 1
2
3 interaction between transthyretin and A β in solution. A saturation transfer difference
4
5 (STD) NMR analysis of the role of iododiflunisal. *J. Med. Chem.* **2017**, *60*, 5749-5758.
6
7
8 40. Gales, L.; Macedo-Ribeiro, S.; Arsequell, G.; Valencia, G.; João Saraiva, M.; Margarida
9
10 Damas, A. Human transthyretin in complex with iododiflunisal: structural features
11
12 associated with a potent amyloid inhibitor. *Biochem. J.* **2005**, *388*, 615-621.
13
14
15 41. Rodrigues, D. A. *Drug-Drug Interactions*, 2nd ed.; CRC Press: New York, 2008.
16
17
18 42. Ahmadian, M.; Suh, J. M.; Hah, N.; Liddle, C.; Atkins, A. R.; Downes, M.; Evans, R. M.
19
20 PPAR γ signaling and metabolism: the good, the bad and the future. *Nat Med.* **2013**,
21
22 *19*, 557-566.
23
24
25 43. Palaninathan, S. K.; Mohamedmohaideen, N. N.; Orlandini, E.; Ortore, G.; Nencetti, S.;
26
27 Lapucci, A.; Rossello, A.; Freundlich, J. S.; Sacchettini, J. C. Novel transthyretin amyloid
28
29 fibril formation inhibitors: synthesis, biological evaluation, and X-ray structural
30
31 analysis. *PLoS One* **2009**, *4*, e6290.
32
33
34
35 44. Petrassi, H. M.; Klabunde, T.; Sacchettini, J.; Kelly, J. W. Structure-based design of *N*-
36
37 phenyl phenoxazine transthyretin amyloid fibril inhibitors. *J. Am. Chem. Soc.* **2000**,
38
39 *122*, 2178-2192.
40
41
42 45. Petrassi, H. M.; Johnson, S. M.; Purkey, H. E.; Chiang, K. P.; Walkup, T.; Jiang, X.;
43
44 Powers, E. T.; Kelly, J. W. Potent and selective structure-based dibenzofuran inhibitors
45
46 of transthyretin amyloidogenesis: kinetic stabilization of the native state *J. Am. Chem.*
47
48 *Soc.* **2005**, *127*, 6662-6671.
49
50
51
52
53
54
55
56
57
58
59
60

- 1
2
3 46. Green, N. S.; Foss, T. R.; Kelly, J. W. Genistein, a natural product from soy, is a potent
4
5 inhibitor of transthyretin amyloidosis. *Proc. Nat. Acad. Sci. U.S.A.* **2005**, *102*, 14545-
6
7 14550.
8
9
10 47. Hurshman, A. R.; White, J. T.; Powers, E. T.; Kelly, J. W. Transthyretin aggregation
11
12 under partially denaturing conditions is a downhill polymerization. *Biochemistry* **2004**,
13
14 *43*, 7365-7381.
15
16
17 48. Klabunde, T.; Petrassi, H. M.; Oza, V. B.; Raman, P.; Kelly, J. W.; Sacchettini, J. C.
18
19 Rational design of potent human transthyretin amyloid disease inhibitors. *Nat. Struct.*
20
21 *Biol.* 2000, *7*, 312-21.
22
23
24 49. Niemietz, C.; Fleischhauer, L.; Sandfort, V.; Guttman, S.; Zibert, A.; Schmidt, H. H.
25
26 Hepatocyte-like cells reveal novel role of SERPINA1 in transthyretin amyloidosis. *J. Cell*
27
28 *Sci.* 2018, *131*, pii: jcs219824.
29
30
31 50. Klein, R.; Klein, B. E.; Cruickshanks, K. J. The prevalence of age-related maculopathy
32
33 by geographic region and ethnicity. *Prog. Retin. Eye Res.* 1999, *18*, 371-389.
34
35
36 51. Basaiawmoit, R. V.; Rattan, S. I. S. Cavalotti C. A. P., Cerulli L. (eds): Age-related
37
38 changes of the human eye. *Biogerontology* 2009, *10*, 95-96.
39
40
41 52. Westermark P.; Sletten, K.; Johansson, B.; Cornwell, G. G. 3rd. Fibril in senile systemic
42
43 amyloidosis is derived from normal transthyretin. *Proc. Natl. Acad. Sci. U. S. A.* **1990**,
44
45 *87*, 2843-2845.
46
47
48
49
50
51
52
53
54
55
56
57

- 1
2
3 53. Wong, W. L.; Su, X.; Li, X.; Cheung, C. M.; Klein, R.; Cheng, C. Y.; Wong, T. Y. Global
4 prevalence of age-related macular degeneration and disease burden projection for
5
6 prevalence of age-related macular degeneration and disease burden projection for
7
8 2020 and 2040: a systematic review and meta-analysis. *Lancet Glob. Health.* **2014**, *2*,
9
10 e106-116.
11
12
- 13 54. Wolf G. Retinol transport and metabolism in transthyretin-"knockout" mice. *Nutr. Rev.*
14
15 **1995**, *53*, 98-99.
16
17
- 18 55. Vogel, S.; Piantedosi, R.; O'Byrne, S. M.; Kako, Y.; Quadro, L.; Gottesman, M. E.;
19
20 Goldberg, I. J.; Blaner, W. S. Retinol-binding protein-deficient mice: biochemical basis
21
22 for impaired vision. *Biochemistry* **2002**, *41*, 15360-15368.
23
24
- 25 56. Quadro, L.; Blaner, W. S.; Salchow, D. J.; Vogel, S.; Piantedosi, R.; Gouras, P.; Freeman,
26
27 S.; Cosma, M. P.; Colantuoni, V.; Gottesman, M. E. Impaired retinal function and
28
29 vitamin A availability in mice lacking retinol-binding protein. *Embo J.* **1999**, *18*, 4633-
30
31 4644.
32
33
34
- 35 57. Quadro, L.; Hamberger, L.; Colantuoni, V.; Gottesman, M. E.; Blaner, W. S.
36
37 Understanding the physiological role of retinol-binding protein in vitamin A
38
39 metabolism using transgenic and knockout mouse models. *Mol Aspects Med.* **2003**,
40
41 *24*, 421-430.
42
43
44
- 45 58. Thompson, C. L.; Blaner, W. S.; Van Gelder, R. N.; Lai, K.; Quadro, L.; Colantuoni, V.;
46
47 Gottesman, M. E.; Sancar, A. Preservation of light signaling to the suprachiasmatic
48
49 nucleus in vitamin A-deficient mice. *Proc. Nat. Acad. Sci. U. S. A.* **2001**, *98*, 11708-
50
51 11713.
52
53
54
55
56
57

- 1
2
3 59. Wolf G. A case of human vitamin A deficiency caused by an inherited defect in retinol-
4 binding protein without clinical symptoms except night blindness. *Nutr. Rev.* **1999**, *57*,
5 258-260.
6
7
8
9
10 60. Seeliger, M. W.; Biesalski, H. K.; Wissinger, B.; Gollnick, H.; Gielen, S.; Frank, J.; Beck,
11 S.; Zrenner, E. Phenotype in retinol deficiency due to a hereditary defect in retinol
12 binding protein synthesis. *Invest. Ophthalm. Vis. Sci.* **1999**, *40*, 3-11.
13
14
15
16
17 61. Alhamadsheh, M. M.; Connelly, S.; Cho, A.; Reixach, N.; Powers, E. T.; Pan, D. W.;
18 Wilson, I. A.; Kelly, J. W.; Graef, I. A. Potent kinetic stabilizers that prevent
19 transthyretin-mediated cardiomyocyte proteotoxicity. *Sci. Transl. Med.* **2011**, *3*,
20 97ra81.
21
22
23
24
25
26
27
28
29
30
31
32
33
34
35
36
37
38
39
40
41
42
43

44
45 **Table of Content Graphic**
46
47
48
49
50
51
52
53
54
55
56
57
58
59
60

